

**FLOW, MIXING AND MASS TRANSFER IN DUAL PLUG
STIRRED LADLES IN THE PRESENCE OF AN UPPER
BUOYANT PHASE.**

A Thesis Submitted

in Partial Fulfillment of the Requirements

for the Degree of

MASTER OF TECHNOLOGY

by

DABBIRU SATISH KUMAR

to the

**DEPARTMENT OF MATERIALS & METALLURGICAL ENGINEERING
INDIAN INSTITUTE OF TECHNOLOGY, KANPUR
SEPTEMBER, 2003**

19 NOV 2003 / MME

पुरुषोत्तम काशीनाथ कैलकर पुस्तकालय

भारतीय प्रौद्योगिकी संस्थान कानपुर

अवधि क्र० A.....145922.....TH

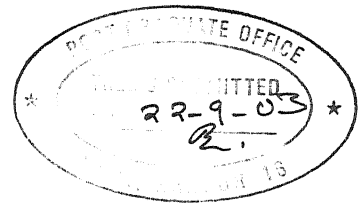
MME/2003/M
D1116



A145922

dedicated to

my parents



CERTIFICATE

This is to certify that the present work “ **FLOW, MIXING AND MASS TRANSFER IN DUAL PLUG STIRRED LADLES IN THE PRESENCE OF AN UPPER BUOYANT PHASE** ” has been carried out by Mr. Dabbiru Satish Kumar (Roll No: Y120606) towards his M.Tech. dissertation under my supervision and that this has not been submitted elsewhere for a degree.

September 22nd, 2003


(Prof. Dipak Mazumdar)

Deptt. of Materials and Metallurgical Engineering.

Indian Institute of Technology, Kanpur

DR. DIPAK MAZUMDAR
Professor
Department of Materials
& Metallurgical Engineering
I.I.T. Kanpur-208 016

ACKNOWLEDGEMENT

I take the opportunity to express a deep sense of gratitude and regard to Dr. Dipak Mazumdar for his astute guidance, invaluable suggestions, discussion and freedom to work. His overly enthusiasm and integral view on research and his mission for providing 'only high-quality work and not less', has made a deep impression on me. I owe him lots of gratitude for having me shown this way of research.

I feel great pleasure on extending my heartfelt and cordial thanks to Dr.A.K.Ray, Mr.Amitava Paul and Mr.Rajiv Singh of Computational Lab Group, RDCIS, SAIL Ranchi for their great coordination and adroit response during the PIV experiments at their place.

I am deeply indebted to all my friends at Hall – V who made my stay at IIT Kanpur a memorable one. I will never forget the sweet moments I spent with Jayanta, Madan, Surendra, Emila, Mukesh, Animesh, Amit, Pramod, Shankar, Amitesh, Sanjay, Ballu, Dj, Gaurav and Rajasekhar.

I am also thankful to Sharmaji and all the technical staff of the department for their direct and indirect assistance towards the project.

Financial assistance received from Ministry of steel, Govt. of India, is gratefully acknowledged.

D. Satish Kumar
Indian Institute of Technology
Kanpur

CONTENTS

	Page
Abstract	i
List of Symbols	ii
List of Figures	iii
List of Tables	vii
CHAPTER I	
INTRODUCTION	1
1.1 Introduction to the Thesis	1
1.2 Literature review	5
1.2.1 Previous work on Fluid flow in Gas Bubble Driven Systems	5
1.2.2 Previous work on Mixing in Gas Bubble Driven Systems	10
1.2.2.1 Effect of Gas Flow Rate on Mixing Time	11
1.2.2.2 Effect of Nozzle Position and Number of Nozzles	14
1.2.2.3 Effect of Second Phase on Mixing Time	15
1.2.3 Previous work on Mass Transfer in Gas Bubble Driven Systems	17
1.3 Scope of the work	22
1.4 Plan of the work	23
CHAPTER II	
FLOW MEASUREMENTS	24
2.1 Introduction	24
2.2 The Physical Model and Operating Parameters	24
2.3 Techniques of Velocity Measurement and their Comparison	26
2.3.1 Laser Doppler Velocimetry	26

2.3.2	Particle Imaging Velocimetry	27
2.3.3	Video Recording	29
2.3.4	Comparison of Effectiveness of PIV, LDV and Video Recording Methods.	31
2.4	Experimental Results	34
2.4.1	Velocity Measurement for Single Plug Bubbling	34
2.4.1.1	Particle Imaging Velocimetry	34
2.4.1.2	Video Recording	43
2.4.2	Velocity Measurement for Dual Plug Bubbling	46

CHAPTER III

MASS TRANSFER AND MIXING MEASUREMENTS 56

3.1	Techniques of mass transfer measurement	56
3.2	Mass Transfer Experiments	58
3.2.1	Experimental Setup	58
3.2.2	Preparation of Liquid	59
3.2.3	Selection of Experimental Variables	60
3.2.4	Experimental Procedure	61
3.2.5	Mass Balance on Tracer: The Governing Equation	62
3.3	Mass Transfer Experimental Results	64
3.4	Discussion of Results	73
3.4.1	Effect of Gas Flow Rate on Mass Transfer	73
3.4.2	Determination of Rate Constant	75
3.4.3	Effect of Gas Flow rate on Mass Transfer Parameter	78
3.4.4	Effect of Nozzle Configuration	80
3.4.5	Effect of Oil Volume Fraction	81
3.4.6	Effect of Location of Sampling on Mass Transfer	83
3.5	Mixing Time Measurements	84
3.5.1	Principles of Electrical Conductivity Measurement Technique	84

3.6	Mixing Time Experiments	85
3.6.1	The Criterion for determination of mixing times	85
3.6.2	Experimental Setup	86
3.6.3	Experimental Procedure	87
3.6.4	Reproducibility of Data	89
3.7	Mixing Time Experimental Results	90
3.8	Discussion of Results	93

CHAPTER IV

CONCLUSION TO THE THESIS	98
---------------------------------	----

CHAPTER V

RECOMMENDATIONS FOR FUTURE WORK	100
--	-----

REFERENCES	101
-------------------	-----

APPENDIX	103
-----------------	-----

ABSTRACT

Fluid flow, mixing and mass transfer in gas stirred ladles were studied through a water model employing mustard oil and water as simulating fluids for slag and metal respectively.

A laboratory method of velocity measurement has been developed using video recording technique. The results were compared with results of established Particle imaging velocimetry (PIV) and Laser Doppler velocimeter (LDV) techniques and found to give a reasonable first hand estimate for the purpose of qualitative analysis. Mixing times were determined by conductivity method using H_2SO_4 as tracer, whereas in the mass transfer experiments the transfer of benzoic acid from water to mustard oil was assessed by volumetric analysis. Gas injection rate, oil volume fraction and nozzle configuration were the parameters included in the study.

The velocity magnitude increased with increasing gas flow rate but the axial and radial velocities are dampened considerably in presence of an upper phase for both single and dual plug bubbling. Mean speed was found to increase as the depth of liquid in the system increases. While the mixing time decreased with the increase of the gas flow rate, the oil layer over the top of the bath extended the mixing time by a factor of 1.5 to 2.25 in the whole range of gas flow rates and at constant gas flow rate, the mixing time was extended with the increase of oil thickness. Mass transfer experiments shows that centric bottom nozzle gas injection leads to higher rate constant of mass transfer as compared to dual and eccentric gas injection. Rate of mass transfer was increased with increase in oil/water volume ratio. Mass transfer is faster for centric nozzle as compared to an eccentric nozzle but mixing times are smaller for eccentric nozzle.

LIST OF SYMBOLS

A	: Interfacial Area, m^2
C_e	: Equilibrium Concentration, gms/l
C_o	: Initial Concentration, gms/l
C_t	: Concentration at time t, gms/l
D,d	: Diameter of Vessel, m
F_c	: Inertial Force
F_σ	: Surface Force
K	: Mass Transfer Parameter/rate Constant, min^{-1}
L	: Bath Depth (Liquid Height), m
m	: Mass, gms
m_f	: Mass Flow rate, gms/sec
Q	: Gas Flow Rate, m^3/sec
Q_B^*	: Transition Gas Flow Rate, m^3/sec
R,r	: Radius of the Vessel, m
t	: Time, min
U_{Mean}	: Mean Recirculation speed, m/sec
U_p	: Plume Velocity, m/sec
V	: Bath Volume, m^3
V_w	: Volume of Water, l
β_m, β, k_w, K_B	: Mass Transfer Coefficient
τ_m	: Mixing Time, sec
ε_m	: Gas Flow Rate, m^3/sec

LIST OF FIGURES

	Page
Figure 1.1: Different methods of melt stirring.	2
Figure 1.2 Schematic view of Gas Stirred Ladle.	3
Figure 1.3: Variation of liquid rise velocity at the plume centerline as a function of gas flow rates [8].	6
Figure 1.4: Characteristic liquid flow pattern in an axisymmetric gas stirred ladle [5].	7
Figure 1.5: Flow patterns of the liquid in the bath generated by blowing gas through porous plug at 1.5 l min^{-1} [11].	7
Figure 1.6: Gas plume shape, fluid flow velocity vectors and turbulent energy dissipation rate at main vertical plane of 80 t ladle for (a) single and (b) dual gas jet conditions respectively[13].	8
Figure 1.7: Plot of total kinetic energy contained in the recirculation aqueous phase vs specific potential energy input rate under various upper slag phase conditions (viz., rigid, fluid and no-slag [15])	9
Figure 1.8: Observed velocity field in the vessel [16] (a) Without oil (b) With oil	10
Figure 1.9: Functional relation between mixing time and specific energy input rate/gas flow rates reproduced from the work of previous investigators. (a) Asai et al.[12] (b) Krishnamurthy et al.[6] and (c) Mazumdar and Guthrie.[3].	13
Figure 1.10: (a) Variation in 95% mixing times with gas flow rate for plug placed at center, one-third, half and two-third radius of ladle base. (b) A plot of mixing time vs. radial position for a single plug for various flow rates.	14
Figure 1.11: Mixing time vs. stirring energy density for three different nozzle patterns with and without oil layer.	16
Figure 1.12: A plot of mixing time as a function gas flow rate for three different arrangement of nozzle with an oil layer present.	16

Figure 1.13:	Relationship between $\beta_m A$ and flow rate in terms of the order of dependence, n , for central tuyere injection. (β_m is written as k_w in the plot)	18
Figure 1.14:	Relation between $k_m / D_i^{1/2}$ and $\varepsilon_m * V^{-2/3}$ (water model).	18
Figure 1.15:	Rate constant of mass transfer versus gas flow rate for centric and eccentric gas injection.	19
Figure 1.16:	Principles of slag emulsification in steel ladles. (a) scheme of detaching process, and (b) equilibrium between inertia force F_c , buoyancy force $F_g \cos \alpha$, and surface force F_σ at the point of droplet detachment.	19
Figure 1.17:	(a) Influence of location of gas injection (top and bottom) on C_t/C_o vs. time for constant gas injection rates. (b) Variation of rate constant K with gas injection rate V	20
Figure 1.18:	Variation in mass transfer coefficient as a function of gas flow rates in high temperature gas-slag-metal system.	21
Figure 2.1:	Principle diagram of Laser Doppler Velocimetry.	26
Figure 2.2:	Basic setup of Particle Imaging Velocimetry.	27
Figure 2.3:	Cross-correlation and localization of the correlation peak.	28
Figure 2.4:	Experimental Setup in the Laboratory	30
Figure 2.5:	Comparison of velocities of PIV, LDV and Video Recording Methods at different Heights from the bottom (a) 3 cms, (b) 9 cms.	32
Figure 2.6:	Comparison of velocities of PIV, LDV and Video Recording Methods at different Heights from the bottom (a) 12 cms, (b) 18 cms.	33
Figure 2.7:	Radial Distribution of axial and radial velocities at 6cm height from the bottom for single plug bubbling without slag.	35
Figure 2.8:	Radial Distribution of axial and radial velocities at 12cm height from the bottom for single plug bubbling without slag.	36
Figure 2.9:	Radial Distribution of axial and radial velocities at 18cm height from the bottom for single plug bubbling without slag.	

Figure 2.10:	Radial Distribution of axial and radial velocities at 24cm height from the bottom for single plug bubbling without slag.	38
Figure 2.11:	Radial Distribution of axial and radial velocities at 6cm height from the bottom for single plug bubbling with slag.	39
Figure 2.12:	Radial Distribution of axial and radial velocities at 12cm height from the bottom for single plug bubbling with slag.	40
Figure 2.13:	Radial Distribution of axial and radial velocities at 18cm height from the bottom for single plug bubbling with slag.	41
Figure 2.14:	Radial Distribution of axial and radial velocities at 24 cm height from the bottom for single plug bubbling with slag.	42
Figure 2.15:	The influence of gas flow rates on mean liquid speed for situations with and without an upper slag phase.	45
Figure 2.16:	The influence of upper phase thickness on mean liquid speed.	45
Figure 2.17:	Radial Distribution of axial and radial velocities at 6 cm height from the bottom for Dual plug bubbling without slag.	47
Figure 2.18:	Radial Distribution of axial and radial velocities at 12 cm height from the bottom for Dual plug bubbling without slag.	48
Figure 2.19:	Radial Distribution of axial and radial velocities at 18 cm height from the bottom for Dual plug bubbling without slag.	49
Figure 2.20:	Radial Distribution of axial and radial velocities at 24 cm height from the bottom for Dual plug bubbling without slag.	50
Figure 2.21:	Radial Distribution of axial and radial velocities at 6 cm height from the bottom for Dual plug bubbling with slag.	51
Figure 2.22:	Radial Distribution of axial and radial velocities at 12 cm height from the bottom for Dual plug bubbling with slag.	52
Figure 2.23:	Radial Distribution of axial and radial velocities at 18 cm height from the bottom for Dual plug bubbling with slag.	53

Figure 2.24:	Radial Distribution of axial and radial velocities at 24 cm height from the bottom for Dual plug bubbling with slag.	54
Figure 3.1:	Schematic diagram of Experimental setup.	58
Figure 3.2:	Schematic diagram of location of bottom nozzles in model.	59
Figure 3.3:	Fractional change of concentration of benzoic acid in water as a function of time for gas injection through central nozzle.	74
Figure 3.4:	Fractional change of concentration of benzoic acid in water as a function of time for gas injection through dual nozzle.	74
Figure 3.5:	Fractional change of concentration of benzoic acid in water as a function of time for gas injection through single asymmetric nozzle.	75
Figure 3.6:	Relationship between $-\ln[(C_t - C_e) / (C_o - C_e)]$ and time for central nozzle injection.	76
Figure 3.7:	Relationship between $-\ln[(C_t - C_e) / (C_o - C_e)]$ and time for dual nozzle injection.	77
Figure 3.8:	Relationship between $-\ln[(C_t - C_e) / (C_o - C_e)]$ and time for single asymmetric nozzle injection.	77
Figure 3.9:	Plot of mass transfer parameter, K as a function of gas flow rate for central nozzle injection.	79
Figure 3.10:	A schematic diagram of top views of oil layer during gas injection of high gas flow rates according to the different arrangements of nozzles.	80
Figure 3.11:	Effect of position of a nozzle on the mass transfer parameter.	81
Figure 3.12:	Fractional change of concentration of benzoic acid in water as a function of time for different slag depths for central nozzle injection.	82
Figure 3.13:	Fractional change of concentration of benzoic acid in water as a function of time for different slag depths for dual nozzle injection.	82
Figure 3.14:	Effect of location of sampling point on mass transfer for central nozzle injection.	83
Figure 3.15:	A schematic diagram of the experimental setup for mixing time measurements.	86
Figure 3.16:	Location of tracer additions with respect to nozzle configuration.	87

Figure 3.17:	A typical tracer response curve illustrating experimentally measured variation of bath electrical conductivity at the monitoring point as a function of time.	89
Figure 3.18:	Experimentally measured mixing times as a function of gas flow rate for three different nozzle configurations without slag.	93
Figure 3.19:	Experimentally measured mixing times as a function of gas flow rate for three different nozzle configurations in presence of slag.	94
Figure 3.20:	Comparison of experimentally measured mixing times as a function of gas flow rate for central single nozzle configuration with and without slag.	95
Figure 3.21:	Comparison of experimentally measured mixing times as a function of gas flow rate for dual nozzle configuration with and without slag.	96
Figure 3.22:	Comparison of experimentally measured mixing times at 1cm, 3cm and 6cm slag depths as a function of gas flow rate for dual nozzle configuration.	97

LIST OF TABLES

	Page
Table 1.1: A summary of experimental configurations and mixing time correlations reported by various investigators[2].	12
Table 2.1: Physical Dimensions of the cylindrical vessel.	24
Table 2.2: Physical parameters used in full scale and experimental model in the present investigation.	25
Table 2.3: Physical properties of fluids used in the present investigation and their comparison with those in full scale system.	25
Table 2.4: Mean recirculation Speeds at different gas flow rates and bath depths.	44
Table 3.1: Mass transfer systems studied by various investigators.	57
Table 3.2: Change in concentration of aqueous phase with time at different gas flow rates for gas injection through central nozzle.	64
Table 3.3: Change in concentration of aqueous phase with time at different gas flow rates for gas injection through dual nozzle.	66
Table 3.4: Change in concentration of aqueous phase with time at different gas flow rates for gas injection through single asymmetric nozzle.	67
Table 3.5: Change in concentration of aqueous phase with time at different gas flow rates for gas injection through central nozzle at 1 cm slag depth.	69
Table 3.6: Change in concentration of aqueous phase with time at different gas flow rates for gas injection through central nozzle at 5 cm slag depth.	69
Table 3.7: Change in concentration of aqueous phase with time at different gas flow rates for gas injection through dual nozzle at 1 cm slag depth.	70
Table 3.8: Change in concentration of aqueous phase with time at different gas flow rates for gas injection through dual nozzle at 5 cm slag depth.	71

Table 3.9:	Change in concentration of aqueous phase with time at different gas flow rates. for gas injection through central nozzle at different sampling positions.	72
Table 3.10:	Values of Mass transfer parameter K for different gas injection configurations.	78
Table 3.11:	Experimentally observed mixing time values for varying flow rates at three different nozzle configurations without slag layer.	90
Table 3.12:	Experimentally observed mixing time values for varying flow rates at three different nozzle configurations in presence of slag layer.	91
Table 3.13:	Ratio of experimental mixing times (τ_m , with slag / τ_m , without slag) for varying flow rates at 3 cm slag depth.	92
Table 3.14:	Experimentally observed mixing time values for varying flow rates at 1cm and 6 cm slag depth for dual nozzle configuration.	92

CHAPTER I

INTRODUCTION

1.1 INTRODUCTION TO THE THESIS

Ladles, torpedo cars and the likes were originally designed for transporting molten iron from the iron blast furnace to steel making vessels, and from there to ingot pouring bays. With the popularity of the continuous casting technology, introduction of new technology such as twin drum strip caster as well as the ever increasing demand for finished steel with superior quality in terms of both cleanliness and composition, molten steel processing in ladles, following tapping from a BOF, have assumed considerable importance. Most recently, the role of ladles has enlarged to include in transit chemical and physical processing operations. Thus, one can now identify three main areas where ladle metallurgy has provided new possibilities.

1. **Chemistry:** By the removal of unwanted elements (viz., S, Si, P, O, C, H and N) from iron and steel, new grades are possible and overall product quality is improved.
2. **Control:** It allows close quality control of physical and chemical characteristics to be achieved (i.e., inclusion type, size and amount, dissolved gas content, etc.).
3. **Productivity:** The main functions of the primary processing vessels are to provide 'raw' iron or steel. They are not interrupted by any secondary refining operations carried out in transfer vessels or ladles.

In recent years there has been a growing interest in "ladle refining processes" as a means of obtaining molten steel at given temperature and composition. The present term "Ladle refining" will be broadly interpreted, to include all the processing operations in the molten state subsequent to the actual steelmaking operations, such

as argon rinsing, induction stirring, vacuum degassing, injection of powders and the like. A schematic of the various stirring techniques is illustrated in Fig. 1.1

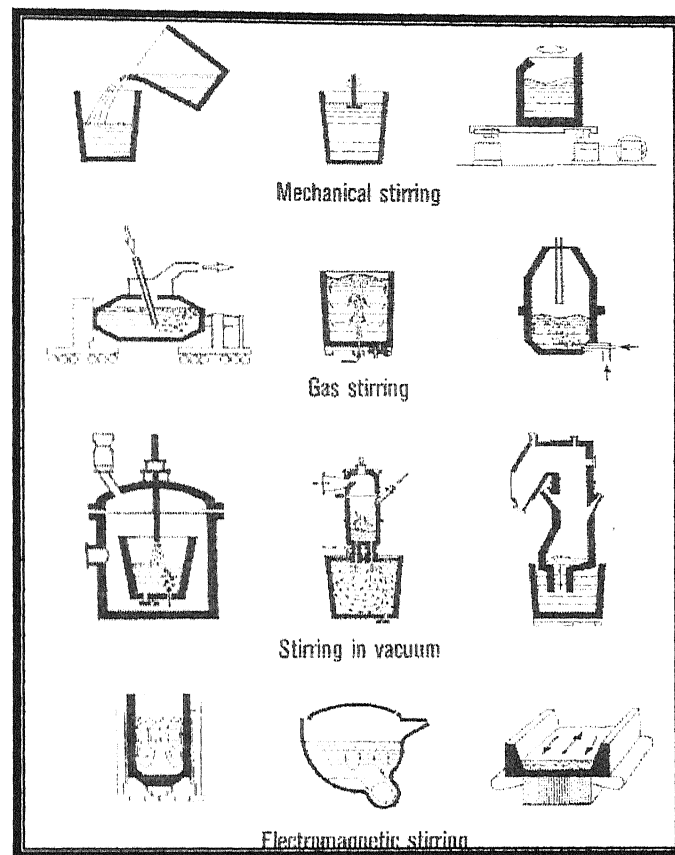


Figure 1.1: Different methods of melt stirring.

Since first envisioned and practiced by Sir Henry Bessemer almost a century and half ago for his bottom blown steel making process, submerged gas injection into melts contained in furnaces, ladles and transfer vessels, has become common in present metallurgical industries. Gas- stirring of steel in ladles is applied on a routine basis, at various stages of melt refining to achieve certain objectives. Similarly, parallel examples can be cited for the non-ferrous industries. For instance submerged gas injection plays a vital role in copper and aluminum industries. A schematic view of gas stirring is shown in Fig 1.2.

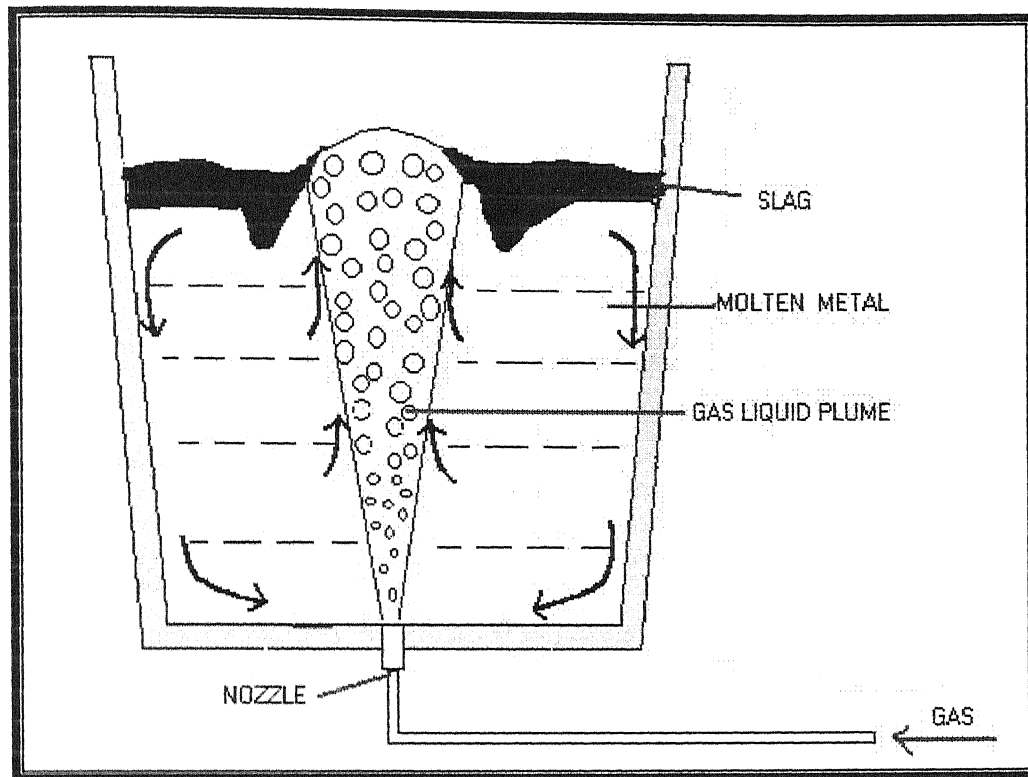


Figure 1.2 Schematic view of Gas Stirred Ladle.

The objectives of such stirring process are:

1. Alloy addition and control of final chemistry
2. Improved deoxidation
3. Improved temperature and composition homogenization
4. Inclusion floatation
5. Desulphurization
6. Inclusion shape control
7. Vacuum degassing for hydrogen and
8. Dephosphorization.

When an inert gas is injected into ladle containing molten steel from the bottom at a moderate flow rate, it comes out of the nozzle/ porous plug/ lance and rises in the form of discrete gas bubbles. These bubbles rise to the top of the bath owing to the buoyancy effect and in doing so, impart momentum to the surrounding liquid inducing good agitation/ circulation. This rising two phase mixture is termed as 'plume'. Liquid rising to

the bath surface goes down into the bath along the vessel walls, causing gross circulation of the liquid. A schematic of this type of flow is shown already in Fig. 1.2. The characteristics of the induced flow, which is invariably turbulent in nature, influences the rate of numerous processes such as dissolution/ melting, dispersion, slag metal reaction etc. and thus plays a decisive role in the overall process performance of the gas stirred ladle systems. As a disadvantage, this process exposes the liquid steel to the atmosphere, resulting nitrogen pickup and reoxidation of steel. It is therefore of interest and concern to know the level of induced agitation in such ladles and its overall bearing on various transport processes (mixing, mass transfer etc.).

The flow is responsible for the general movement of the liquid, and as a consequence, also for mixing within the melt. Details of fluid flow and mixing depend on the physical properties of the liquid, on the geometry of the vessel, on the arrangement of the nozzles, and on the flow rate of the gas introduced. Consequently, to optimize a stirring process the dependence of fluid flow and mixing on the parameters mentioned above must be known. However, direct observation and measurements in steelmaking reactors are often difficult owing to the high operating temperatures ($\sim 1600^\circ \text{C}$), massive reactor size and visual opacity of the melt. Consequently, **Physical Modelling** has been routinely applied as a reasonable alternative to gain vital understanding and useful insight of steel making processes. Physical models have helped to understand liquid metal flows and the associated mass transfer processes in converters, ladles, tundishes and molds. The primary goal is to use such physical models to derive ideas about the characteristics of the real system, inexpensively and conveniently. Ample evidence available within the literature indicates that the results derived from physical modeling investigations correspond reasonably accurately with the actual and hence can be considered as an effective tool for steelmaking process analysis and design.

1.2 LITERATURE REVIEW

Considerable efforts have been made during the last three decades or so to investigate gas injection operations in steel making ladles. On this basis of literature search, a brief review of this is presented in this section. For the sake of convenience the studies have been categorized in three sections (1) Fluid flow, (2) Mixing, (3) Mass transfer.

1.2.1 Previous work on Fluid flow in Gas Bubble Driven Systems

In order to optimize the stirring process, detailed information regarding flow patterns, fluid velocity and turbulence which depend on the physical properties of the liquid, the geometry of the vessel, arrangement of nozzles and flow rate of gas is needed. The physical characteristics of the gas-liquid (viz., air-water, mercury-nitrogen etc.) plumes of relevance to ladle processing have been investigated extensively [1-6]. Gas volume fraction, bubble frequency and bubble rise velocities within the two phase region, have been measured by numerous investigators in vessel of widely varying geometries and gas flows for a number of gas-liquid systems.

Apart, from the measurements of various parameters within the rising two phase plume region, gas induced liquid flows have also been measured and reported by various investigators. To this end, widely different flow measuring devices and techniques have been applied. These include an electromagnetic flow meter [7], a drag probe [8], Laser Doppler Velocimetry[9], combined electro-resistivity probe and Laser Doppler Velocimetry[4,5], video recording and so on. Measurements on individual phase velocities within the two phase zone, as well as in the bulk liquid, have all been reported. It has been found that the centerline liquid velocity at the plume axis, at any given gas flow rate, was practically independent of the height of the ladle [8]. The only deviations from this trend were observed near the injection nozzle and near the free surface. This is illustrated in Fig. 1.3.

The experimental observations [10, 5] appear to confirm that hydrodynamic conditions at an orifice or nozzle are not critical to plume rise velocity over a significant portion of the axial height. Under ladle refining conditions, one can therefore anticipate nearly constant bubble and liquid velocities in the major portion of the upwelling two phase region.

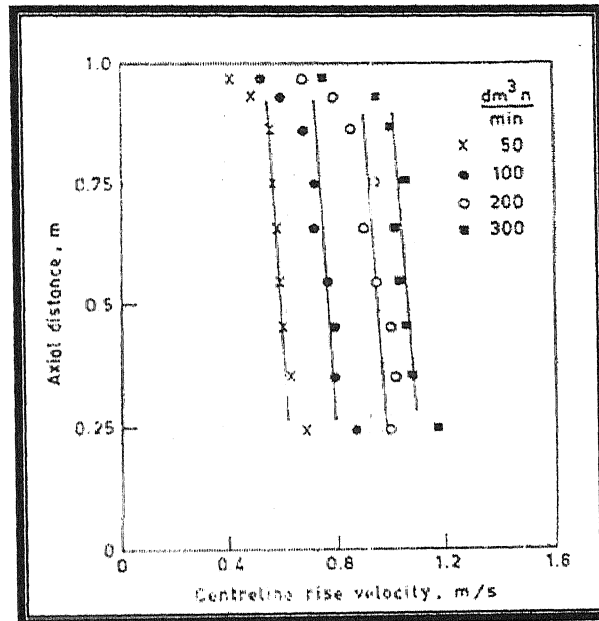


Figure 1.3: Variation of liquid rise velocity at the plume centerline as a function of gas flow rates [8].

One may further note that near the surface, the rising liquid loses a significant portion of its vertical momentum in favor of an upwelling spout and is thereby forced to flow, radially outward from the plume's axis. Fig. 1.4 shows [5] experimentally measured flow patterns in an axisymmetric gas stirred water model ladle. There, a relatively high vertical velocity at the plume axis is readily apparent. It has been established that the position and the number of nozzles influence fluid flow pattern and in turn the mixing and mass transfer as well. General fluid flow patterns and the inactive zones for different nozzles arrangements are shown in Fig 1.5[11].

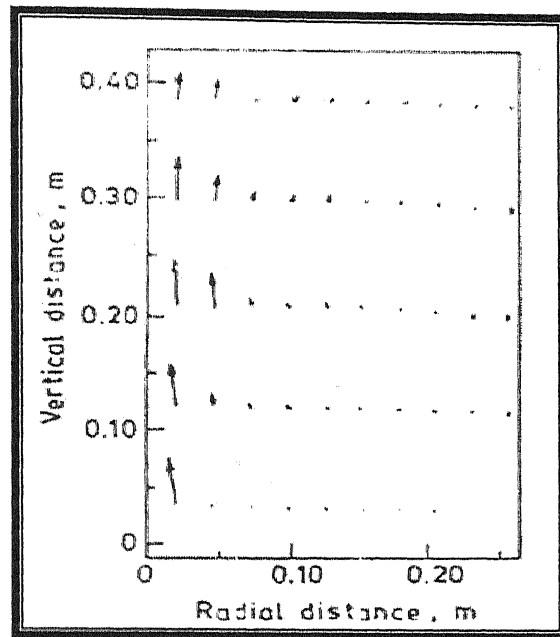


Figure 1.4: Characteristic liquid flow pattern in an axisymmetric gas stirred ladle [5].

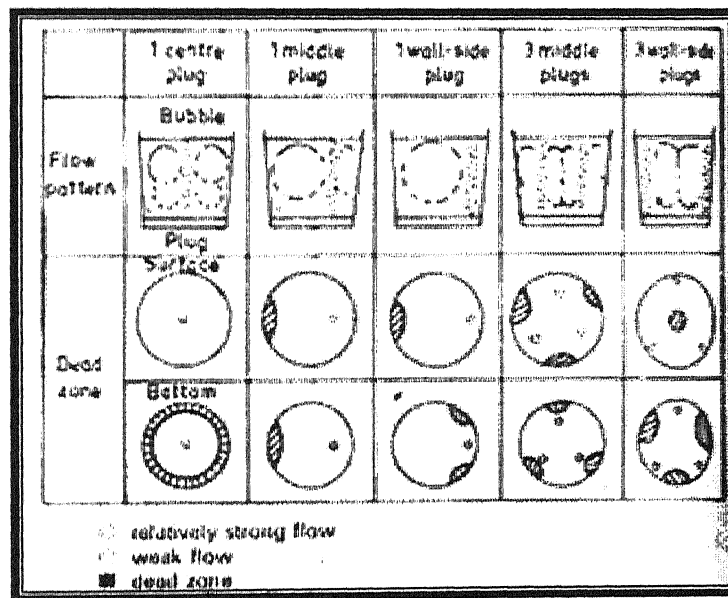


Figure 1.5: Flow patterns of the liquid in the bath generated by blowing gas through porous plug at 1.5 l min^{-1} [11].

For double plug bubbling, more gentle flow and equivalent mixing time vs single off centre bubbling were obtained, using equal net flows of gas into the ladle [12]. The mid

radius placement of a plug represents an optimum location for single-plug bubbling, while diametrically opposed, mid radius placement of bubblers is recommended for double plug bubbling[12]. In this respect, the fluid flow fields of an 80 t ladle with 2.0 m bottom diameter, 2.5 m upper diameter and 2.8 m height are shown in Fig 1.6.

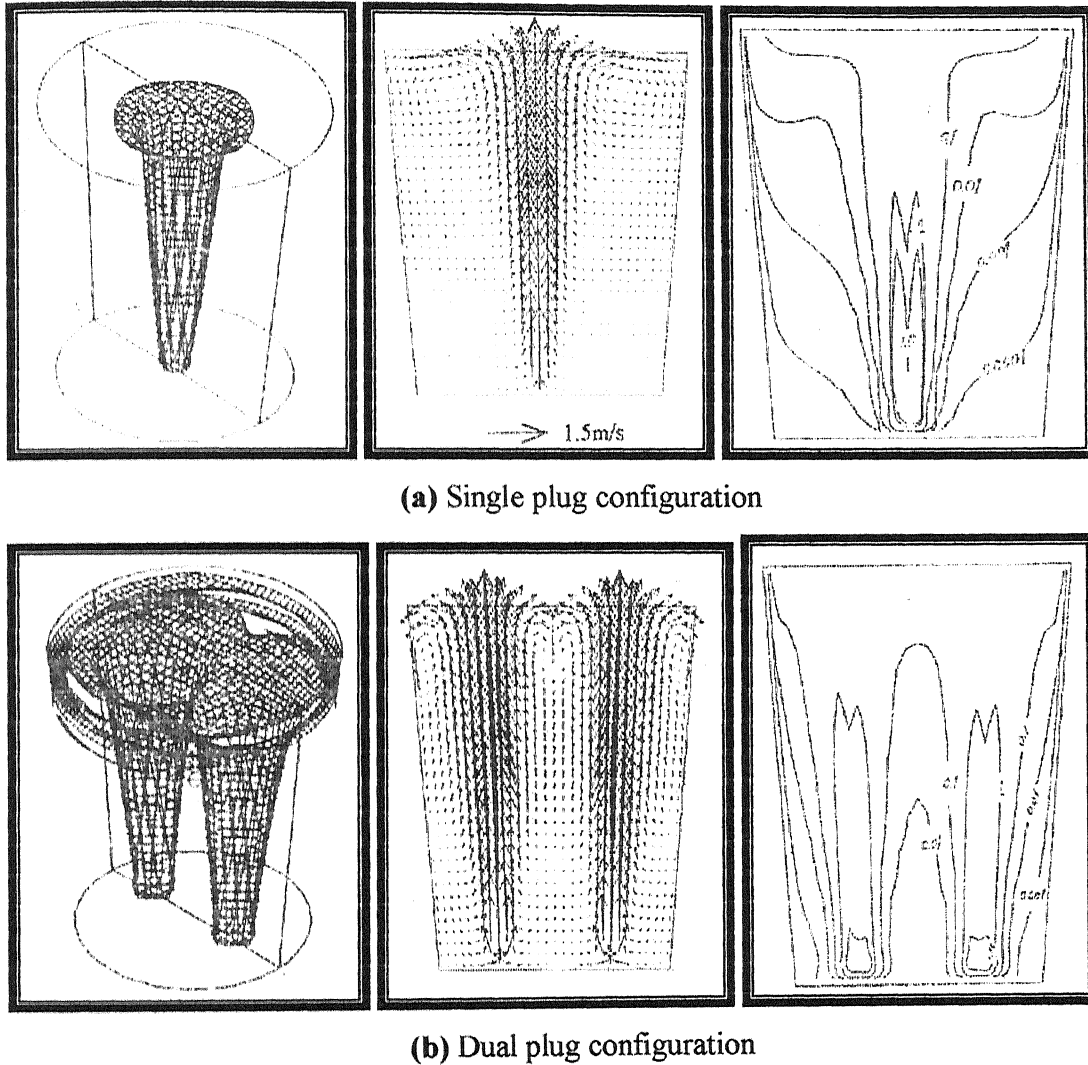


Figure 1.6: Gas plume shape, fluid flow velocity vectors and turbulent energy dissipation rate at main vertical plane of 80 t ladle for (a) single and (b) dual gas jet conditions respectively[13].

Fig 1.6 also shows the distribution of turbulence energy dissipation rate at the main vertical plane and the gas plume shape for both the case. The gas is much better dispersed for the case with two nozzles than with one nozzle [13].

In contrast to the large number of experiments carried out on air-water systems [1-7] physical model studies on hydrodynamics of equivalent gas-metal-slag systems have been rare. Some investigations [14] on slag metal interactions under relatively high gas flow rates (e.g., corresponding to BOF steelmaking) suggested that gas bubbling can lead to generation of droplets torn from around the rim of the plume.

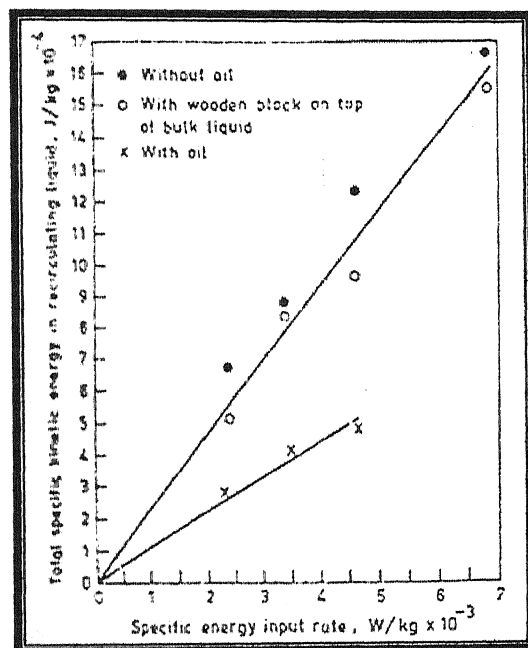


Figure 1.7: Plot of total kinetic energy contained in the recirculation aqueous phase vs specific potential energy input rate under various upper slag phase conditions (viz., rigid, fluid and no-slag [15])

It was observed experimentally [15] that at any gas flow rate, the kinetic energy of mean and fluctuating motions (i.e., the total kinetic energy of motion in system) are considerably reduced in presence of the top buoyant phase. The deformation of the upper buoyant phase together with its entrainment in the bulk phase liquid was found to be responsible for the observed rates of energy dissipation and slowing of the lower phase liquid. This is illustrated in Fig 1.7, in which the variation in total kinetic energy contained in the recirculation aqueous phase is plotted against the specific energy input rate, for various upper slag phase conditions (viz., rigid, fluid and no-slag condition are

shown). The visual observations of liquid flow patterns in such systems appear to indicate that in the immediate vicinity of the two phase interface (water and oil as well as mercury and paraffin), the flow is considerably different to an equivalent no oil/paraffin situation. Careful examination of the region close to interface suggested that the subsurface velocities adjacent to free surface are perfectly horizontal, whereas they become deflected downwards by about 30° with upper layer as shown in Fig. 1.8 [16]. However, it is still not known how and to what degree, the presence of such an upper phase (slag phase) affects the various flow variables such as bulk velocity, turbulence etc in an actual industrial steel refining ladle. Since the mixing characteristics of gas stirred ladles depend on both convection and eddy diffusion effects [17], these latter parameters must evidently affect the dynamics and efficiencies of metal processing operations in ladles.

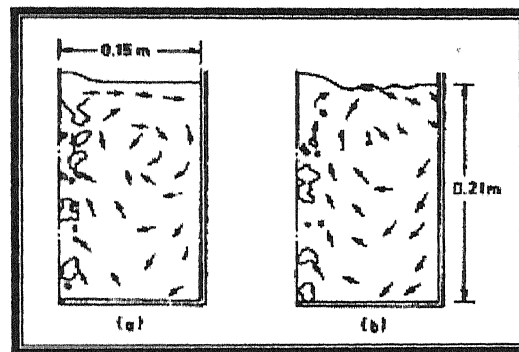


Figure 1.8: Observed velocity field in the vessel [16].

(a) Without oil (b) With oil

1.2.2 Previous work on Mixing in Gas Bubble Driven Systems

Mixing of liquids in metals and materials processing operations has been a subject of discussion and research for many years. Mixing not only reduces the non-uniformities or gradients in concentration and temperature of a liquid bath, but also enhances chemical reactions by bringing reactants together and removing products from reaction sites. The phenomenon of mixing is a result of combination of transport processes, namely, molecular diffusion, convective flow and eddy diffusion. Molecular diffusion, which is a result of intermolecular activity, is basically driven by concentration gradient between

various space points. On the other hand, eddy diffusion is promoted by the collision of different sized eddies while they are being transported by bulk flow.

Since molecular diffusion is an extremely slow process, mixing in liquid baths is generally carried out through forced convection and/or eddy diffusion by agitating the bath (typically termed as macro mixing) Although it is easier and more economical to stir room temperature liquid baths using mechanical agitation, mixing in many high temperature metallurgical processes is promoted primarily by gas injection. Examples of such processes include (i) converter steelmaking, (ii) homogenization of steel with respect to temperature and composition in ladles, (iii) Conversion of copper matte to metal in converters etc. In converter steel making, bottom gas injection provides improved stirring of the metal bath and enhances the effectiveness of top blown oxygen in combined steel making.

Considerable amount of theoretical and experimental work has been carried out to date and reported in the literature on macro-mixing phenomena in ladles [18, 19]. The present brief review outlines mainly the influences of various operating parameters on mixing time.

1.2.2.1 Effect of Gas Flow Rate on Mixing Time

It has been established that the mixing time decreases with increasing flow rate [17,20,21,22,23,24,25,26,27,28]. But at high gas flow rate the effect is not pronounced. Mixing times were measured via different experimental techniques and to this end, various criteria were applied. As a consequence, a variety of functional relationships between mixing times, specific energy input rate and operating variables (e.g., L, R and Q) have been proposed. To illustrate these, experimental conditions, together with the various proposed mixing time correlations reported in the literature, have been summarized [19] and presented in Table 1.1. It is evident from the table that whiles some of the expressions results in similar estimates but still there are discrepancies. As an example of this, in Figs. 1.9 (a) through 1(c), functional relationships between experimentally

Investigators	Exp. Technique	Mixing Criteria	Vessel Dimension and mass of fluid	Specific gas flow rates(m ³ /min/T)	Mixing time correlation
Nakanishi et al. [25]	pH	Undefined	L=0.465m, D=0.42m;64 kg	0.015 to 0.06	$\tau_m = 800 \epsilon_m^{-0.4}$
Asai at al. [28]	Electrical conductivity	99%	L=0.405,0.2 & 0.10 m, L/D=0.5 to 1;52 kg to 0.4 kg	0.019 to 0.90	$\tau_m = 274 \epsilon_m^{-0.4} L^{-1} R^{1.36}$
Sinha and McNallan[26]	pH	97.7%	L=0.48m, D=0.45m;76 kg	0.02 to 0.4	$\tau_m = 692 \epsilon_m^{-0.89}$
Stapurewicz and Themelis[27]	Photocell	95%	L=0.67 to 1.0m, D=0.66m;310 kg (max)	0.13 to 0.96	$\tau_m = 164 \epsilon_m^{-0.39} L^{0.39}$
Mietz and Oeters[23]	Electrical conductivity & colorometry	955	L=1.0m, D=0.63m;311 kg	0.038 to 0.29	$\tau_m = C_1 Q_g^{-n}$ C ₁ and n are functions of tracer addition and monitoring locations.
Mazumdar and Guthrie[17]	Electrical conductivity	95% Bulk	L=0.5 to 1.1m, D=1.12m;1000 kg	0.012 to 0.06	$\tau_m = 37 \epsilon_m^{-0.33} L^{-1} R^{1.66}$
Krishnamurty et al. [22]	Electrical conductivity	99.9%	L=0.1 to 0.45m, D=0.48m;81 kg (max)	0.11 to 2.67	$\tau_m = C_1 Q_g^{-n}$ C ₁ and n are functions of flow regime and liquid depth.

Table 1.1: A summary of experimental configurations and mixing time correlations reported by various investigators [2].

measured mixing times and energy input rates (or gas flow rates) reported by the different groups of investigators [28, 22, 17] are illustrated.

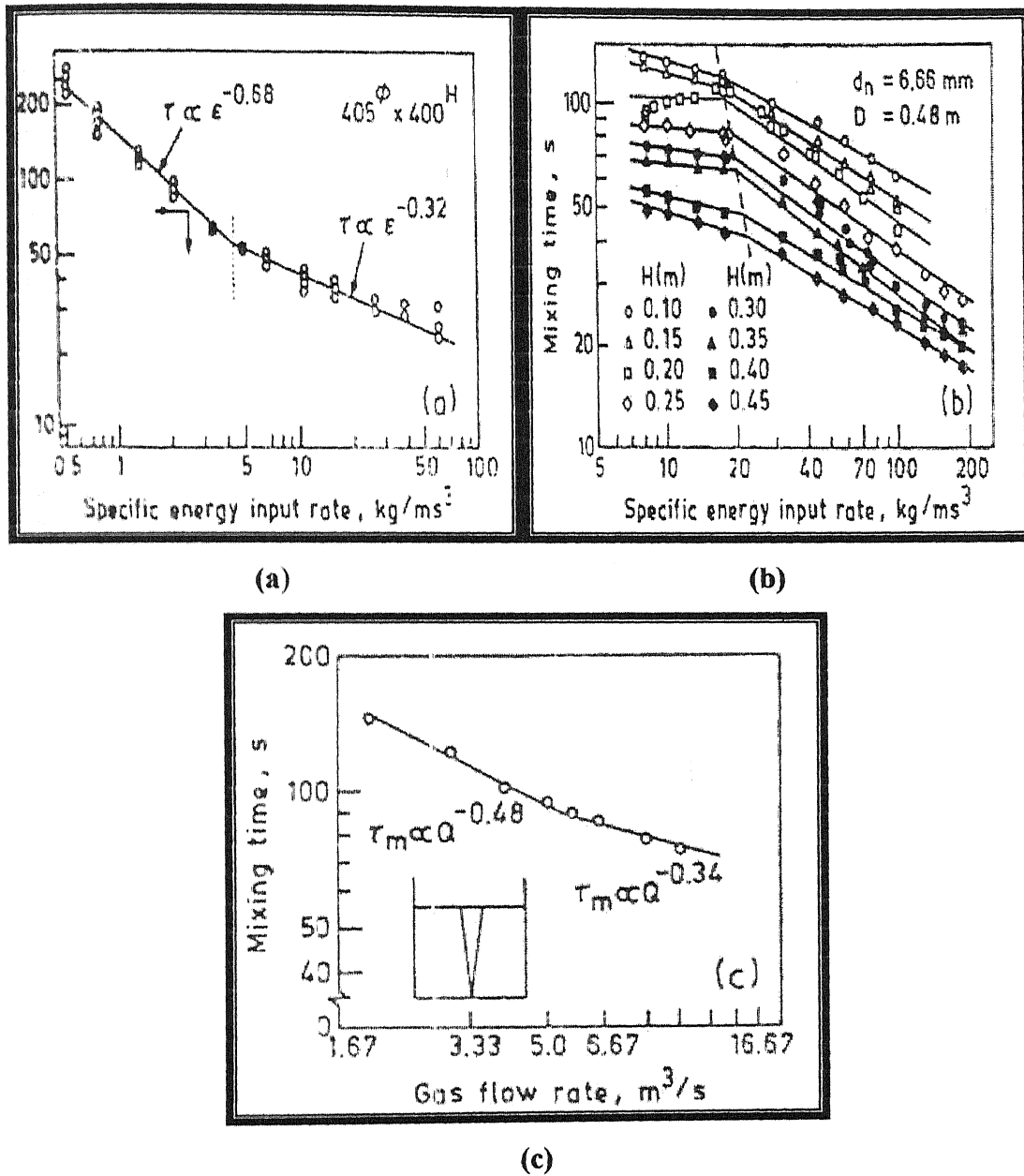


Figure 1.9: Functional relation between mixing time and specific energy input rate/gas flow rates reproduced from the work of previous investigators. (a) Asai et al.[28] (b) Krishnamurthy et al.[22] and (c) Mazumdar and Guthrie.[17].

As a possible reason for shift in the functional relationship between ϵ_m and τ_m many arguments have been proposed by the investigators, although such arguments have not

been often adequately supported with direct experimental evidence, It appears that different hydrodynamic phenomena are at play under different operating regimes.

1.2.2.1 Effect of Nozzle Position and Number of Nozzles

It has been established that the position and number of nozzles influence mixing as well as mass transfer rates. It has been established that an asymmetric nozzle arrangement resulted in superior transport close to the bottom of the vessel compared with symmetrically placed nozzles [7]. For certain nozzle numbers and arrangements, there can be multiple circulation loops in the bath. Such circulation patterns, e.g. that observed in a bubble column, through increasing mass transfer rates, affect mixing rates adversely [22]. It has been found that the mixing rates increased (or mixing times decreased) as the position of the nozzle moved from centre towards the vessel walls [29].

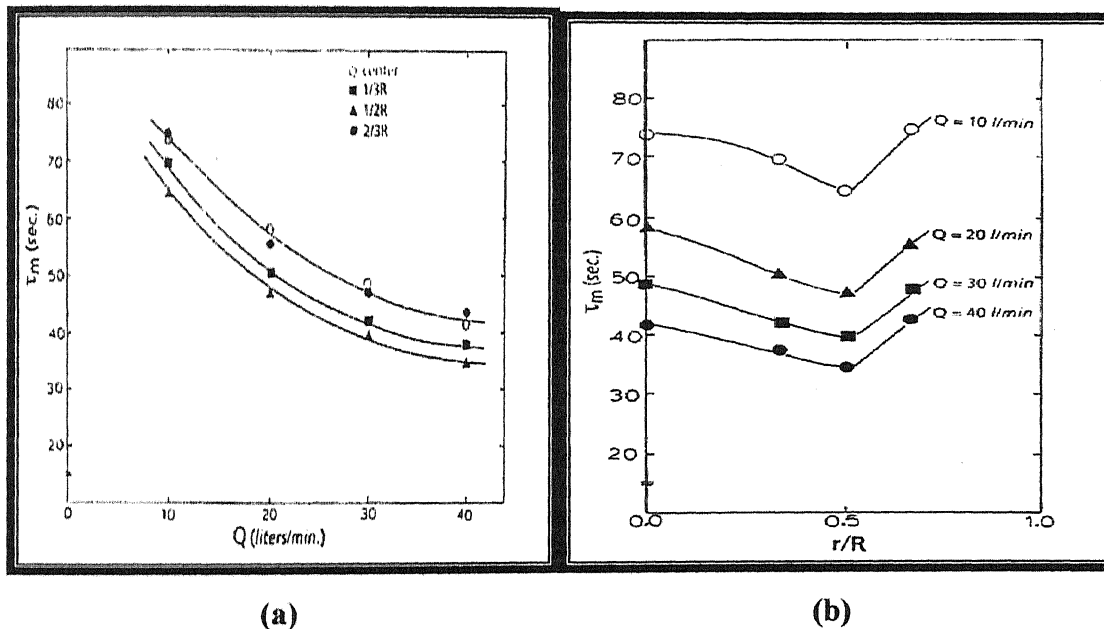


Figure 1.10: (a) Variation in 95% mixing times with gas flow rate for plug placed at center, one-third, half and two-third radius of ladle base. **(b)** A plot of mixing time vs. radial position for a single plug for various flow rates.

A mid radius placement of a porous plug represents an optimum location for single-plug bubbling, while diametrically opposed, mid radius placement of bubblers is

recommended for double plug bubbling [30]. Figure 1.10 (a) shows that mixing time decreases according to $\sim 1/3$ power to gas flow rate for various bubbler locations. On the other hand, Figure 1.10 (b) shows mixing time for the radial position for a single nozzle for different gas flow rate. It can be concluded from the above that as one moves away from the center toward half radius position for the plug, mixing time decreases, giving minimum mixing time at half radius position of the plug and then again increases as one moves toward the wall of the vessel [30].

1.2.2.2 Effect of Second Phase on Mixing Time

Often the agitated metallurgical baths are covered with slag. Therefore, it is desirable to know the effect of the second phase on hydrodynamics and mixing. It is found that mixing time increases in the presence of second phase [29, 31,32]. Mixing times measured with a simulated slag tended to be considerably different to those for equivalent “no slag” situations [29]. Figure 1.11 shows a plot of mixing time in terms of stirring energy density. Similarly, Figure 1.12 shows a plot of mixing time as a function of gas flow rate for center, an off center, and a side nozzle with an overlaying oil layer. It is seen that, in presence of an oil layer, mixing times is significantly longer regardless of injection pattern. Such observations can be readily rationalized, since the hydrodynamic state of the vessel, at any gas flow rate, is known to be different in presence of an overlying second phase [29] liquid. The upper slag phase dissipates a part of the input energy rate and therefore, mixing times in the ladle, in the presence of the overlying second phase liquid will be somewhat longer than those to be expected under an equivalent no slag situation.

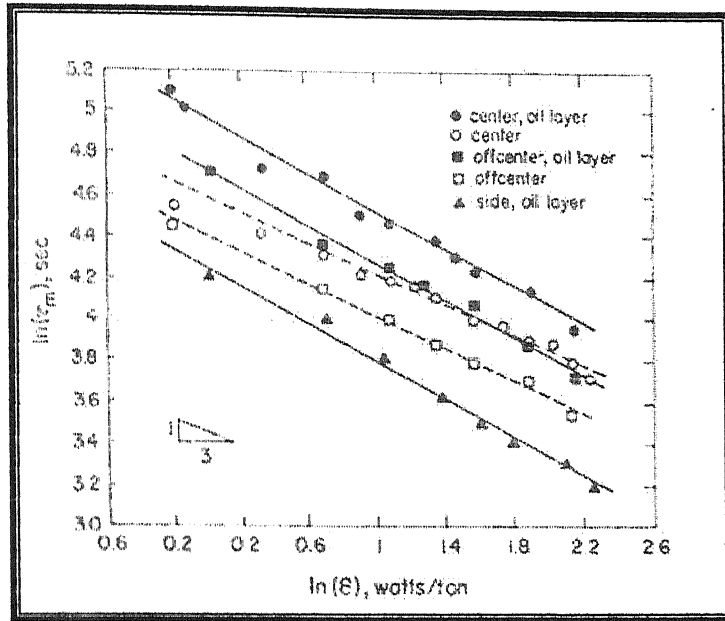


Figure 1.11: Mixing time vs. stirring energy density for three different nozzle patterns with and without oil layer.

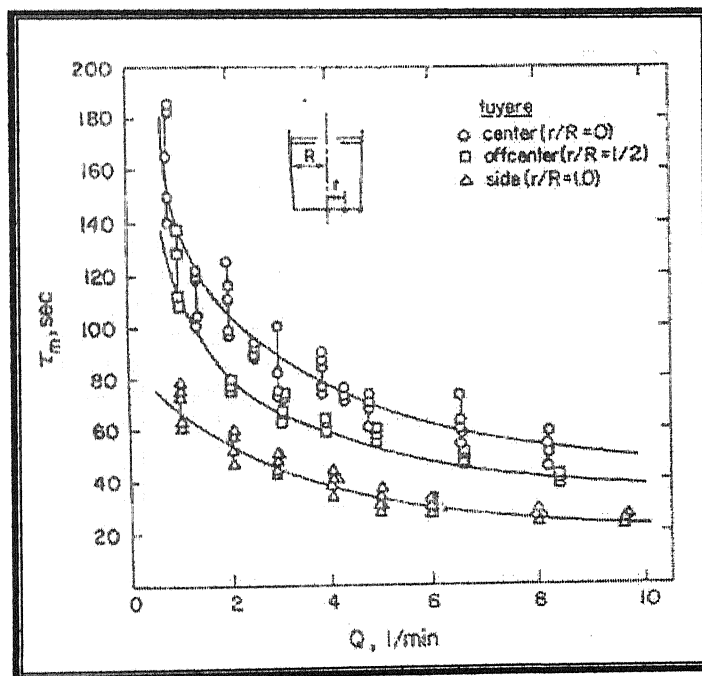


Figure 1.12: A plot of mixing time as a function gas flow rate for three different arrangement of nozzle with an oil layer present.

1.2.3 Previous work on Mass Transfer in Gas Bubble Driven Systems

One of the main tasks of ladle metallurgy treatment is desulphurisation of liquid steel produced in a converter or electric arc furnace. For this purpose, a high-basic slag with low iron oxide content is charged on top of the melt. Acceleration of metal-slag reactions is achieved by stirring the bath with inert gas injected through a lance or bottom nozzle. To achieve ultra low sulphur contents, additional injection of desulphurizing powder is necessary.

From economic considerations and process optimizations, in addition to the final sulphur content the rate of desulphurisation is important. This latter parameter is determined by rate of sulphur transfer from the metal to the slag phase/desulphurisation compounds. To develop more insight into such interfacial transfer processes, fundamental studies are being routinely conducted in room temperature models. In investigations carried out over a wide range of gas flow rates, sometimes strong increases of the rate constant were detected if the gas flow rate exceeds a critical value. Explanations were found from observations of emulsification phenomena in model systems where considerable amounts of emulsified slag droplets only occurred beyond a certain gas flow rate [29, 33].

In the case of a gas stirred system it is difficult to measure interface area. So volumetric mass transfer ($\beta_m A$) and K is generally reported to know the extent of mass transfer. In gas-stirred systems, broadly speaking, the $\beta_m A$ parameter, for any given vessel dimension has been found to be proportional to Q^n . Value of n has been found to be different in different ranges of gas flow rate [29] as shown in Figure 1.13. Inert gas was injected from bottom axisymmetrically. Oil simulated the slag phase, and water simulated the metal phase.

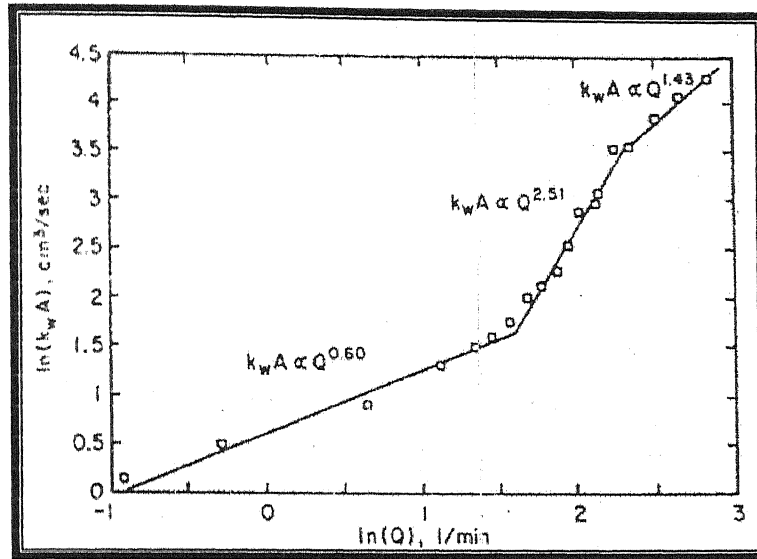


Figure 1.13: Relationship between $\beta_m A$ and flow rate in terms of the order of dependence, n , for central tuyere injection. (β_m is written as k_w in the plot)

Figure 1.13 shows three regimes in $\ln(\beta_m A)$ vs. Q curve, with different values of n . Some model experiments using KCl and Benzoic acid as solute [34], reveals that $k_{m,I} \propto D_i^{-1/2}$ approximately. Figure 1.14 shows $k_{m,I} \propto D_i^{-1/2}$ as a function of $\epsilon_m * V^{-2/3}$, where V is bath volume.

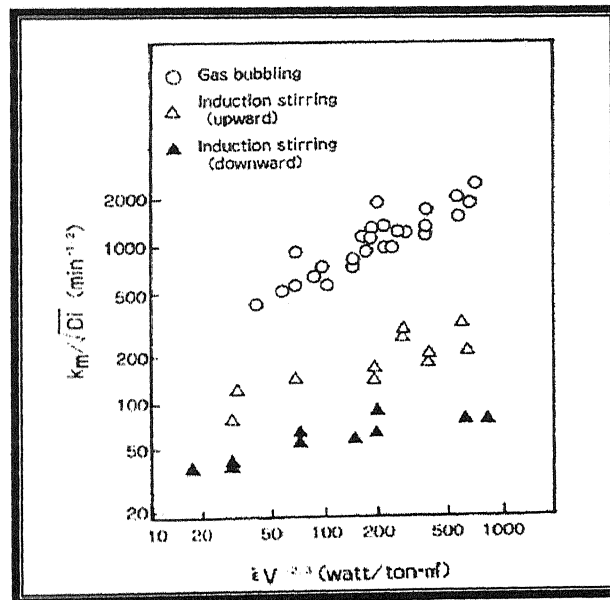


Figure 1.14: Relation between $k_m / D_i^{1/2}$ and $\epsilon_m * V^{-2/3}$ (water model).

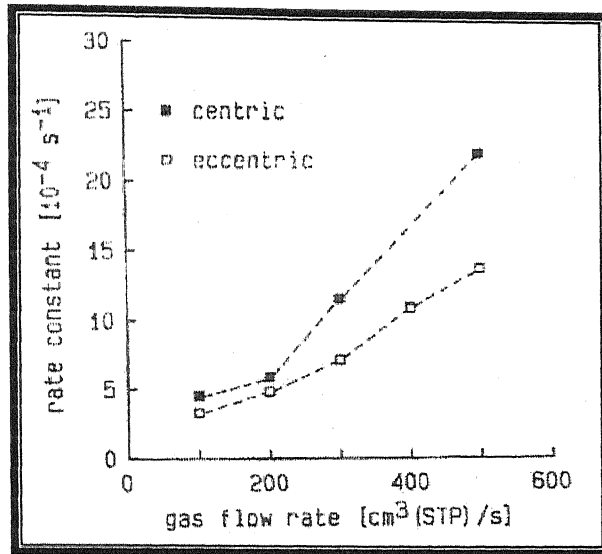


Figure 1.15: Rate constant of mass transfer versus gas flow rate for centric and eccentric gas injection.

Fig 1.15 shows the effect of gas flow rate on rate constant for centric and eccentric gas injection [35]. Mass transfer of tracer from water to slag phase increases with increasing gas flow rate for centric as well as eccentric nozzle. But comparing concentration changes for both nozzle arrangements, considerable faster mass exchange can be noticed when using centric gas injection.

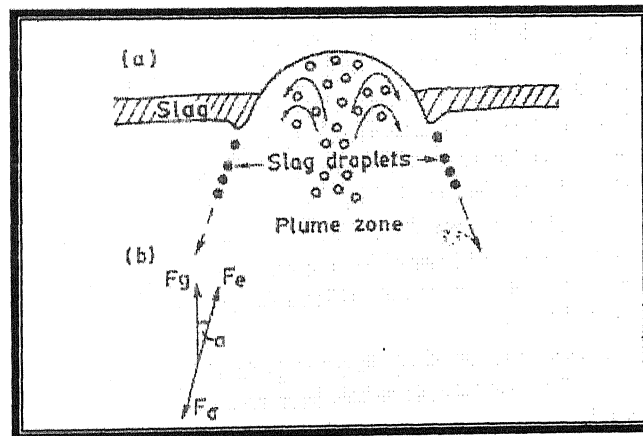


Figure 1.16: Principles of slag emulsification in steel ladles. (a) scheme of detaching process, and (b) equilibrium between inertia force F_e , buoyancy force $F_g \cos \alpha$, and surface force F_σ at the point of droplet detachment.

Formation of oil-in-water and slag-in-metal *emulsion* increases the liquid – liquid interfacial area by even a factor of about 100. Consequent large enhancement in $\beta_m A$ parameter has been well established. The mechanism of drop formation is shown schematically [35] in Figure 1.16. When the inertia force due to liquid circulation exceeds surface tension and buoyancy force at slag layer on plume edge, slag droplets form. The volumetric mass transfer coefficient (K'_B) is dependence on the bottom gas flow rate varies at the transition gas flow rate, Q_B^* [36]. In the low Q_B range, K'_B is a strong function of Q_B and increases slightly with Q_B beyond Q_B^* . it was also found that K'_B increases slightly with the increase with increase in N from 2 to 4 and then decreases with further increase in N , also K'_B decreases with increasing r/R . Bottom injection was found to yield higher mass transfer rate that top injection [37] Fig 1.17 (a). The results also show that the rate constant for the process of mass transfer increases abruptly within a very narrow region of gas injection rate as shown in Fig. 1.17 (b) Increase in oil volume fraction was also found to increase the mass transfer rate.

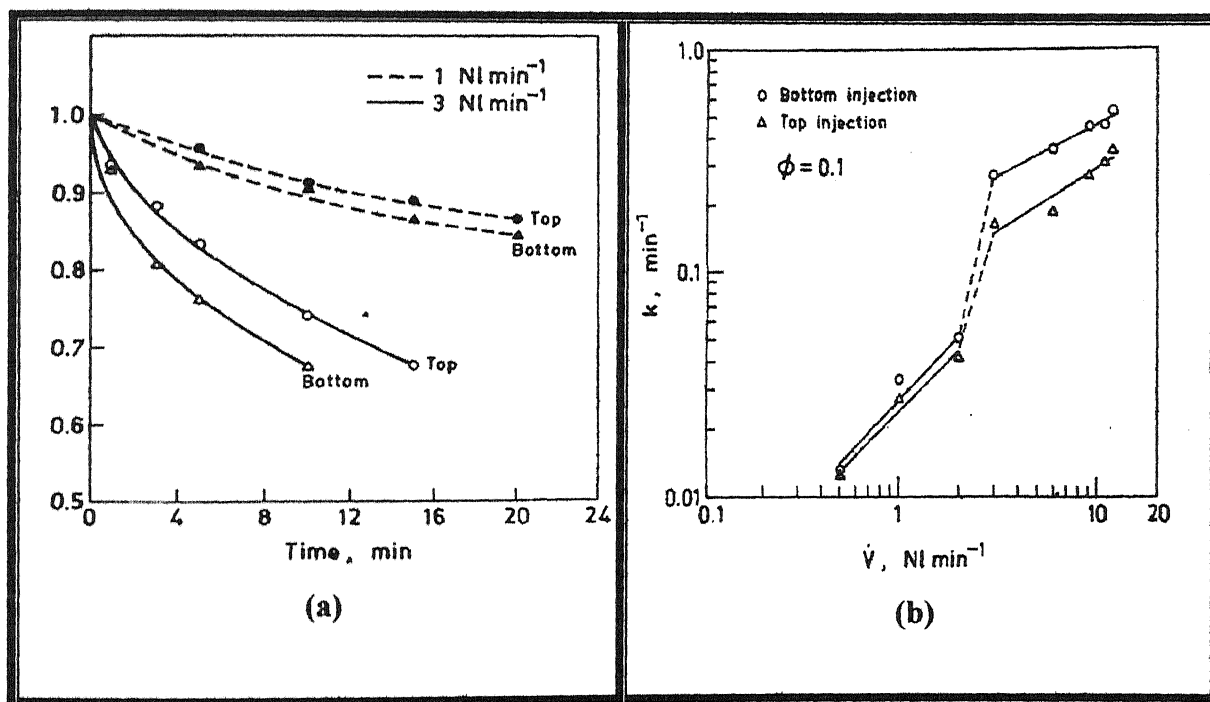


Figure 1.17: (a) Influence of location of gas injection (top and bottom) on C_t/C_o vs. time for constant gas injection rates. (b) Variation of rate constant K with gas injection rate \dot{V}

Flow visualization studies reported so far [29,35,15,] on bubble stirred oil-water systems indicate that the oil-water interface (slag-metal interface) can undergo considerable disturbances and therefore, produce a host of complex physical phenomena, such as extensive deformation of the interface, formation of oil ligaments, droplet generation and entrainment, *etc.* Thus at relatively low gas flow rates, the interface remains relatively unperturbed but with increasing flow rates, oil ligaments and droplets tend to form at the water-oil interface leading to a significant increase in the oil – water interfacial area. At still higher specific flow rates, the entire oil layer breaks down into numerous droplets leading to the formation of an oil-water emulsion. Experimentally measured [38] volumetric mass transfer coefficient ($= K_w A$) as a function of gas flow rates are illustrated in Fig 1.18. There, corresponding to these three operating regimes, different function relationships are seen to govern interphase mass exchange rates. Experiments have indicated that an off-centered nozzle position hinders mass transfer rates as compared to central nozzle position. This trend as one would note here, is contrary to observations made on mixing times, which are found to be accelerated by an eccentric nozzle position in the bath [35,12].

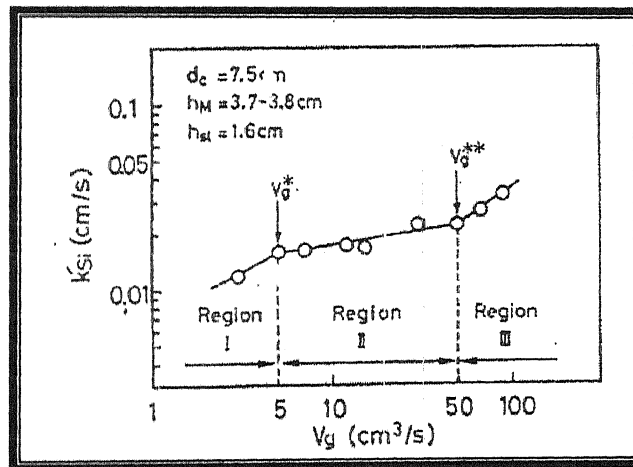


Figure 1.18: Variation in mass transfer coefficient as a function of gas flow rates in high temperature gas-slag-metal system.

1.3 SCOPE OF THE WORK

From the literature review presented above part, it is clear that fluid flow, mixing and mass transfer studies have been of concern to researchers and numerous studies have been reported in the literature on this subject. In these symmetrically and asymmetrically placed lances/tuyeres/ porous plugs have been used as a gas injection devices and studies have been reported on both gas-liquid, as well as gas-liquid-slag, systems for wide range of vessel geometries and gas flow rates. Despite many cold model studies taken up over the years, there remains considerable scope in broadening the applicability of the models and their performances.

From the literature it is clear that under practical refining conditions, significant energy can be dissipated by an upper slag, and that fluid flow will be a function of slag thickness, density, aspect ratio of the vessel etc. Further experimental work is needed to adequately quantify such phenomena.

The experimental studies for mixing time calculations considered in the literature essentially carried out in water models in which the effect of an upper buoyant phase on mixing phenomenon was neither properly simulated nor investigated. Questions still exists concerning optimum stirring conditions for faster mixing (e.g., Location of plugs, no of plugs, gas flow rates and other variables.)

Similarly despite of many cold model studies on mass transfer there still remains scope to study the influence of different combination of nozzles on the mass transfer between slag and metal phase for varying gas flow rates. In addition to such there are several less investigated areas such as the effect of slag volume on the kinetics of mass transfer, that require fresh attention.

It is to these all aspects that the present thesis has been primarily concerned with.

1.4 PLAN OF THE WORK

The main body of the thesis consists of six chapters. **Chapter 1** presents a brief summary of the previous work carried out by various researchers to investigate gas injection operations in steel making ladles, In **Chapter 2**, Fluid flow measurements are dealt in detail, which included the various techniques of measurement, velocity measurement for single and dual plug bubbling, with and without slag. **Chapter 3** covers the mass transfer and mixing studies (with and without slag) carried out for various nozzle configurations and varying flow rates and their analysis. **Chapter 4** summarizes the general conclusions derived from the present work and the thesis ends with the recommendations for future work in **Chapter 5**.

CHAPTER II

FLOW MEASUREMENTS

2.1 INTRODUCTION

The efficiency of the processing operations carried out in steel making reactors are intrinsically related to the fluid flow phenomena. The exchange of mass, momentum and heat between the gas and the liquid depend to a large extent on the motion in the liquid. Therefore a detailed knowledge of fluid flow is required for better understanding of the physics involved and for process design and optimization. The present chapter is aimed at developing some understanding of the flow in a twin plug stirred system in the presence of an upper buoyant phase through physical model studies.

2.2 THE PHYSICAL MODEL AND OPERATING PARAMETERS

In order to describe the fluid flow and physical nature of slag metal interactions during the submerged gas injection in ladles, a small Perspex vessel filled with water has been employed in the present investigation. A 3 cm thick layer of mustard oil was poured on the top of water so as to simulate the slag layer of an industrial system. The vessel was provided with a central nozzle/tuyere ($d = 0.005\text{m}$) at its base, through which air was injected.

Parameters	Model Vessel
Diameter, m	0.30
Maximum height, m	0.45
Nozzle Diameter, m	0.005

Table 2.1: Physical Dimensions of the cylindrical vessel.

The physical parameters used in the full scale and the present system are listed in Table 2.2 While the physical properties of the molten steel and water model systems are shown in Table 2.3

Physical Parameters	Full Scale 150t ladle	Model 0.08 cylindrical tank of Perspex sheet.
Height,(m, as filled)	3.75	0.3
Diameter, (m)	3.75	0.3
Liquid	Steel/slag	Water/oil

Table 2.2 Physical parameters used in full scale and experimental model in the present investigation.

Fluid	Physical property	Molten steel system at 1600°C	Water model at room Temperature
Overlying second phase	Density, kg/m ³	2700	910
	Viscosity, kg/(m-s)	0.3	0.1
Bulk liquid phase	Density, kg/m ³	7000	1000
	Viscosity, kg/(m-s)	6.7×10^{-3}	1.1×10^{-3}

Table 2.3 Physical properties of fluids used in the present investigation and their comparison with those in full scale system.

For the present investigation the geometrical scaling factor was taken 0.08 with respect to a full scale ladle of 150 T and the flow rates were kept such that it correspond to the range of gas flow rates practiced in ladle refining operations. Referring to Table 2.3, it is seen that kinematic viscosities of molten steel and slag are practically equivalent to those of water and mustard oil. However the interfacial tension of the high temperature slag-metal system is considerably greater than that for the oil-water system and it is therefore not possible to considered similarity between surface tension forces between the model and the full scale systems.

2.3 TECHNIQUES OF VELOCITY MEASUREMENT AND THEIR COMPARISON

Various types of velocimeters are available for fluid velocity measurements at room temperature such as Pitot tube, hot wire/film Anemometers, Reaction probe, Karman Vortex Probe, Magnet Probe, LDV, PIV, Melting Probe etc. But these velocimeters are not applicable to measure velocities of molten metal that are typically at temperature of over 1000° C. The measurement of liquid flows in the water model was done using simple video recording method developed in the lab (see later ; viz., sec. 2.3.3). However it is a crude method and therefore results derived from such measurements are liable to some errors. Therefore, to cross check the results from Video recording, more sophisticated flow measurement device PIV (Particle imaging Velocimetry) was applied. reported velocity data obtained via LDV (laser Doppler Velocimetry) for a similar system was also applied. The LDV and PIV systems utilized in fluid flow measurement in present investigation are described briefly in the subsequent paragraphs.

2.3.1 Laser Doppler Velocimetry

Laser Doppler velocimetry is a well-proven technique that measures fluid velocity accurately and non-invasively. Laser Doppler Velocimetry allows a non-invasive measurement of flow velocity by means of the well-known Doppler Effect.

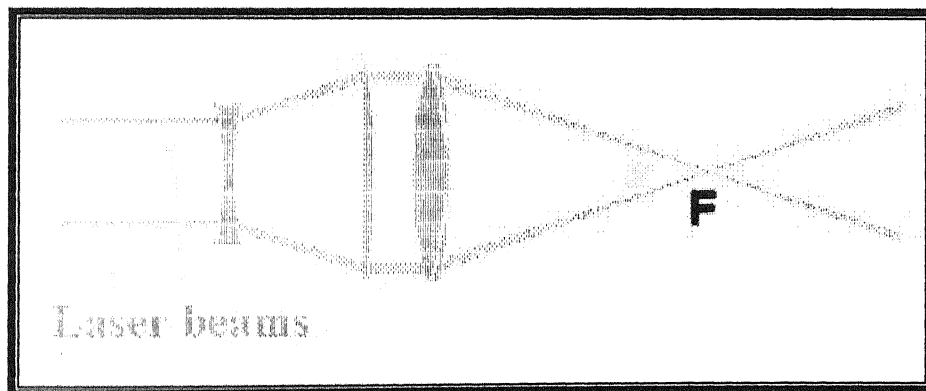


Figure 2.1: Principle diagram of Laser Doppler Velocimetry.

Laser light illuminates the flow, and light scattered from particles in the flow is collected and processed. In practice, a single laser beam is split into two equal-intensity beams which are focused at a common point (F) in the flow field. An interference pattern is formed at the point where the beams intersect, defining the measuring volume. Particles moving through the measuring volume scatter light of varying intensity, some of which is collected by a photo-detector. The resulting frequency of the photodetector output is related directly to particle velocity. If additional laser beam pairs with different wavelengths (colors) are directed at the same measuring volume two, and even three, velocity components can be determined simultaneously. Typically, the blue and green or blue, green, and violet lines of an argon-ion laser are used for multi-component measurements. If one of the beams in each beam pair is frequency shifted, the LDV system can also measure flow reversals.

2.3.2 Particle Imaging Velocimetry

Particle imaging Velocimetry is a optical technique used to measure velocities in fluid flow fields by capturing images of illuminated particles within the flow field. The particle velocity is calculated from the distance the particle moves between two pulses of a light source. The micron sized particles are seeded into the intake flow of the cylinder.

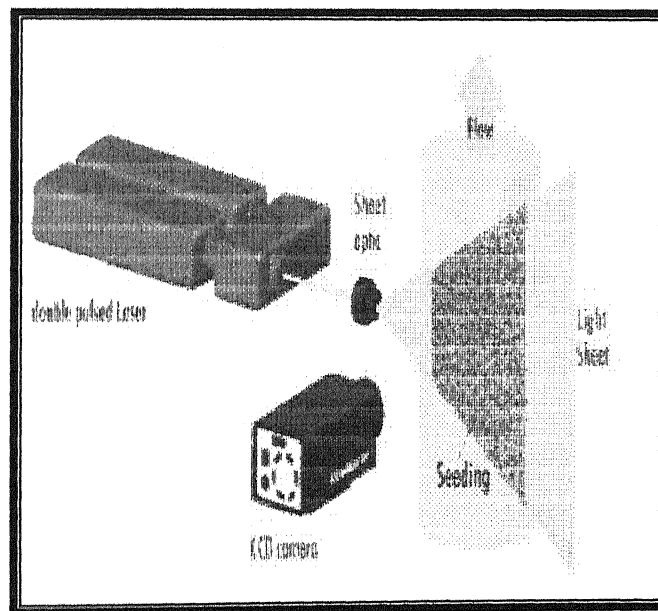


Figure 2.2: Basic setup of Particle Imaging Velocimetry.

The cylinder is optically accessed for the light source and digital capture camera. The diagram below shows the basic setup of a PIV system. The working fluid in the vessel has to be seeded first with spherical tracer particles which don't influence the flow. Then a pulsed laser light sheet is generated on the plane in which flow is to be determined. Pictures from the planar flow field are taken with a CCD camera at the right angle to the illuminated plane, one at time t and the second at time $t + dt$. The pictures are digitized, in order to compare them. The first shows the initial position of the tracer particles and the second pair, their position after the movement. The frames are subdivided in smaller windows called interrogation regions. For each window a displacement vector of a group of particles is calculated by cross correlation method. It is repeated for each interrogation area. Finally it is converted into a velocity vector field. There exist a few post processing methods in order to get the optimal vector field. From these the vorticity field and the streamlines can be calculated. PIV measures whole velocity fields by taking two images shortly after each other and calculating the distance individual particles traveled within this time. From the known time difference and the measured displacement, the velocity is calculated.

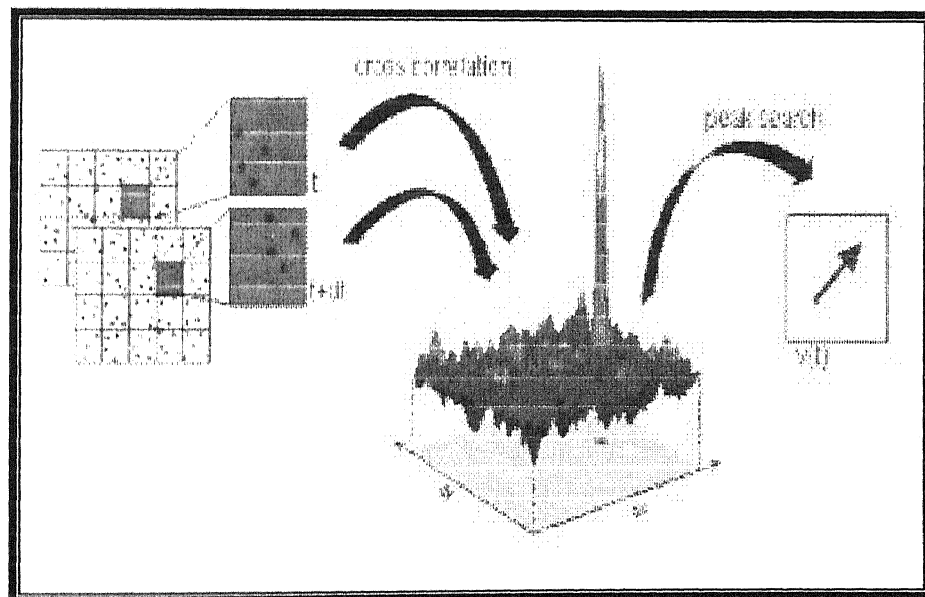


Figure 2.3: Cross-correlation and localization of the correlation peak.

Since the flow can be quite fast one has to avoid blurred images and that's one reason to use laser pulses. They are only 6-10 ns long and freeze any motion. The other reason is that only laser light can be focused into a thin enough light sheet so that only particles in that plane are imaged. Otherwise the scattered light from particles in other planes would make this measurement impossible. A special camera is utilized so that it can store the first image (frame) fast enough to be ready for the second exposure. The 'dead' time between the frames when the camera is 'blind' is only 1000 μ s. For the present investigation, experiments were conducted on model setup (as described earlier) at RDCIS, SAIL, Ranchi. Mustard oil was used to simulate slag for those experiments in which an upper buoyant fluid was used. System setup, laser sequencing, image capture, data analysis and display was accomplished using a comprehensive software package 'INSIGHT' operating on Windows-NT platform for PC. INSIGHT together with the powerful graphic software Tec-Plot provides the necessary information on the flow in an elegant fashion.

2.3.3 Video Recording

The experimental setup for video recording technique is shown in Fig 2.4. It is similar to the PIV setup except that instead of a laser beam, a light beam is used from the top. To provide a stable and rigid platform for experiments to be conducted, the tank and flow meters were mounted in semi permanent steel super. . In addition to this a lighting arrangement using 3X1000 W halogen bulbs contained in a air circulated aluminum box was fabricated on a rail immediately atop the super structure. The objective of this was to illuminate the central vertical plane of a vessel for direct visualization of flow in that plane. Experiments were carried for central nozzle injection at different flow rates and slag (mustard oil being used as simulating agent) depths. Prior to any measurement, blowing was continued for sufficient time such that near steady state conditions can be achieved after which small rectangular pieces of special paper (which are more or less neutrally buoyant) were added to the bath. For determining the flow field, a 3cm \times 3cm grid network was constructed on the front of the vessel imaging from the central plane. The camera in the front of the vessel is focused on the illuminating plane and recording was done for 4-5 mins at each flow rate. From the recording at least 5 particles'

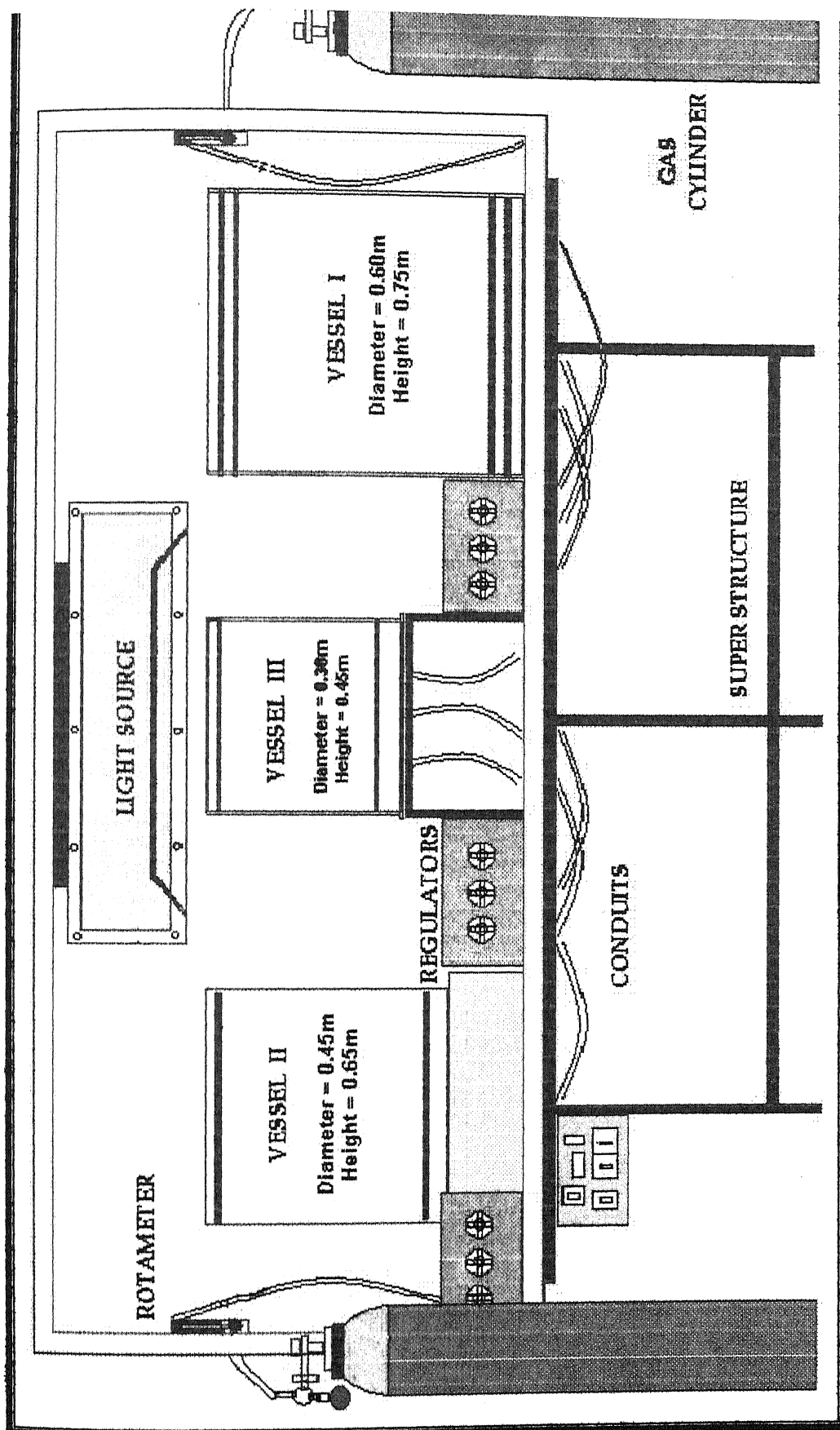


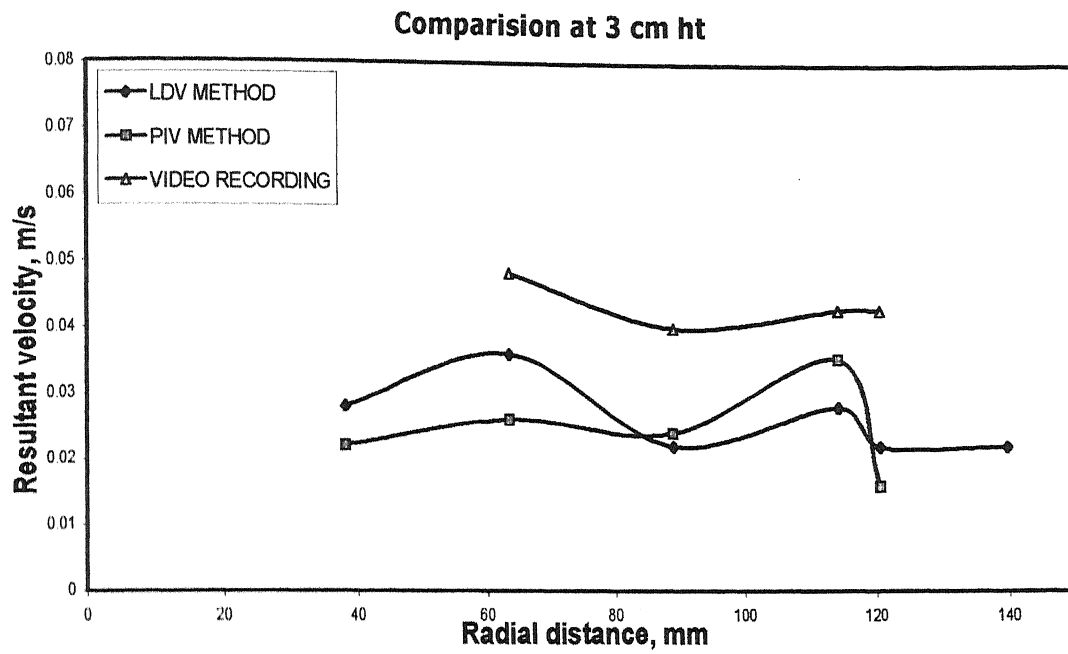
Figure 2.4: Experimental Setup in the Laboratory.

trajectories were taken in each grid. On the basis of the distance travelled and elapsed time average velocity was measured. Detailed measurements of the experimental data on velocity fields are summarized in the appendix

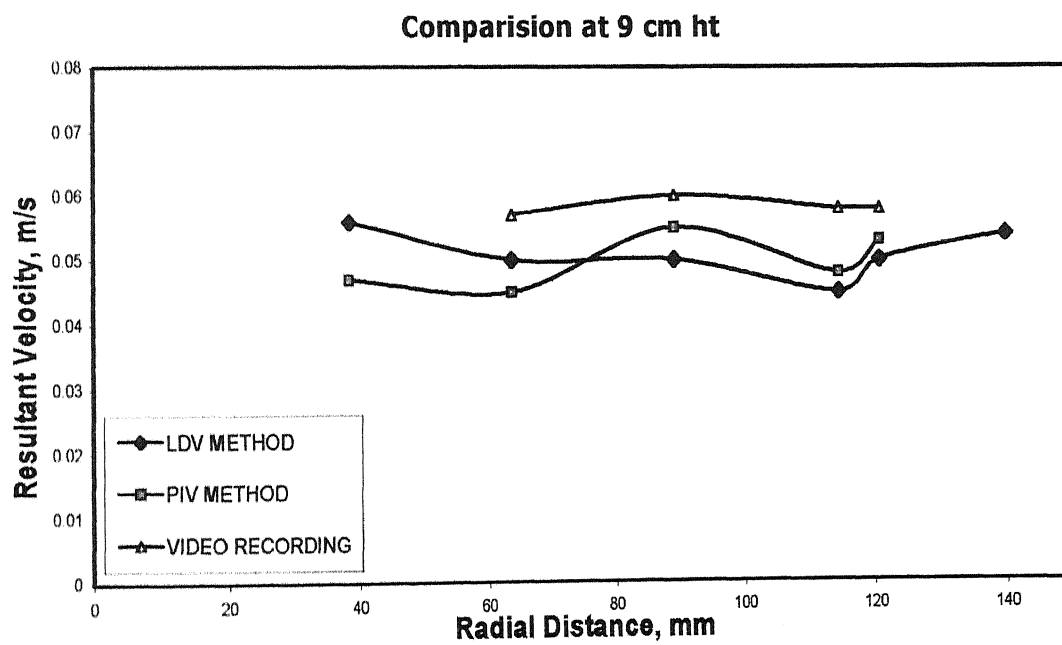
2.3.2 Comparison of Effectiveness of PIV, LDV and Video Recording Methods.

Video recording method developed in the lab, as pointed out already, is a relatively crude method of measuring flows. However a reasonable first hand estimate for the purpose of qualitative analysis can be derived through such measurement technique.

In Fig. 2.5 and Fig. 2.6 experimentally measured resultant flows on the central vertical plane on the laboratory scale water model ($D=30\text{cms}$ and $L=21\text{cms}$, central nozzle and no slag) is compared with PIV and LDV(obtained from a reported earlier work) at four different bath depths from bottom. From the above figures, it can be seen that the video recording method, despite being crude, can provide reasonable estimate of velocity. Flow phenomena in gas stirred ladles are essentially transient (owing to wandering of bubble plume, periodic formation and collapse of the spout are some of the reasons). Therefore some differences between measurements are likely to exist. In view of the above results it can be considered that velocity magnitude inferred from video recording can be applied as a first approximation for rate calculations (dissolution, melting etc.) in such gas agitated systems.

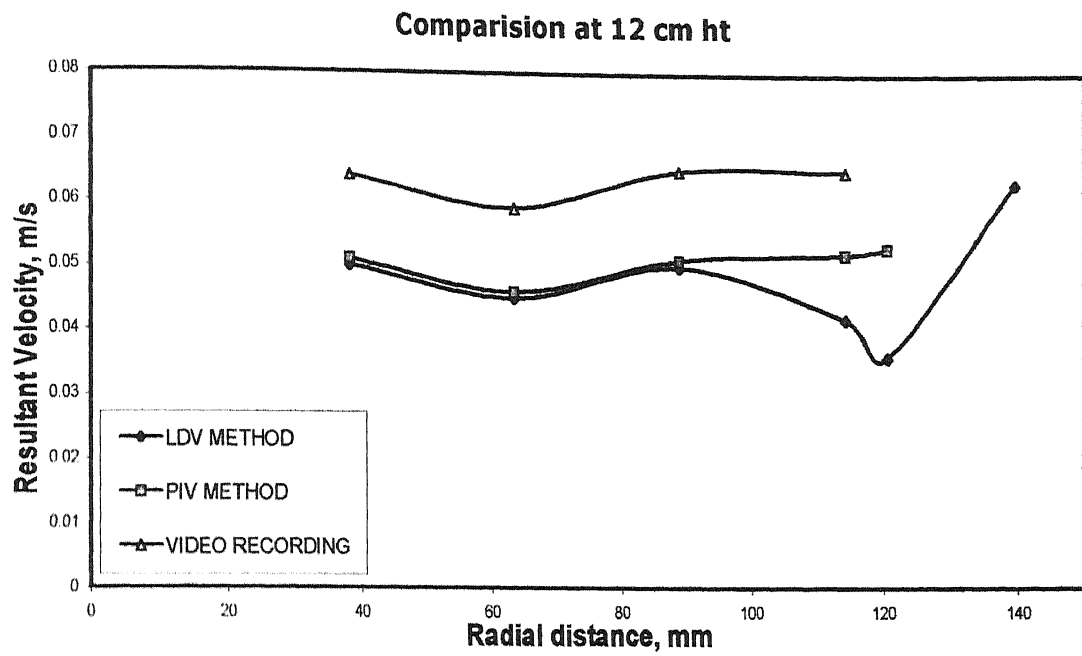


(a)

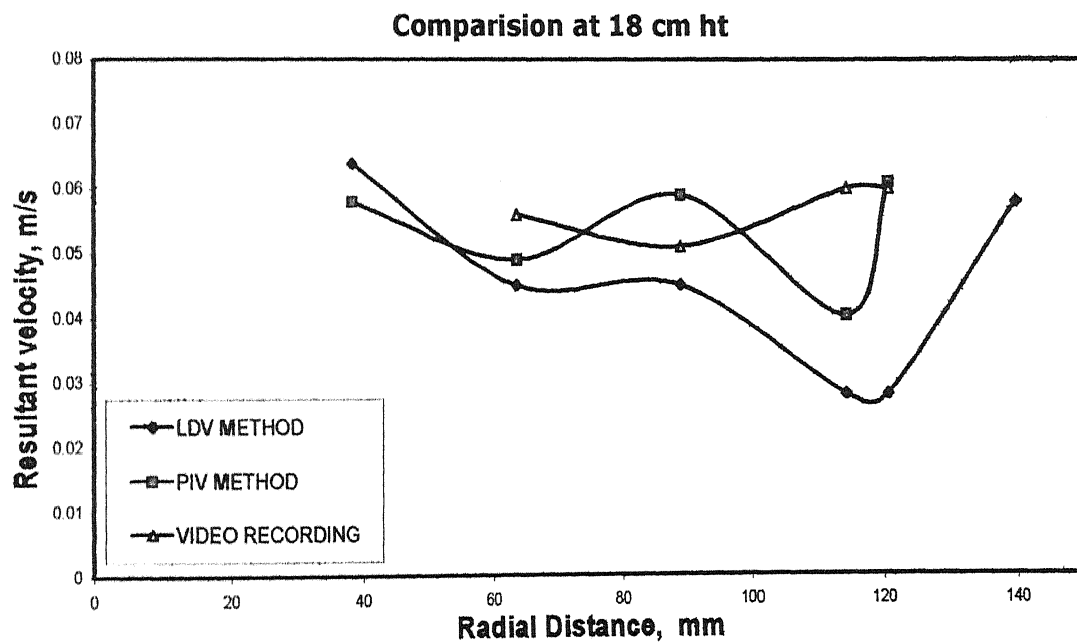


(b)

Figure 2.5: Comparison of velocities of PIV, LDV and Video Recording Methods at different Heights from the bottom (a) 3 cms, (b) 9 cms. (D=30cms and L=21cms, Central nozzle and No slag)



(a)



(b)

Figure 2.6: Comparison of velocities of PIV, LDV and Video Recording Methods at different Heights from the bottom (a) 12 cms, (b) 18 cms. ($D=30\text{cms}$ and $L=21\text{cms}$, Central nozzle and No slag)

2.4 EXPERIMENTAL RESULTS

Experiments were carried out by Particle imaging velocimetry (PIV) system for single and dual plug bubbling with and without slag and using video recording method for single plug bubbling in presence of slag. Parameters involved were slag depth and gas flow rate. In the following sections results and analysis of the flow measurements are presented.

2.4.1 Velocity Measurement for Single Plug Bubbling

2.4.1.1 Particle Imaging Velocimetry

Particle imaging velocimetry (PIV) experiments were conducted for single plug bubbling with (3cm thickness) and without slag layer to investigate the effect of an upper buoyant phase on velocity profile at $L/D = 1$. The radial distribution of axial and radial velocity components at four different heights (6,12,18,24 cms from bottom) are shown in Fig 2.7 to Fig 2.10 for a slag less situation while in presence of slag, results are presented in Fig 2.11 to Fig 2.14 respectively. These indicate:

1. The velocity magnitude increases with increasing gas flow rate
2. Near the plume axial velocity is positive while near the wall the same is negative.
This produces the recirculatory loop in the vessel
3. The axial and radial velocities both are dampened considerably in presence of an upper phase.

The above observations indicate that refining efficiencies of gas stirred system would be higher at higher gas flow rates. Furthermore transport processes in a slag less system are expected to be superior to an equivalent system with slag.

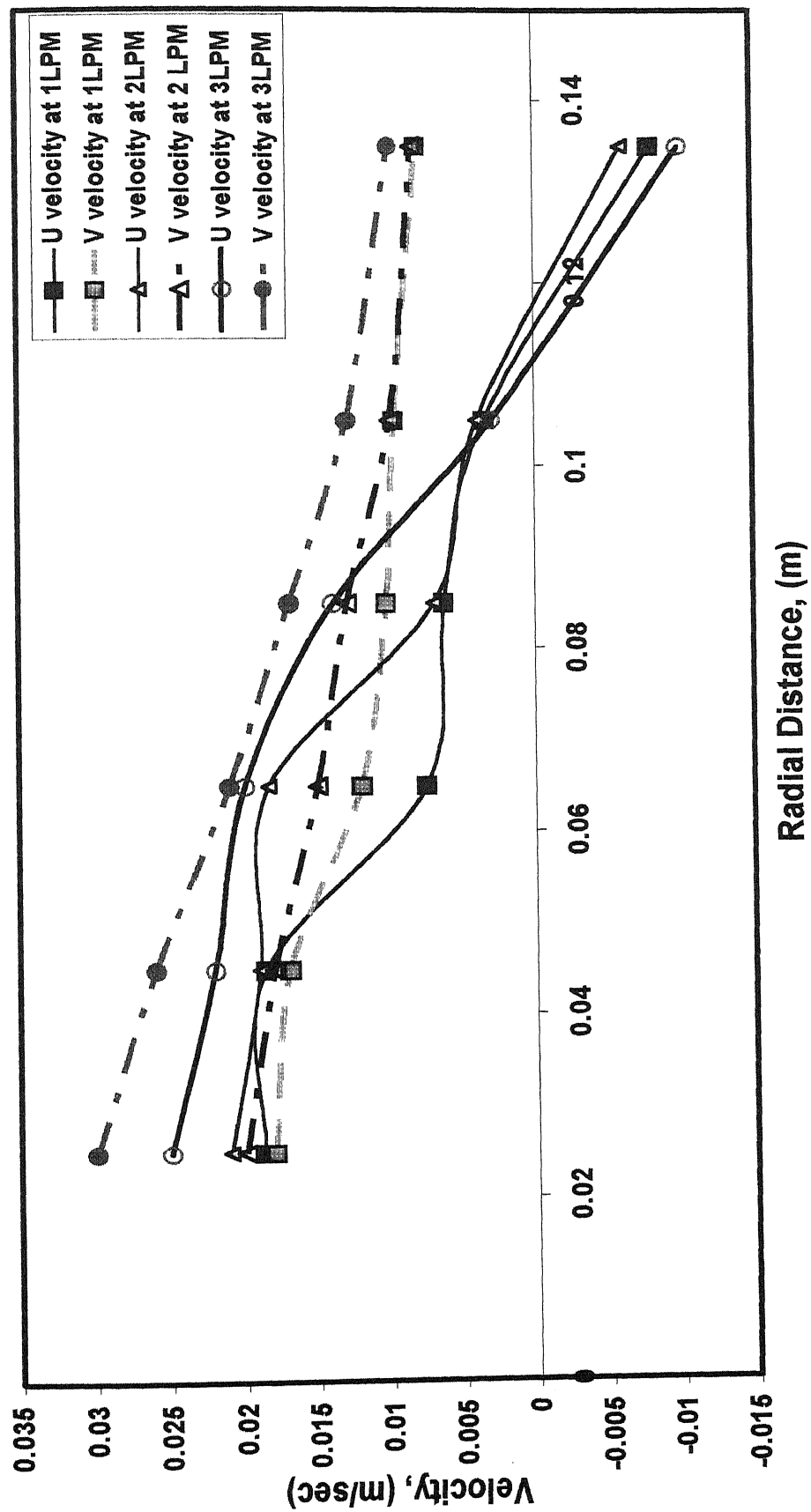


Figure 2.7: Radial Distribution of axial and radial velocities at 6cm height from the bottom for single plug bubbling without slag
(Central nozzle, $L/D = 1$)

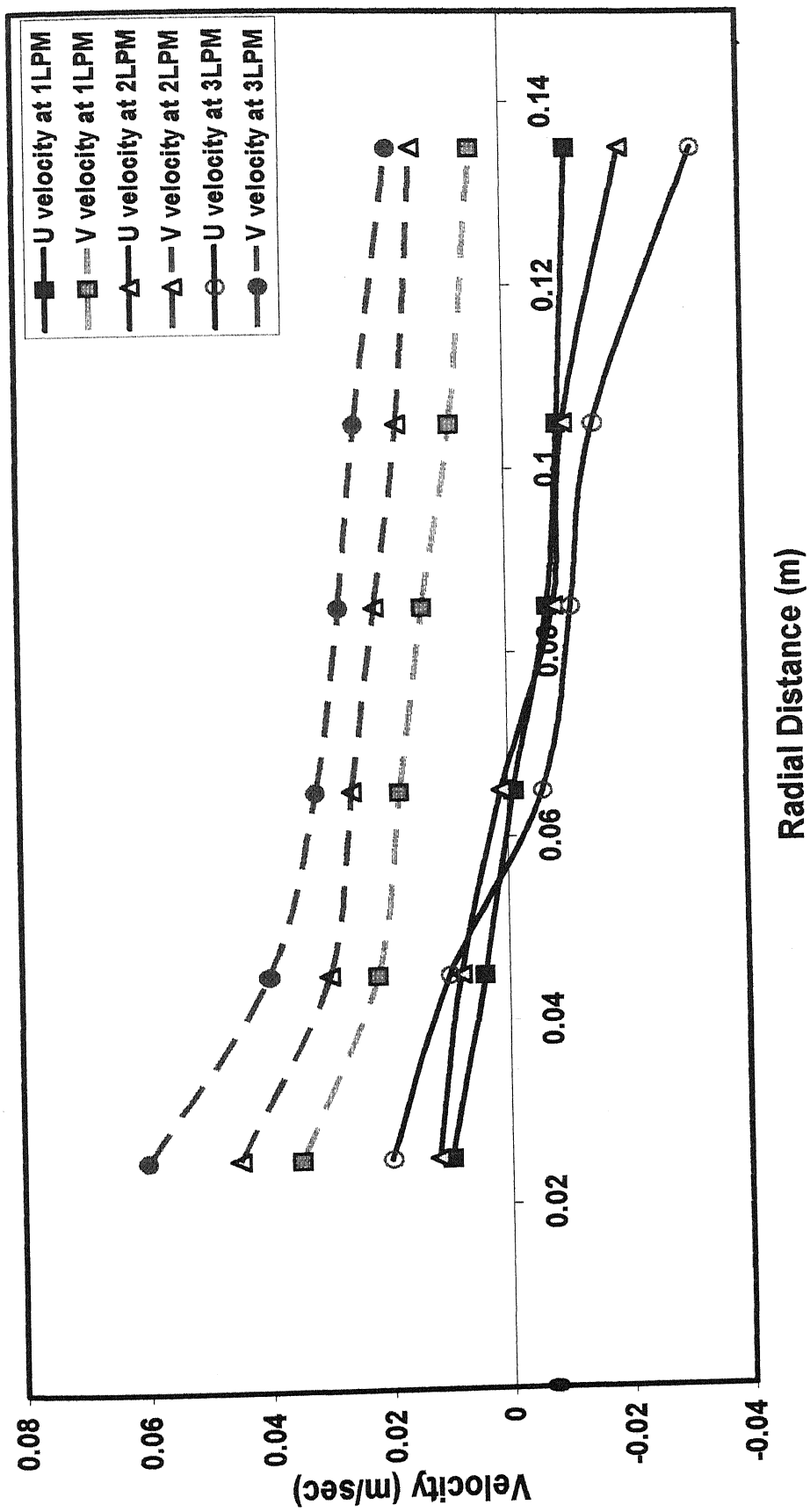


Figure 2.8: Radial Distribution of axial and radial velocities at 12cm height from the bottom for single plug bubbling without slag.
(Central nozzle, $L/D = 1$)

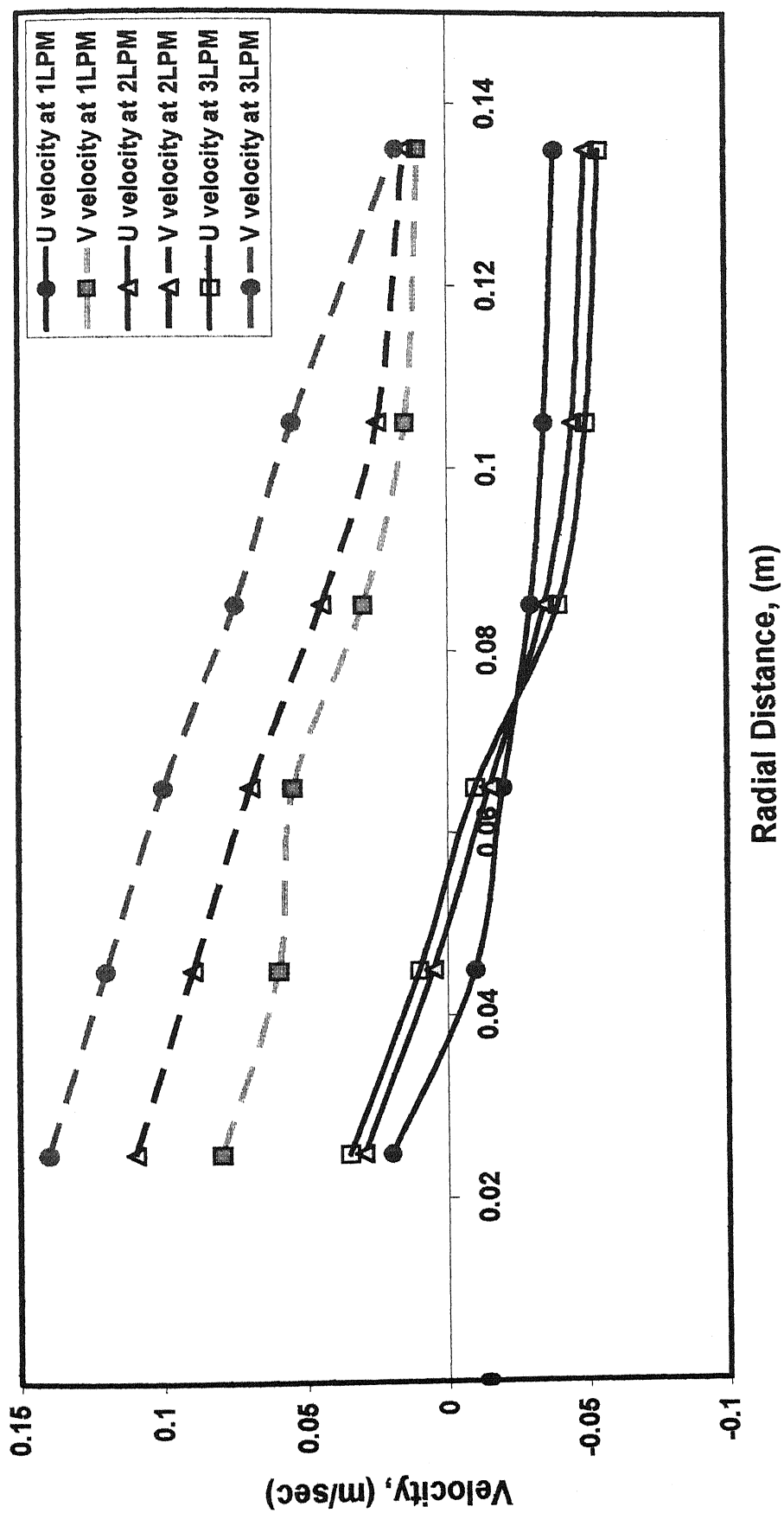


Figure 2.9: Radial Distribution of axial and radial velocities at 18cm height from the bottom for single plug bubbling without slag.
(Central nozzle, $L/D = 1$)

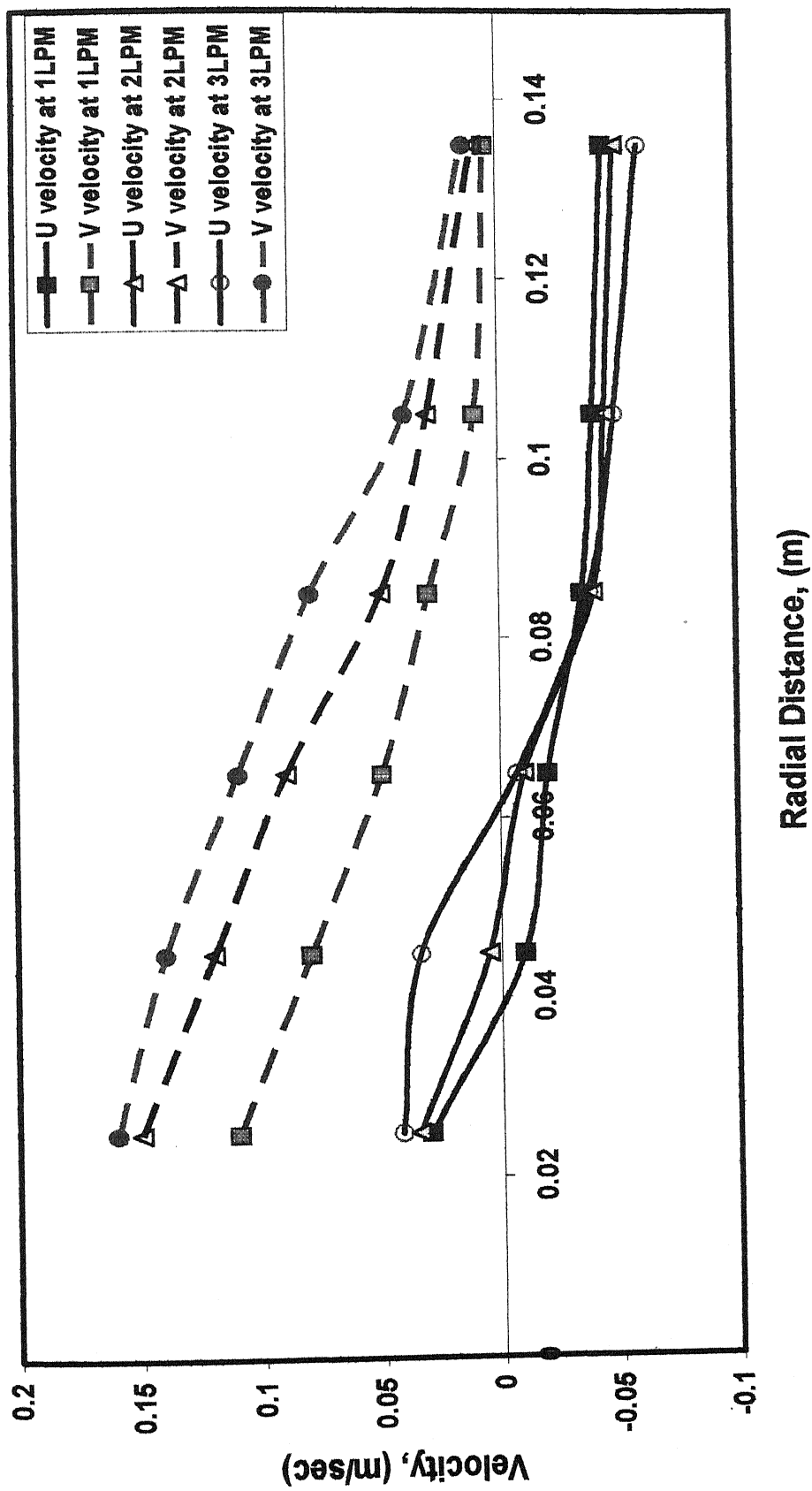


Figure 2.10: Radial Distribution of axial and radial velocities at 24cm height from the bottom for single plug bubbling without slag.
(Central nozzle, $L/D = 1$)

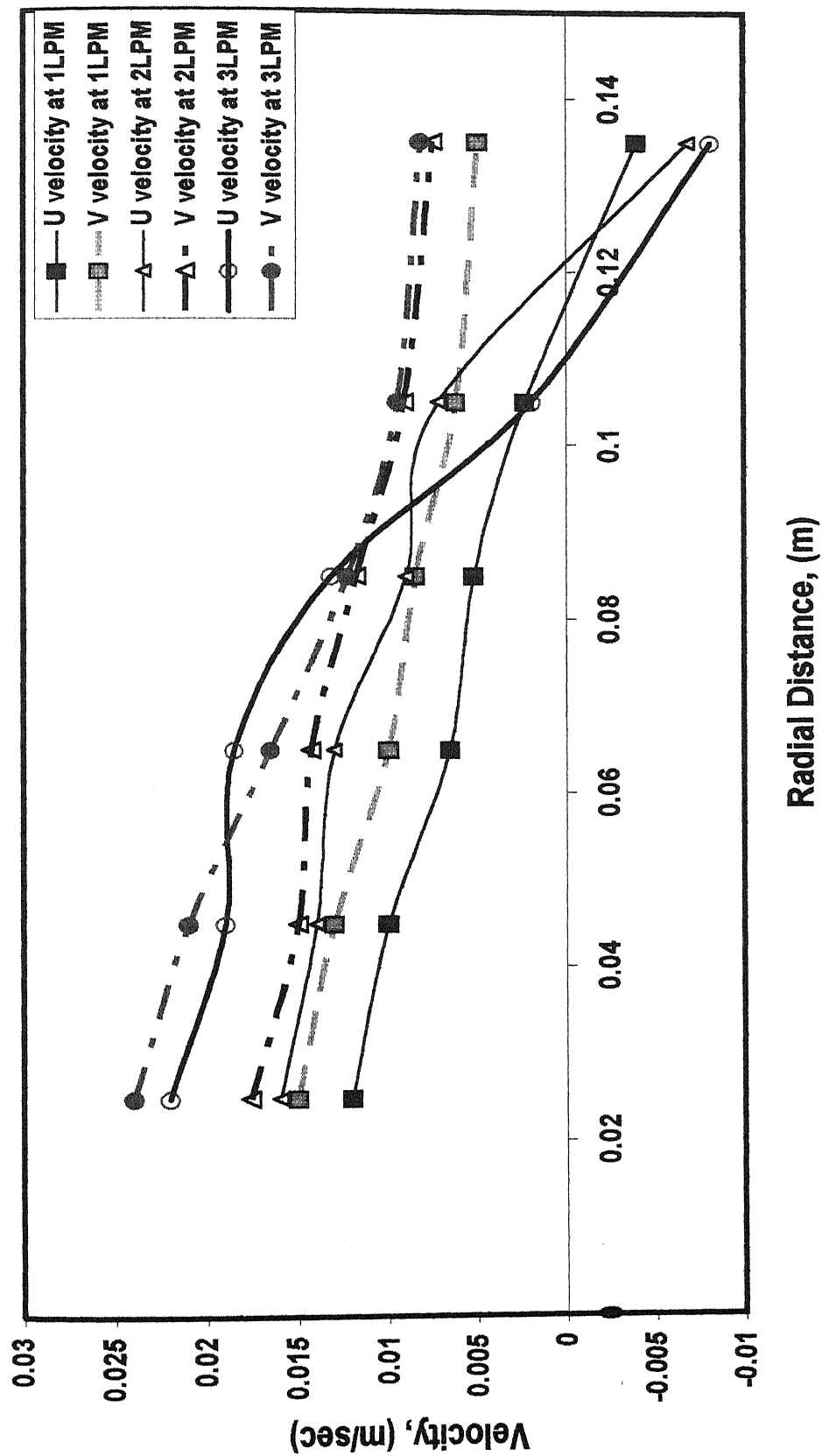


Figure 2.11: Radial Distribution of axial and radial velocities at 6cm height from the bottom for single plug bubbling with slag.
(Central nozzle, 3 cm Slag Depth, $L/D = 1$)

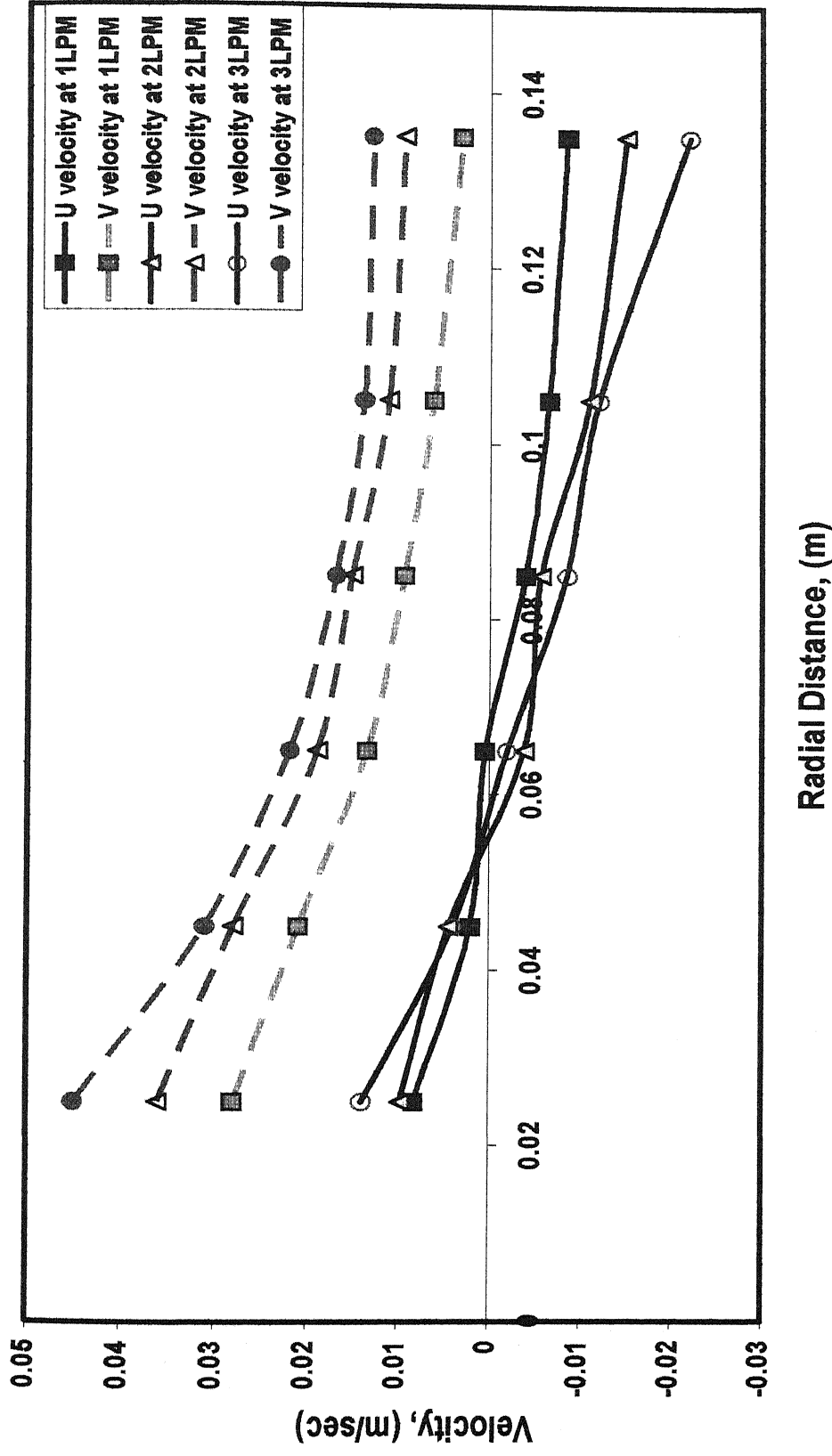


Figure 2.12: Radial Distribution of axial and radial velocities at 12cm height from the bottom for single plug bubbling with slag.
(Central nozzle, 3 cm Slag Depth, $L/D = 1$)

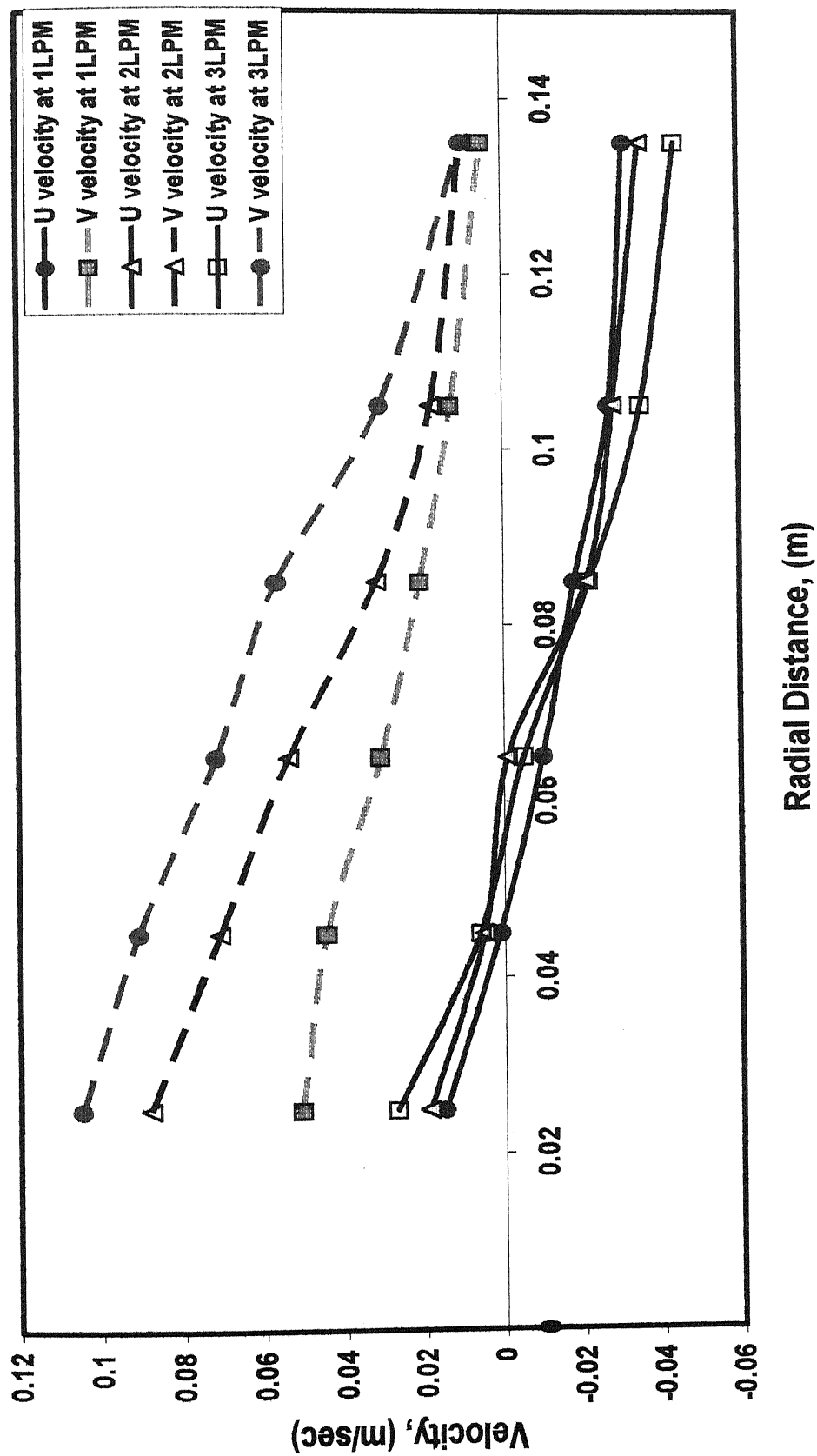


Figure 2.13: Radial Distribution of axial and radial velocities at 18cm height from the bottom for single plug bubbling with slag.
(Central nozzle, 3 cm Slag Depth, $L/D = 1$)

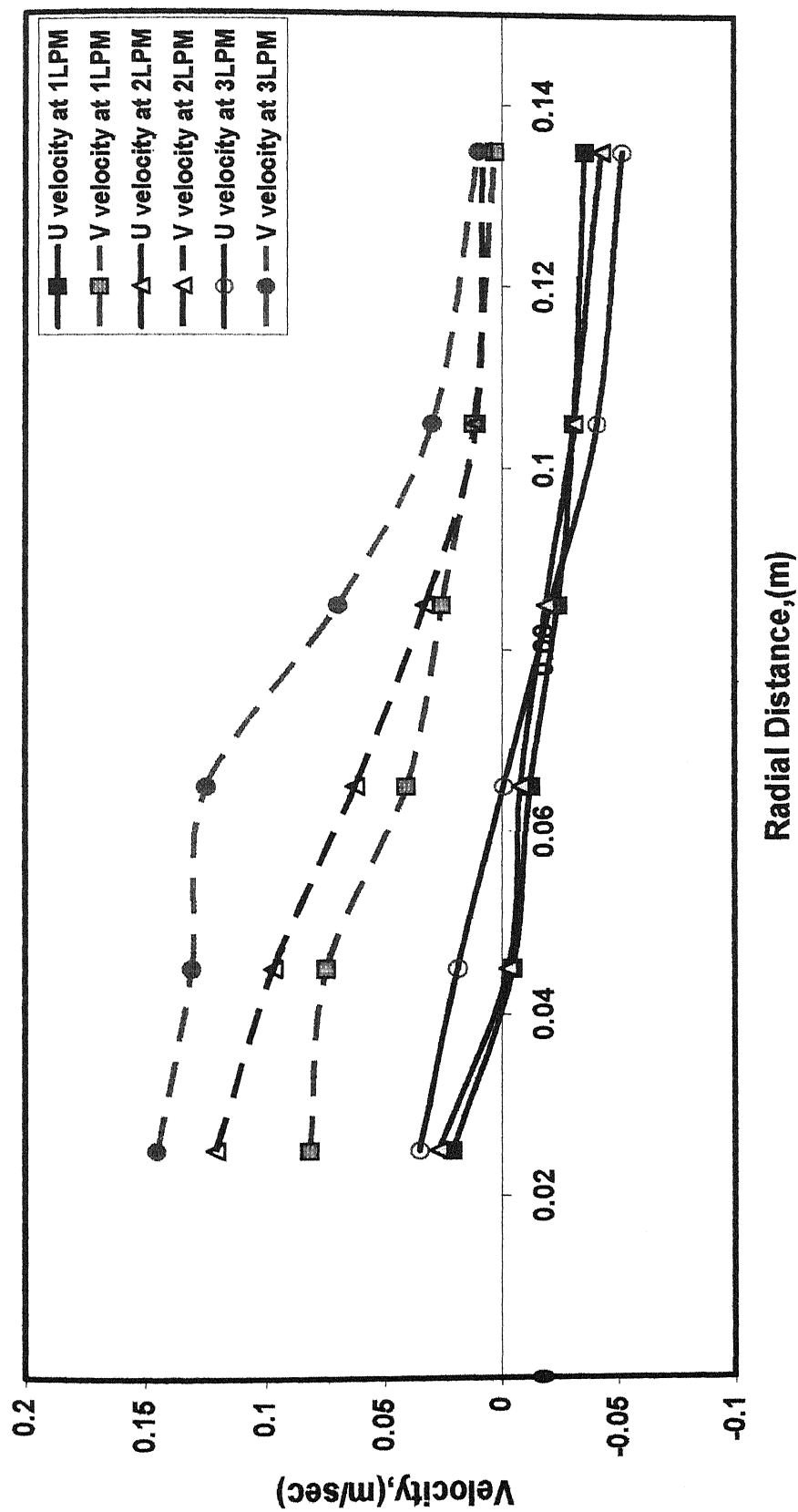


Figure 2.14: Radial Distribution of axial and radial velocities at 24 cm height from the bottom for single plug bubbling with slag.
(Central nozzle, 3 cm Slag Depth, $L/D = 1$)

2.4.1.1 Video Recording

Video recording technique was used to determine the velocity profile for single nozzle bubbling only. For the sake of estimating velocity magnitude, the video tapes were evaluated by transferring information from the video tape to plane papers as pointed out earlier. The detailed results are presented in the appendix while a summary of some derived parameters from the measured flow is presented in the subsequent paragraph.

Using the data sheets obtained from the video recording the mean recirculation speed of the bath was calculated. To determine the mean recirculation speed the average velocity was found in each grid of the data sheet prepared. The velocities at the unmeasured grids were extrapolated using the adjacent grid values. Then volumetric average was found out using the following formula.....

$$U_{Mean} = \frac{\sum Vol \times Vel}{\sum Vol} \dots\dots\dots(2.1)$$

in which vol refers to the volume of the control volume. Since in the video recording method it is not possible to determine the centre-line plume velocity because of bubble interference, consequently mean speed was estimated by considering a theoretically predicted centre-line velocity from the following formula, viz.

$$U_p = 3.3 Q^{1/3} L^{1/4} R^{-5/8} \dots\dots\dots(2.2)$$

In Eq.(2.2) Q, L and R are respectively the gas flow rate, bath depth and radius of the vessel . The estimates of mean speed thus derived together with equivalent estimates for a slag less situation are shown in Table 2.4. The mean speed for a slag less situation is calculated using following established relation,

$$U_{Mean} = 0.79 Q^{1/3} L^{1/4} R^{-5/8} \dots\dots\dots(2.3)$$

	Bath Depth (m)	Slag Depth (m)	Dia of the Vessel (m)	Gas Flow Rate (m ³ /sec)	Mean liquid Recirculation Speed, (ms ⁻¹)		
					Experimental (Without plume velocity)	Predicted	Experimental (With plume velocity)
1	0.27	0.03	0.3	1.6×10^{-5}	0.0335	0.0471	0.0416
2	0.27	0.03	0.3	3.2×10^{-5}	0.0368	0.0593	0.0465
3	0.27	0.03	0.3	4.8×10^{-5}	0.0469	0.0679	0.0586
4	0.29	0.01	0.3	3.2×10^{-5}	0.0395	0.0604	0.0498
5	0.25	0.05	0.3	3.2×10^{-5}	0.0345	0.0582	0.0446

Table 2.4: Mean recirculation Speeds at different gas flow rates and bath depths.

This shows that when the plume region is taken into account the mean speed is somewhat higher. This is to be expected since the gas liquid region moves much faster than the bulk liquid. Table 2.4 also shows that in the presence of an upper slag

1. As the gas flow rate is increased, the mean speed increases and
2. The mean speed increases as the depth of liquid in the system increases

which are equivalent to those for a slag less system. In addition to these the presence of an upper phase is seen to slow down the moving bulk liquid by as much as 15 to 20% These are shown graphically for two key process variables namely, the gas flow rate and slag depths in Figs. 2.15 and 2.16 respectively

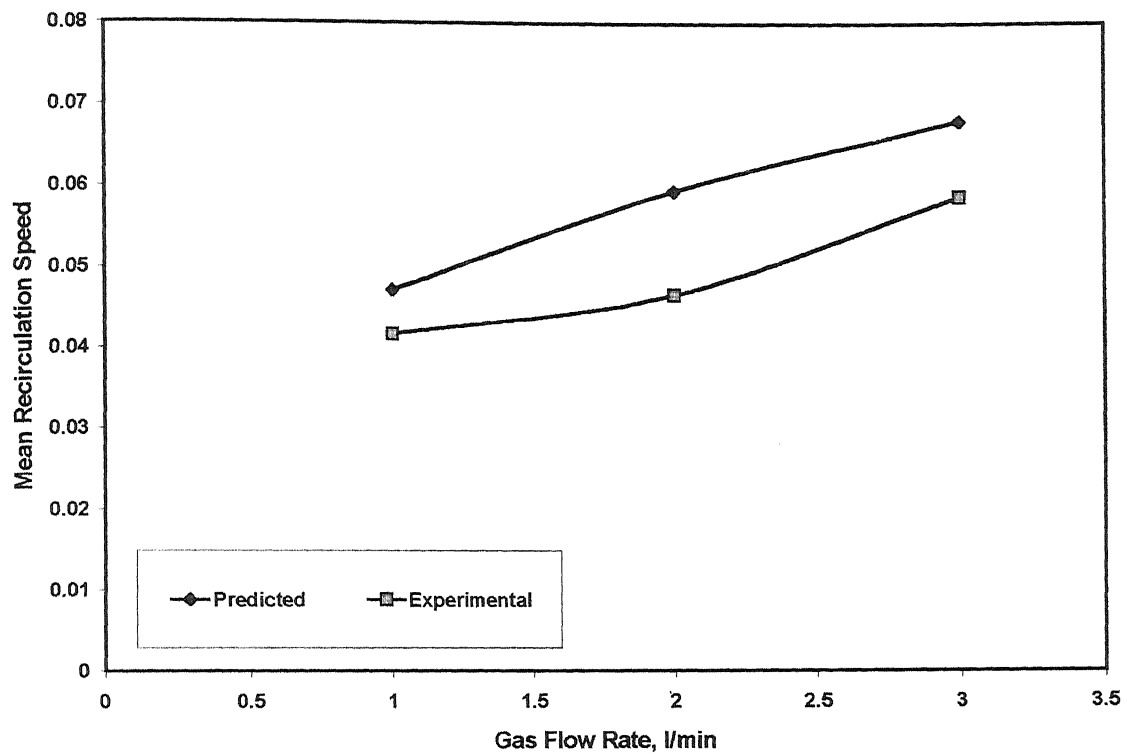


Figure 2.15: The influence of gas flow rates (l/min) on mean liquid speed (ms⁻¹) for situations without and with 0.03m of an upper slag phase.

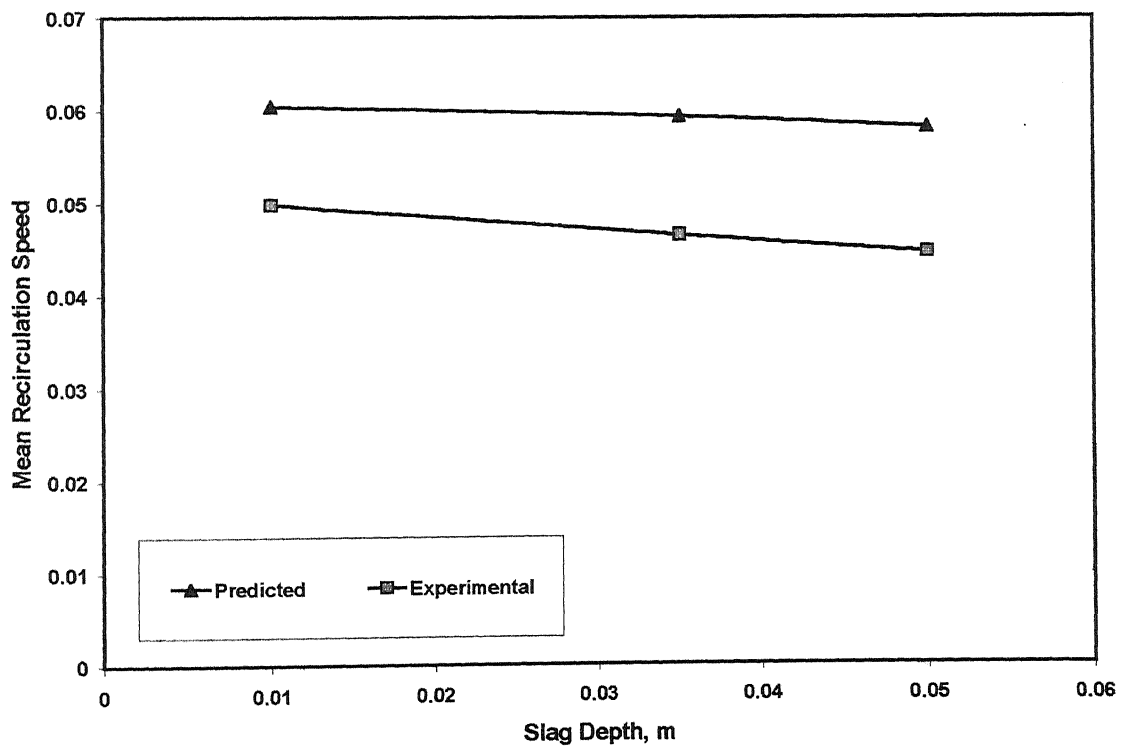


Figure 2.16: The influence of upper phase thickness on mean liquid speed (m/sec).

2.4.2 Velocity Measurement for Dual Plug Bubbling

Particle image velocimetry (PIV) experiments were carried out for dual plug bubbling to map the velocity on the central vertical plane. The radial distribution of axial and radial velocity components of flow at four different heights (6,12,18,24 cms from the bottom) vertical plane for no slag condition are shown in Fig 2.17 to Fig 2.20 and in presence of a slag in Fig 2.21 to Fig 2.24 respectively.

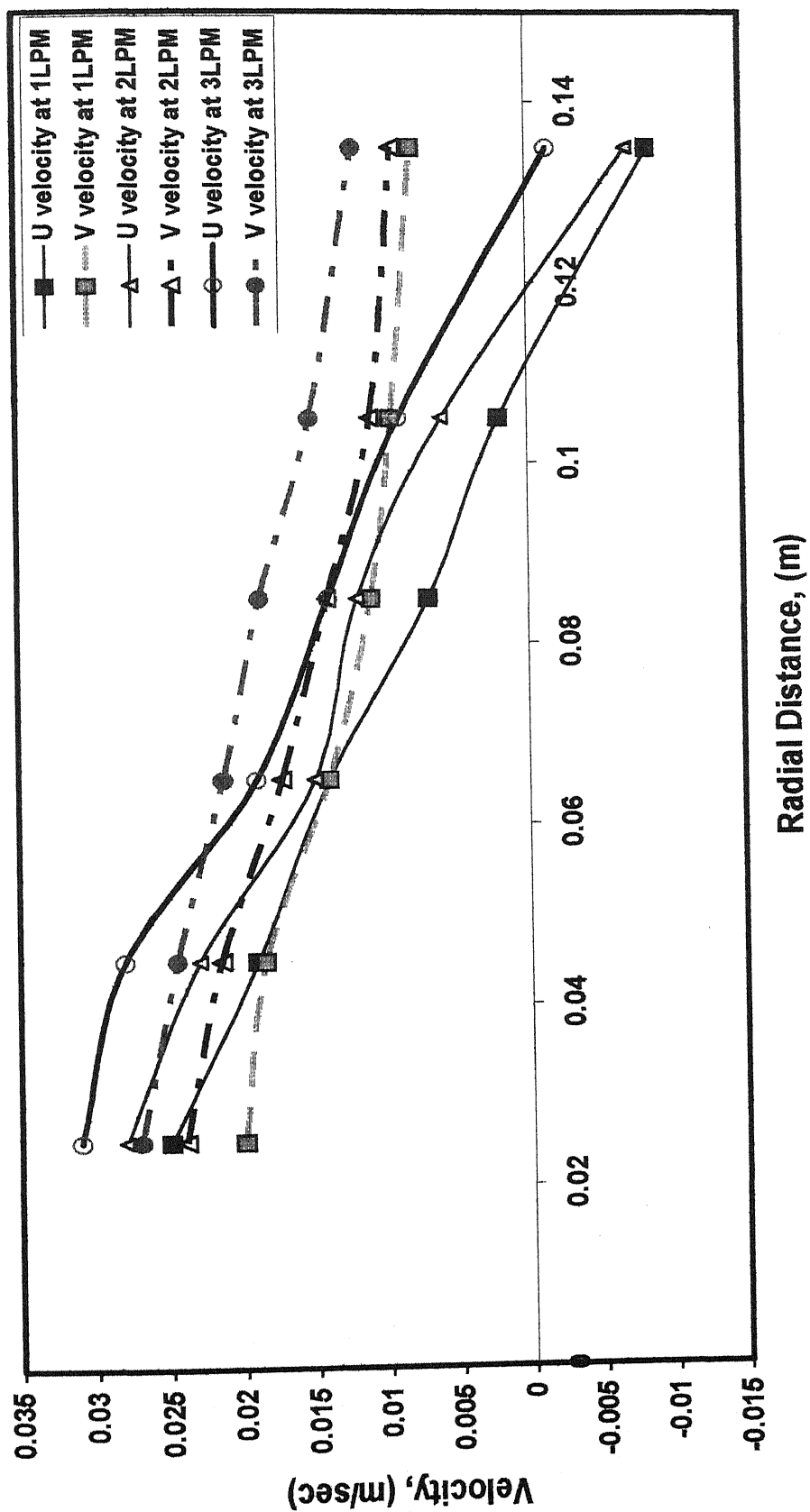


Figure 2.17: Radial Distribution of axial and radial velocities at 6 cm height from the bottom for Dual plug bubbling ($-R/2$, $+R/2$) without slag ($L/D = 1$).

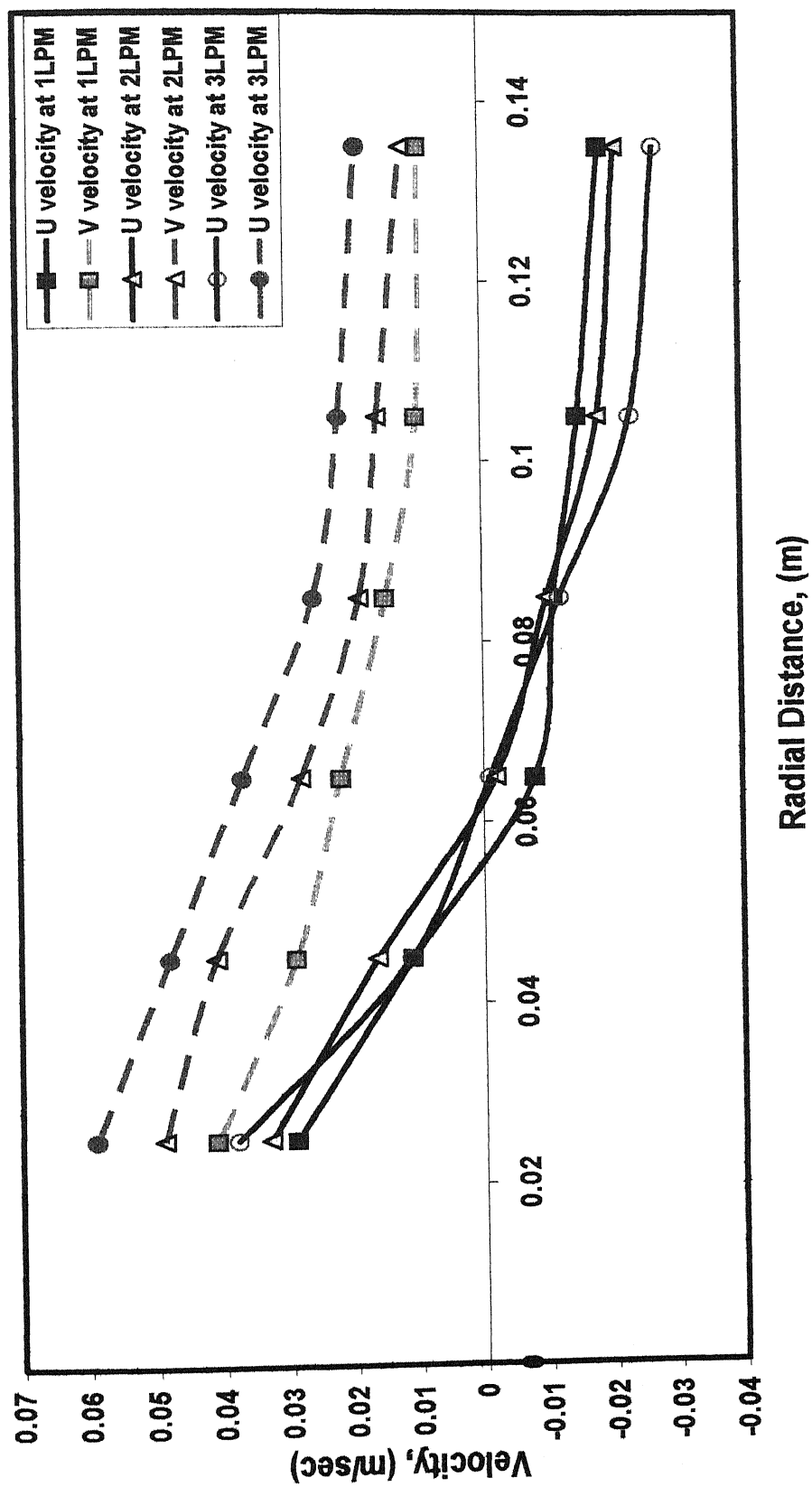


Figure 2.18: Radial Distribution of axial and radial velocities at 12 cm height from the bottom for Dual plug bubbling ($-R/2$, $+R/2$) without slag ($L/D = 1$).

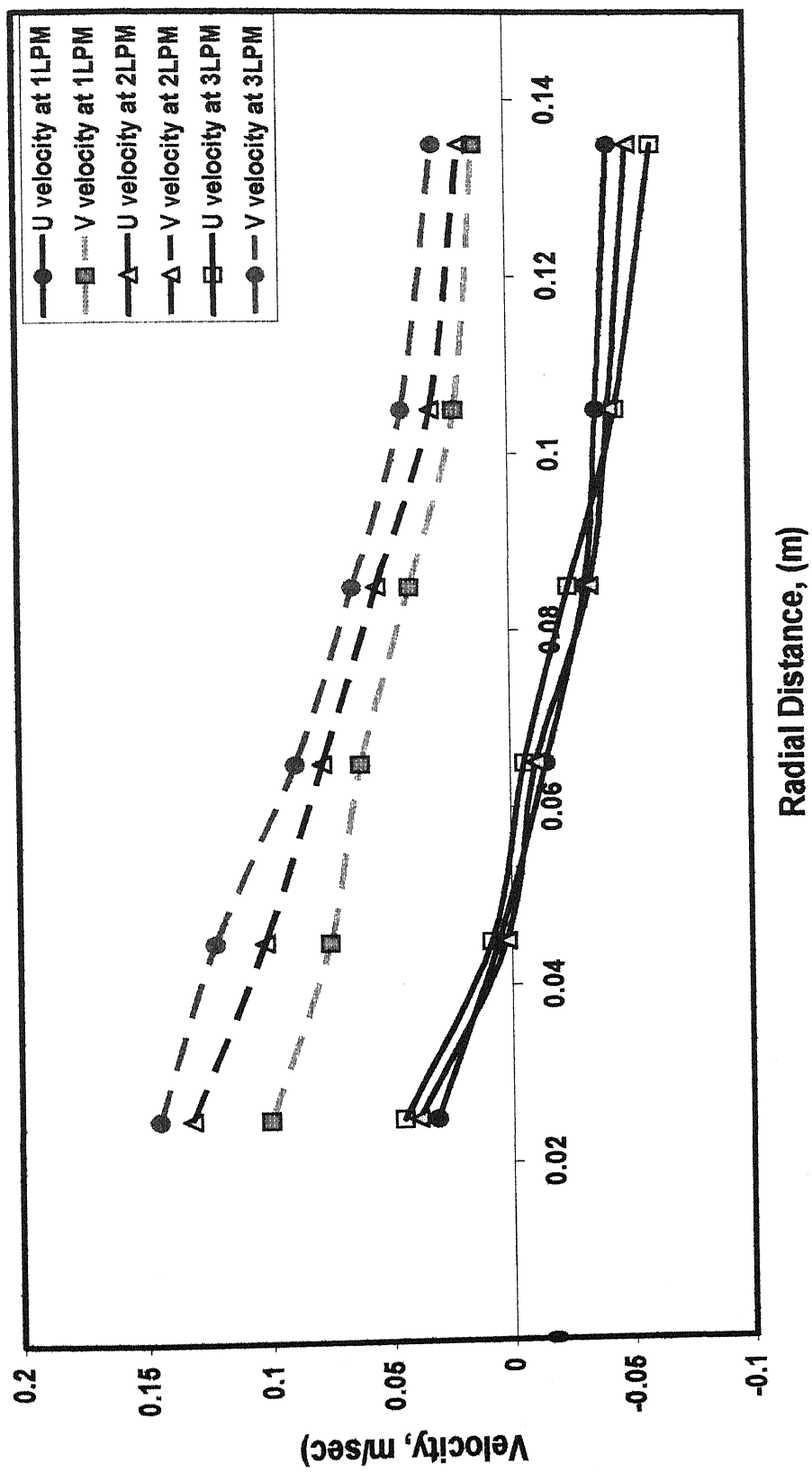


Figure 2.19: Radial Distribution of axial and radial velocities at 18 cm height from the bottom for Dual plug bubbling ($-R/2$, $+R/2$) without slag ($L/D = 1$).

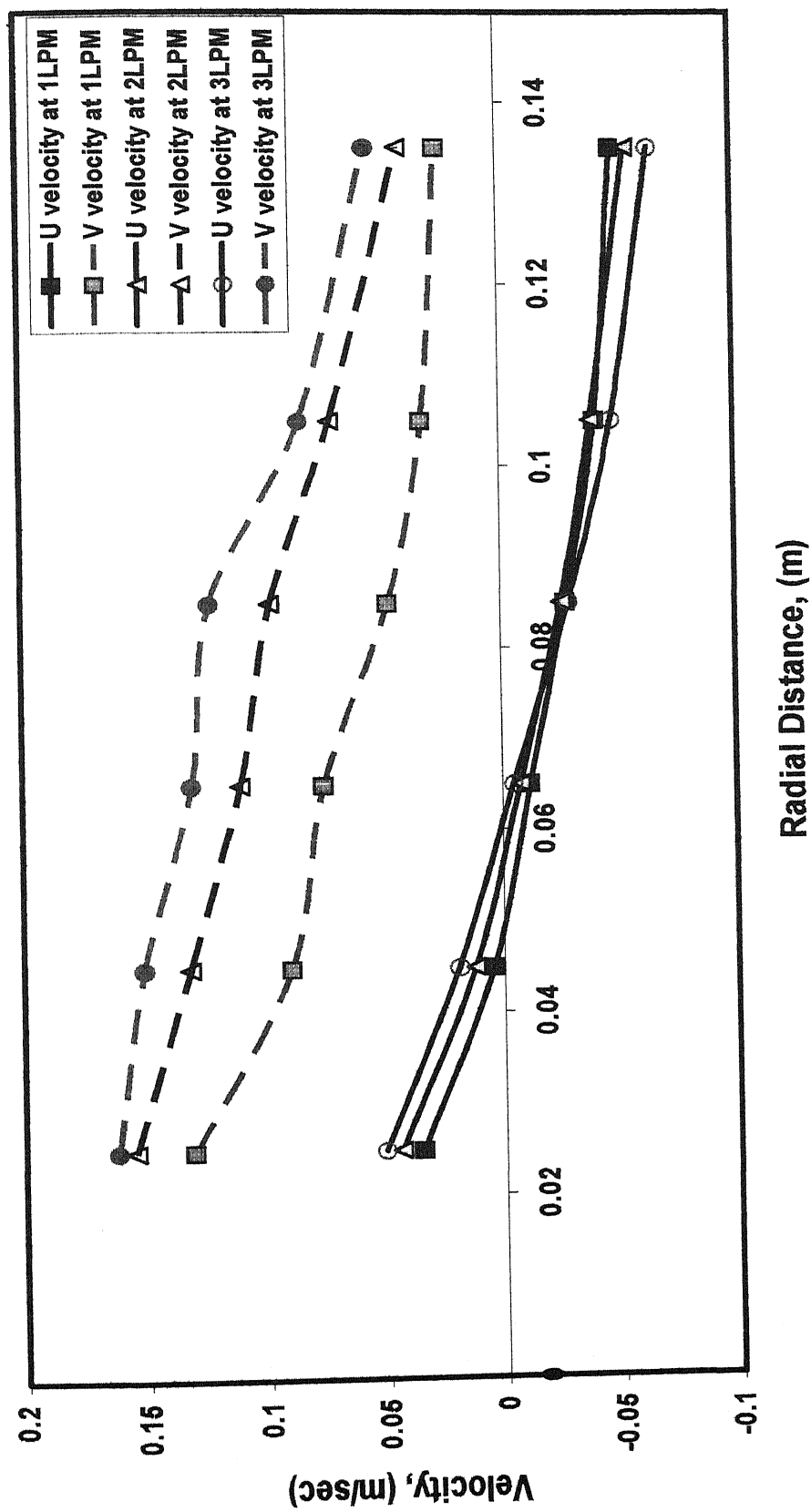


Figure 2.20: Radial Distribution of axial and radial velocities at 24 cm height from the bottom for Dual plug bubbling ($-R/2$, $+R/2$) without slag ($L/D = 1$).

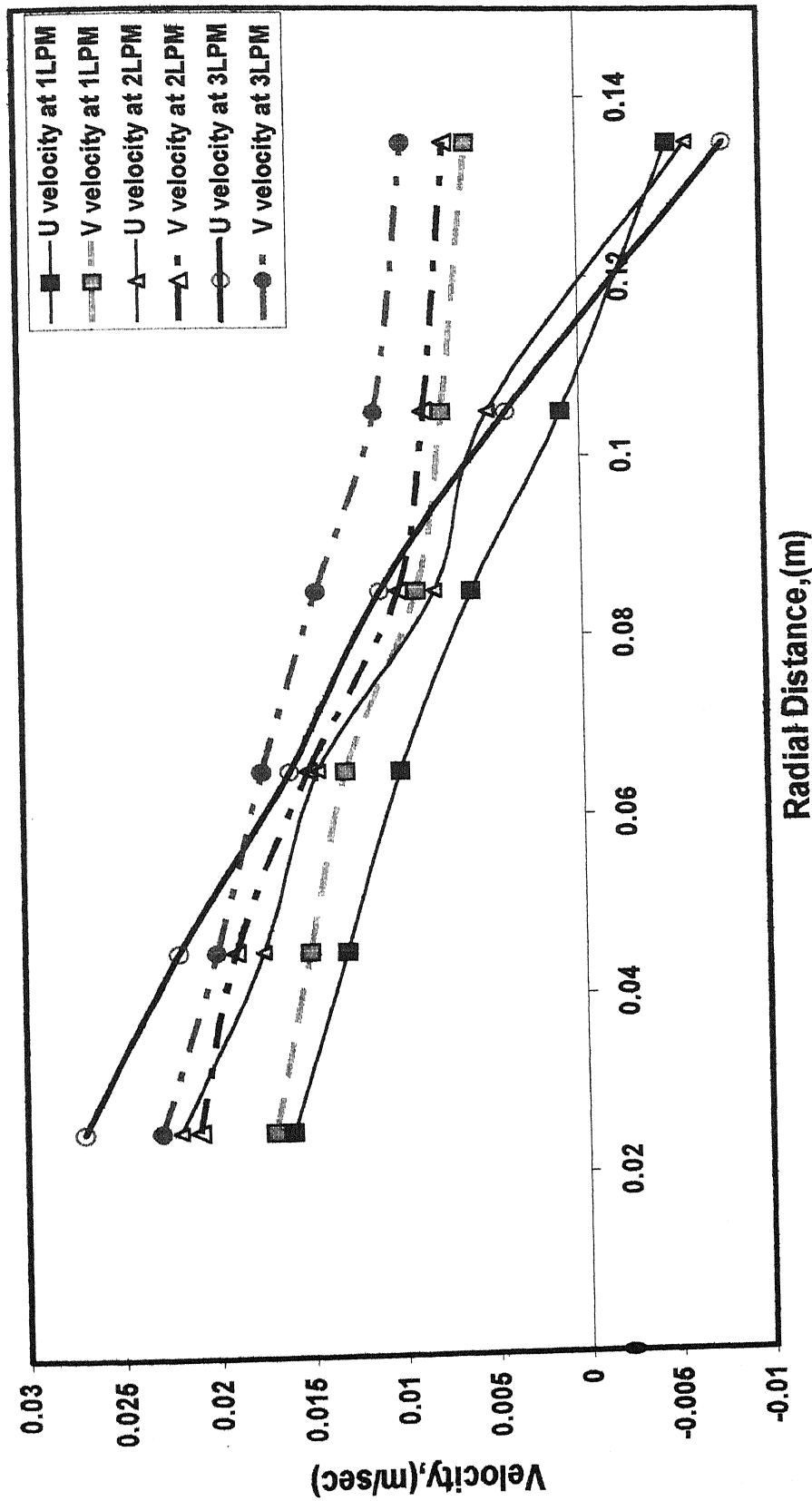


Figure 2.21: Radial Distribution of axial and radial velocities at 6 cm height from the bottom for Dual plug bubbling ($-R/2$, $+R/2$) with slag (3 cm Slag Depth, $L/D = 1$).

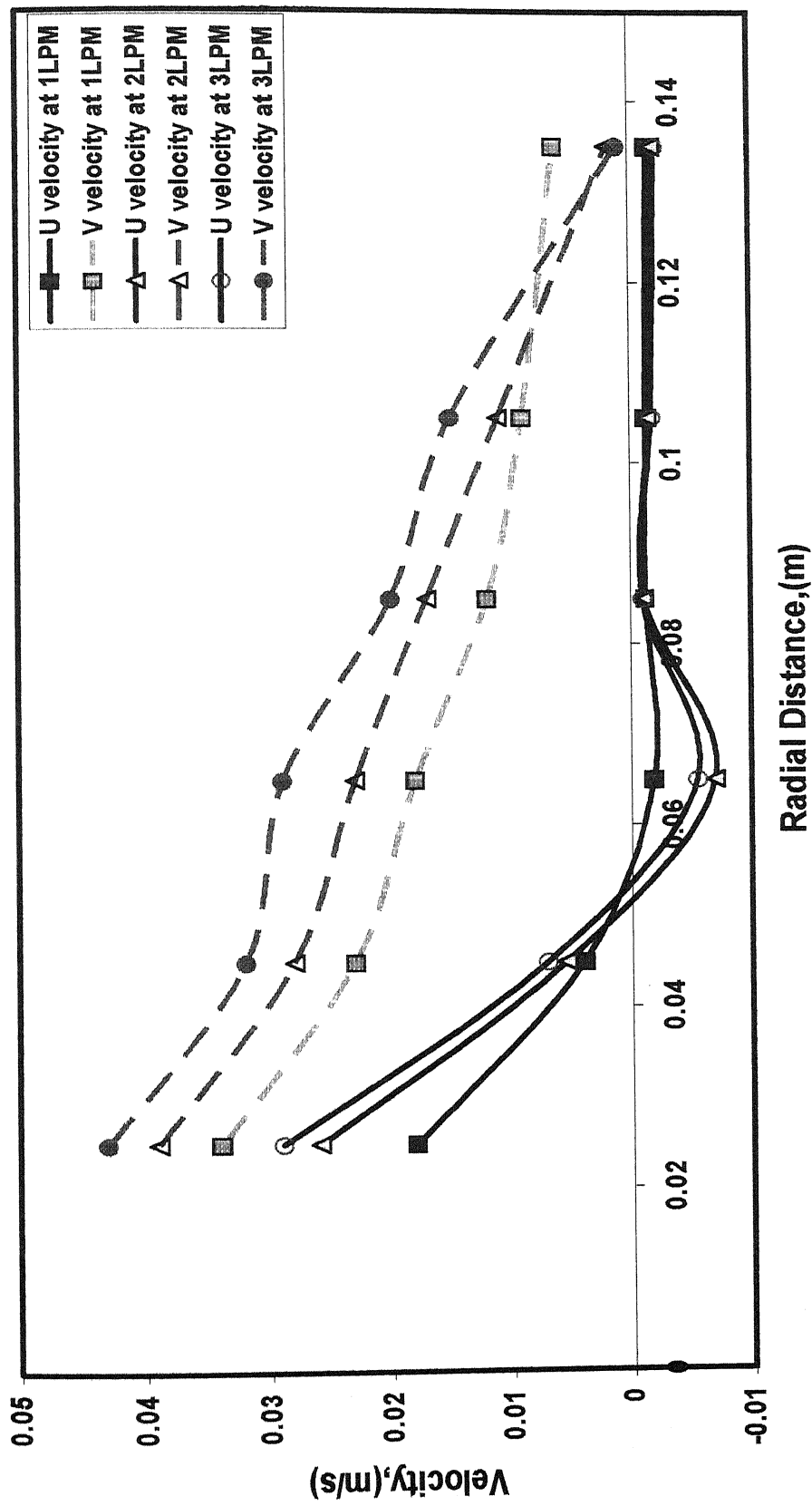


Figure 2.22: Radial Distribution of axial and radial velocities at 12 cm height from the bottom for Dual plug bubbling ($-R/2$, $+R/2$) with slag (3 cm Slag Depth, $L/D = 1$).

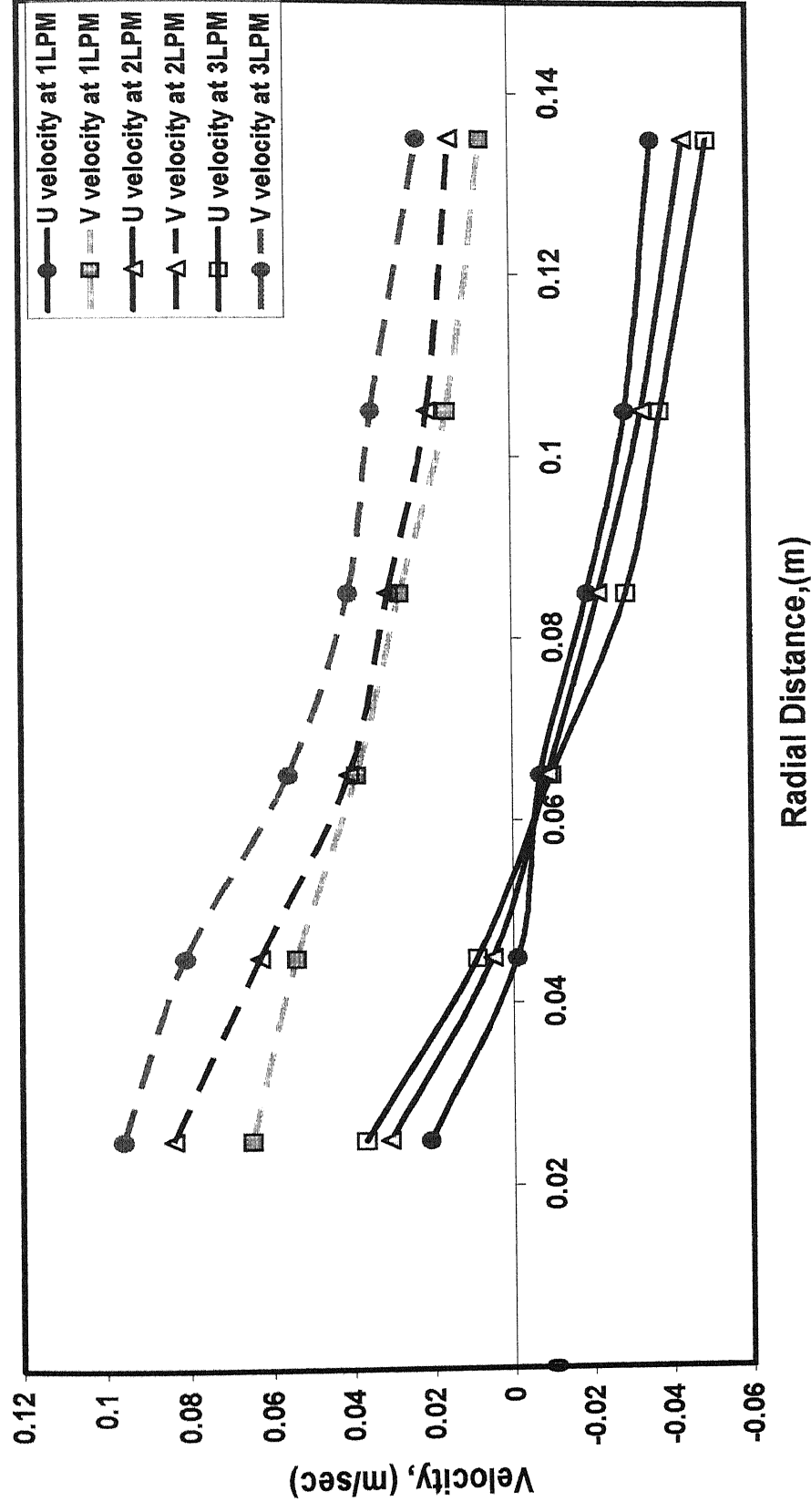


Figure 2.23: Radial Distribution of axial and radial velocities at 18 cm height from the bottom for Dual plug bubbling ($-R/2$, $+R/2$) with slag (3 cm Slag Depth, $L/D = 1$).

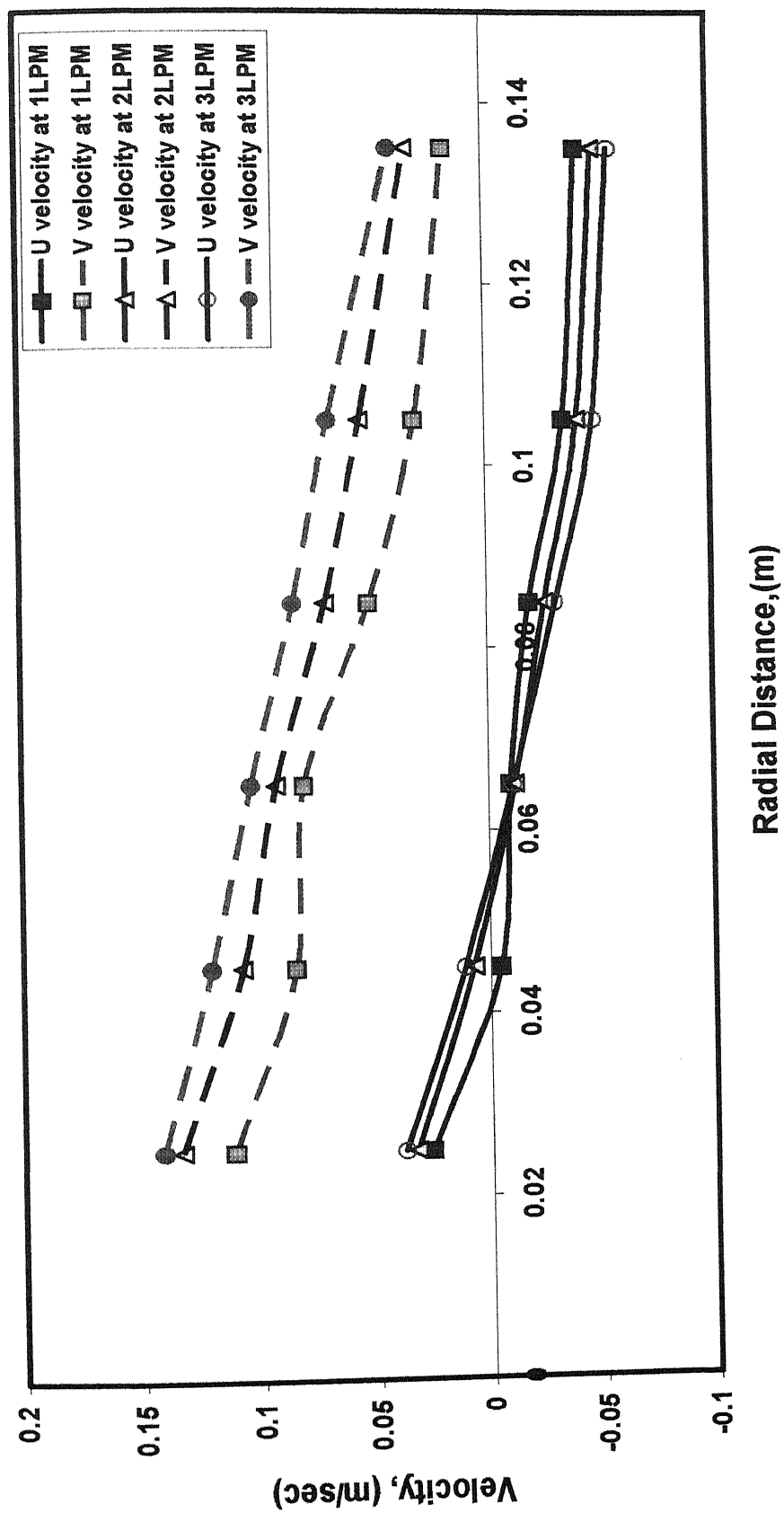


Figure 2.24: Radial Distribution of axial and radial velocities at 24 cm height from the bottom for Dual plug bubbling ($-R/2$, $+R/2$) with slag (3 cm Slag Depth, $L/D = 1$).

The following general observation can be made from the preceding plots:

- i. The velocity magnitude increases with increasing gas flow rate
- ii. Near the plume axial velocity is positive while near the wall the same is negative.
This produces the recirculatory loop in the vessel
- iii. The axial and radial velocities both are dampened considerably in presence of an upper phase and finally
- iv. The magnitude of the flows are similar to those for single plug bubbling at equivalent flow rates

The last observation appears to indicate that not much improvement in refining efficiency is to be expected at equivalent gas flows. In addition the measurements reported so far appears to indicate that differential behavior between a single plug and twin plug stirred ladle are not significantly altered by the presence of an upper slag phase

CHAPTER III

MASS TRANSFER AND MIXING MEASUREMENTS

3.1 TECHNIQUES OF MASS TRANSFER MEASUREMENT

Interfacial (e.g., slag-metal) mass transfer in metallurgical reactors plays an important role in determining the efficiency of various metal processing operations. Naturally researchers have been studying mass transfer phenomena in such reactors under different conditions and to this end a variety of techniques have been applied. A summary of these are presented in Table 3.1. Many investigators [29,34,35,36,37,39,40,41,42,43,44,45,46] have studied mass transfer of a species between two immiscible liquids with bubble stirring for cold and hot models using a tracer transfer method. In these, water and organic fluids (oil [29,37,39,40,41,44,45,46], benzene[36,42,43], cyclohexane[35] etc.) were used as simulating fluids to represent the metal slag phases respectively. Principally, the intensity of slag-metal reactions has been studied by monitoring the transport of a tracer, which has an equilibrium partition ratio between water and the upper liquid phase. In such systems owing to the difficulties in estimating the effective slag-metal interfacial area accurately under gas stirring conditions, a volumetric mass transfer coefficient ($= KA$; K = aqueous phase mass transfer coefficient) has often been applied to quantify the experimental results.

A low temperature mass transfer system for distribution of solute between two immiscible liquid phases is selected for the present study. Such a system is easier to handle in the laboratory than the molten metal / slag. Water is used to simulate liquid steel and Mustard oil is used as model slag, while Benzoic acid represents the dissolved substance to be extracted into the slag phase. Benzoic acid was chosen because it can be determined by titrating it against KOH. This combination of liquids was selected after reviewing various systems studied by different investigators, as summarized in Table 3.1.

System	Investigator	Liquid to simulate		Exchange Material	Technique used for analysis.
		Steel	Slag		
1	Kim and Fruehan [29]	Water	Paraffin oil	Thymol	Ultra Violet Spectroscopy
2	Matway et al[39,40]	Water	Paraffin oil	β Naphthol	Ultra Violet Spectroscopy
3	Schlarb and Froberg[41]	Water	White oil	Caprylic acid	
4	Paul and Ghosh[42]	Water	Benzene	Iodine	Standard titration using Sodium Thiosulphate
5	Singh and Ghosh[36]	Water	Benzene	Iodine	Standard titration using Sodium Thiosulphate
6	Koria and Shamsi[37]	Water	Paraffin oil	Benzoic acid	Standard titration using KOH
7	Kikuchi et al[43]	Water	Benzene	Acetophenone	Spectrometer
8	Koria and George[44]	Water	Paraffin oil	Benzoic acid	Standard titration using KOH
9	Koria and Pal [45]	Water	Paraffin oil	Benzoic acid	Standard titration using KOH
10	Ogawa and Onoue[46]	Water	KCl coated Polystyrol particles	KCl	Electrical Conductivity.
12	Mietz,Schneider and Oeters[35]	Water	Cyclohexane	Iodium Crystals	Spectrophotometer

Table 3.1: Mass transfer systems studied by various investigators.

3.2

MASS TRANSFER EXPERIMENTS

3.2.1 Experimental Setup

A schematic diagram of the experimental setup is shown in Fig 3.1. This Perspex model having a scale factor of 0.08 with respect to full scale 150 tonne ladle, has a bottom diameter of 30 cm and height of 45 cm. Physical dimensions of the vessel and the physical properties of the liquids used is given in the Tables 2.1, 2.2 and 2.3 respectively.

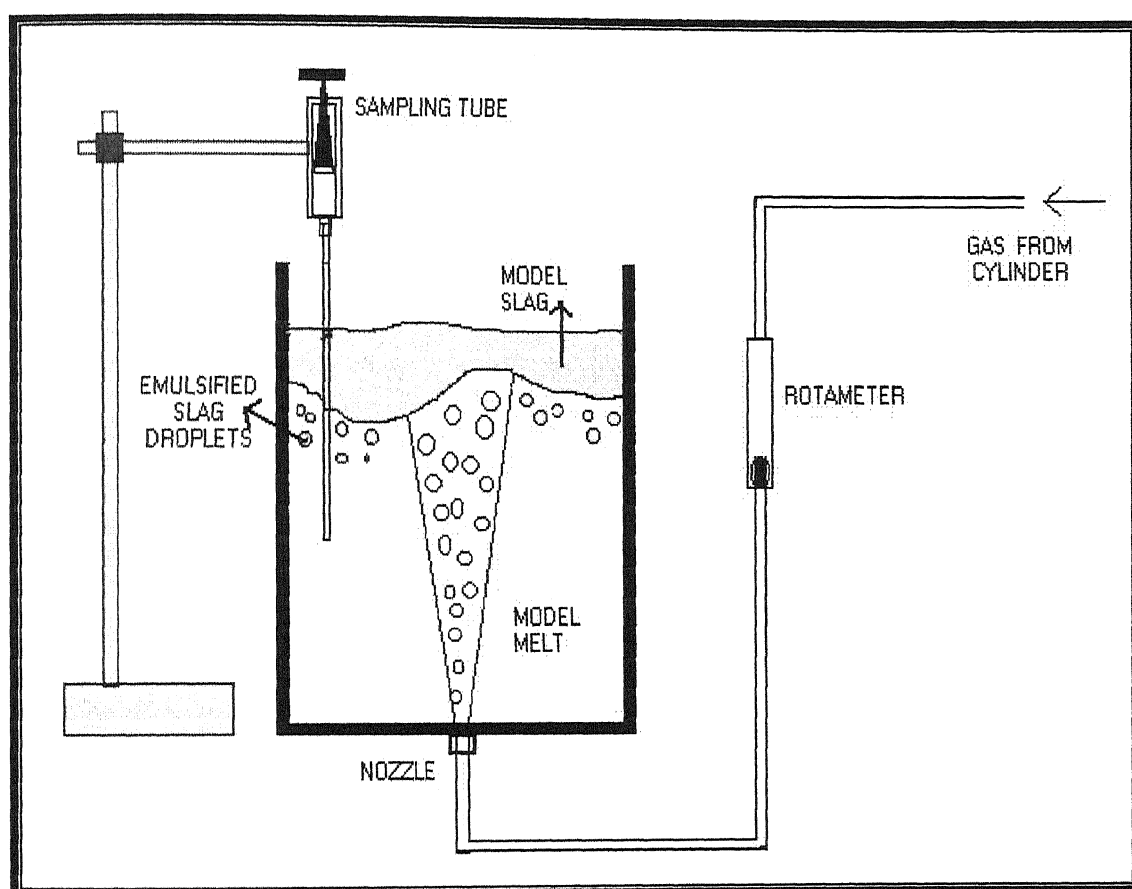


Figure 3.1: Schematic diagram of Experimental setup.

At the base of the vessel three nozzles were fitted ($R=0$, $+0.5R$ and $-0.5R$) to facilitate gas injection, one at the centre, one each at diametrically opposite-half radius positions as shown in Fig 3.2 The nozzle locations were identified from the literature for optimal fluid flow and mixing conditions in the system. All the vessels were kept inside a

relatively bigger square cross sectioned vessel. The space between the two tanks was filled with water to avoid optical distortions during the flow visualization. The lower end of each vessel was sealed against the bottom of the square vessel by a neoprene gasket and sealing rubber gel at the contact point before applying pressure from the top to avoid any intermixing of water. The air/N₂ flow rate was monitored by rotameters on each gas line leading to a nozzle, which had a diameter of 0.5 cm. A fixed arrangement was made to hold the sampling tube at the fixed height from where the samples were taken at regular intervals. For the convenience of experimental study, the vessel together with the flow meters, needle valve etc. was mounted on semi permanent steel superstructure. The liquid was usually filled to a height of 27 cm. Some experiments were also carried out by changing the liquid height.

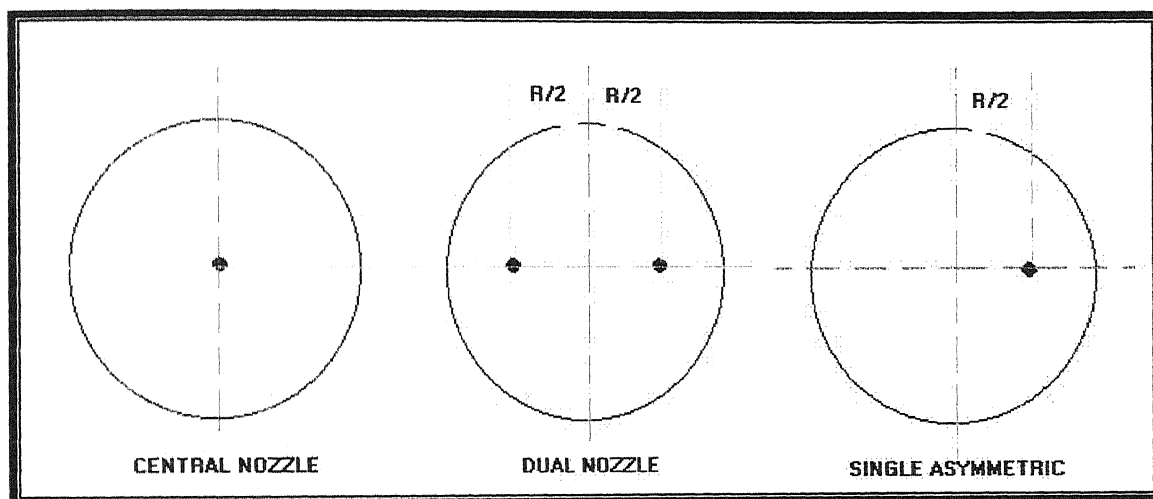


Figure 3.2: Schematic diagram of location of bottom nozzles in model.

3.2.2 Preparation of Liquid

Phase I (i.e., the bulk phase) is an aqueous solution of benzoic acid and is prepared carefully so that for each experiment the nearly same strength of aqueous solution is available. A saturated solution of benzoic acid is made by dissolving 2.32 gm/liter in water and filtering it to obtain a clear solution. The strength of benzoic acid solution is determined by titrating it against (0.02 N) KOH. For this standard oxalic acid and KOH solutions are prepared. A standard solution of KOH cannot be prepared by direct

weighing. So an approximately (0.1 N) solution of KOH is prepared by dissolving 5.6 gm of KOH in one liter of distilled water. Subsequently, 25 ml of the standard oxalic acid is pipetted out into a conical flask and titrated against the prepared KOH solution using phenolphthalein as the indicator. The end point is the first appearance of a permanent pink colour. The experiment is repeated till consecutive concordant values are obtained so as to ascertain the normality of KOH.

$$25 \text{ ml of oxalic acid} = 25.5 \text{ ml of KOH}$$

$$\text{Normality of KOH} = (0.1 \times 25) / 25.4 = 0.0984$$

The solution of KOH thus prepared is diluted 5 times and used for titrating benzoic acid solution. Phase II is a predetermined amount of Mustard oil which was over the benzoic acid solution to act as the upper buoyant slag phase.

3.2.3 Selection of Experimental Variables

The effect of following variables is studied in the present experimental study.

a) Nozzle configuration:

Three different configurations of nozzles for bottom injection are studied in the present investigation. The arrangement is shown in Fig. 4.3.

b) Gas flow rate:

Gas flow rate is varied from 1 l/min to 6 l/min. This large range of gas flow rate is taken for better understanding of the two phase behavior. Furthermore such flow rates correspond to the range of gas flow rates practiced in ladle refining operations

c) Slag depths:

Three different slag depths of 1cm, 3cm and 5cm, above the liquid phase were employed for the experiments at a constant aspect ratio ($L/D = 1$).

d) Sampling location.

To study the effect of the location of sampling point, samples were taken from three different locations, one from the centre, one from the top and one from the bottom.

3.2.4 Experimental Procedure

In each experiment (e.g., specific operating conditions), transfer rate of benzoic acid from water to oil was measured as a function time. In the beginning, 26.5 lts of water containing 1 - 1.2 gms/lit of benzoic acid is filled in the vessel up to the height of 27 cms. Mustard oil is then gently poured along the side of the vessel over the benzoic acid solution up to 30 mm height. This is approximately equivalent to the steel slag volume ratio encountered in actual practices (normally the slag to metal ratio in ladle treatment is less than 0.1). Air/N₂ is injected at predetermined rate by adjusting the gas tap and stop watch is simultaneously started. After the stirring is started, 25 ml benzoic acid solution samples are taken out of the water using a sampling tube, as a function of time and in some cases as a function of position in the ladle. Depending on the gas flow rates and the slag depths, the sampling times for mass transfer experiments ranged between 30 to 45 mins with 7 to 10 samples taken after the start of the flow. One experiment was continued for a long time (1.5-2 hrs) to determine the equilibrium concentration C_e . The samples were allowed to settle for some time such that any carried over oil can float up. Subsequently, the aspirated sample was filtered (using filter paper) to obtain clear water samples. The sample thus obtained was titrated against the (0.02N) KOH solution using phenolphthalein indicator to exactly determine the concentration of transferring species in the sample. The reproducibility of the results is checked by taking two samples practically simultaneously. Experiments were done for different conditions of gas flow rates, nozzle positions and slag depths as pointed out already. For each experiment fresh solutions of benzoic acid and mustard oil were used.

3.2.5 Mass Balance on Tracer: The Governing Equation

From the principle of conservation of mass, the change in the concentration of solute benzoic acid) in aqueous solution is (for explanation, see list of symbols).....

$$\frac{dC_t}{dt} = - \frac{m_T}{V_w} \quad (3.1)$$

$$C_t = m / V_w \quad (3.2)$$

By linear expression, the irreversible mass flux is mostly combined with the corresponding thermodynamic forces.

$$m = L (C_t - C_e) \quad (3.3)$$

$$L = \beta_m A \quad (3.4)$$

Using equations (3.1) and (3.3) and integrating with initial condition $C_t (t = 0) = C_0$ yields

$$C_t = C_e + (C_0 - C_e) \exp\left(-\frac{Lt}{V_w}\right) \quad (3.5)$$

By equating (3.5),

$$L = \frac{V_w}{t} \ln \frac{(C_t - C_e)}{(C_0 - C_e)} \quad (3.6)$$

$$\ln \frac{(C_t - C_e)}{(C_0 - C_e)} = - \frac{Lt}{V_w} \quad (3.7)$$

Where, C_t = Concentration at time t

C_0 = Initial Concentration

C_e = Equilibrium Concentration

A = Interfacial Area

V_w = Volume of Water

t = Time

β = Mass Transfer Coefficient.

m = Mass

m_T = Mass Flow rate

So,

$$\ln \frac{(C_t - C_e)}{(C_o - C_e)} = -K t \quad (3.8)$$

$$K = \frac{\beta_m A}{V_w} = \text{Rate Constant} \quad (3.9)$$

A principal difficulty in this type of representation is that the actual slag-metal interfacial area (A) is many times larger than the planner surface area due to unevenness of the interface formation in such gas agitated slag-metal systems. A is a function of gas flow rate, etc. Moreover, it is a difficult task to properly determine A . Hence, experimental rate measurement yields the value of the βA parameter, where β is specific rate constant. When mass transfer is rate controlling, then $\beta = \beta_m$ and we obtain the βA parameter on the basis of Eq. (3.9). βA has a dimension of ($\text{ms}^{-1} \times \text{m}^2$), i.e., $\text{m}^3 \text{s}^{-1}$. Sometimes the K parameter of dimension $(\beta A/V) \text{ s}^{-1}$ is preferred, where V is the volume of the concerned liquid. Equation (3.9) can be used to determine the rate constant (K) at known equilibrium concentration C_e by measuring the concentration C_t in dependence of the time. K value provides an idea of the rate of tracer transport from the bulk aqueous phase to the upper buoyant phase and therefore yields a measure of how well or bad the phases are stirred.

3.3

MASS TRANSFER EXPERIMENTAL RESULTS

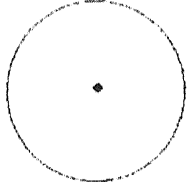
The mass transfer between two immiscible liquids, oil and water simulating slag and steel respectively was measured in a scale model of a ladle. The mass transfer rate was measured as a function of common design parameters used in actual steel making such as gas flow rate and nozzle position. Some experiments were also done for varying slag depths.

Volume of aqueous phase = 26.5 lts (up to 27 cm height)

Volume of oil phase = 2lts (up to 3.0 cm height above the aqueous level)

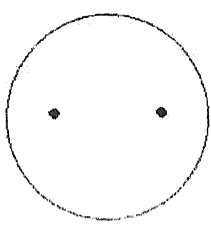
Volume of aqueous phase sample collected at different intervals = 25 ml

Table 3.2: Change in concentration of aqueous phase with time at different gas flow rates for gas injection through central nozzle.

Experimental conditions	Time (min)	Vol of KOH used (ml)	Wt of acid per liter bath (gm)	(Ct / Co)
1 LPM 	0	11.4	1.022534	1
	5	11.2	1.004595	0.982456
	10	11	0.986656	0.964912
	15	10.8	0.968717	0.947368
	20	10.7	0.959747	0.938596
	25	10.4	0.932838	0.912281
	30	10.3	0.923869	0.903509
	35	10.1	0.90593	0.885965
	40	9.9	0.88799	0.868421
	45	9.8	0.879021	0.859649
2 LPM	0	11.6	1.040474	1
	5	11.1	0.995626	0.956897
	10	10.9	0.977686	0.939655
	15	10.7	0.959747	0.922414
	20	10.5	0.941808	0.905172
	25	10.3	0.923869	0.887931
	30	10.2	0.914899	0.87931
	35	10	0.89696	0.862069
	40	9.7	0.870051	0.836207
	45	9.6	0.861082	0.827586

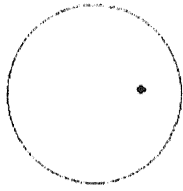
3 LPM	0	11.6	1.040474	1
	5	10.8	0.968717	0.931034
	10	10.5	0.941808	0.905172
	15	10.3	0.923869	0.887931
	20	10.1	0.90593	0.87069
	25	9.9	0.88799	0.853448
	30	9.8	0.879021	0.844828
	35	9.6	0.861082	0.827586
	40	9.4	0.843142	0.810345
	45	9.3	0.834173	0.801724
<hr/>				
4 LPM	0	12.1	1.085322	1
	5	11.2	1.004595	0.92562
	10	10.5	0.941808	0.867769
	15	9.9	0.88799	0.818182
	20	9.5	0.852112	0.785124
	25	9.3	0.834173	0.768595
	30	9.1	0.816234	0.752066
	35	8.9	0.798294	0.735537
	40	8.7	0.780355	0.719008
	45	8.6	0.771386	0.710744
<hr/>				
5 LPM	0	13.4	1.201926	1
	5	11.7	1.049443	0.873134
	10	10.5	0.941808	0.783582
	15	9.7	0.870051	0.723881
	20	9.3	0.834173	0.69403
	25	8.9	0.798294	0.664179
	30	8.7	0.780355	0.649254
	35	8.6	0.771386	0.641791
	40	8.4	0.753446	0.626866
	45	8.3	0.744477	0.619403
<hr/>				
6 LPM	0	12.9	1.157078	1
	5	11.1	0.995626	0.860465
	10	9.9	0.88799	0.767442
	15	8.9	0.798294	0.689922
	20	8.5	0.762416	0.658915
	25	8.3	0.744477	0.643411
	30	8.1	0.726538	0.627907
	35	7.9	0.708598	0.612403
	40	7.8	0.699629	0.604651
	45	7.7	0.690659	0.596899

Table 3.3: Change in concentration of aqueous phase with time at different gas flow rates for gas injection through dual nozzle.

Experimental conditions	Time (min)	Vol of KOH used (ml)	Wt of acid per liter bath (gm)	(Ct / Co)
2 LPM 	0	11.4	1.022534	1
	5	11	0.986656	0.964912
	10	10.8	0.968717	0.947368
	15	10.7	0.959747	0.938596
	20	10.4	0.932838	0.912281
	25	10.3	0.923869	0.903509
	30	10.1	0.90593	0.885965
	35	10	0.89696	0.877193
	40	9.8	0.879021	0.859649
	45	9.7	0.870051	0.850877
3 LPM	0	11.5	1.031504	1
	5	10.9	0.977686	0.947826
	10	10.6	0.950778	0.921739
	15	10.4	0.932838	0.904348
	20	10.2	0.914899	0.886957
	25	10.1	0.90593	0.878261
	30	9.9	0.88799	0.86087
	35	9.8	0.879021	0.852174
	40	9.6	0.861082	0.834783
	45	9.5	0.852112	0.826087
4 LPM	0	13.6	1.219866	1
	5	12.7	1.139139	0.933824
	10	11.9	1.067382	0.875
	15	11.3	1.013565	0.830882
	20	11	0.986656	0.808824
	25	10.9	0.977686	0.801471
	30	10.7	0.959747	0.786765
	35	10.6	0.950778	0.779412
	40	10.4	0.932838	0.764706
	45	10.3	0.923869	0.757353
5 LPM	0	12.1	1.085322	1
	5	11.1	0.995626	0.917355
	10	10.2	0.914899	0.842975
	15	9.6	0.861082	0.793388
	20	9.3	0.834173	0.768595
	25	8.7	0.780355	0.719008
	30	8.4	0.753446	0.694215
	35	8.2	0.735507	0.677686

	40	8	0.717568	0.661157
	45	7.9	0.708598	0.652893
6 LPM	0	11.5	1.031504	1
	5	10.3	0.923869	0.895652
	10	9.1	0.816234	0.791304
	15	8.8	0.789325	0.765217
	20	8.5	0.762416	0.73913
	25	8.1	0.726538	0.704348
	30	7.8	0.699629	0.678261
	35	7.6	0.68169	0.66087
	40	7.4	0.66375	0.643478
	45	7.3	0.654781	0.634783

Table 3.4: Change in concentration of aqueous phase with time at different gas flow rates for gas injection through single asymmetric nozzle.

Experimental conditions	Time (min)	Vol of KOH used (ml)	Wt of acid per liter bath (gm)	(Ct / Co)
1 LPM 	0	11.6	1.040474	1
	5	11.3	1.013565	0.974138
	10	11.3	1.013565	0.974138
	15	11.1	0.995626	0.956897
	20	11	0.986656	0.948276
	25	10.9	0.977686	0.939655
	30	10.8	0.968717	0.931034
	35	10.6	0.950778	0.913793
	40	10.4	0.932838	0.896552
	45	10.3	0.923869	0.887931
2 LPM	0	12.3	1.103261	1
	5	11.9	1.067382	0.96748
	10	11.7	1.049443	0.95122
	15	11.5	1.031504	0.934959
	20	11.4	1.022534	0.926829
	25	11.2	1.004595	0.910569
	30	10.9	0.977686	0.886179
	35	10.8	0.968717	0.878049
	40	10.8	0.968717	0.878049
	45	10.7	0.959747	0.869919

3 LPM	0	11.3	1.013565	1
	5	10.8	0.968717	0.955752
	10	10.7	0.959747	0.946903
	15	10.4	0.932838	0.920354
	20	10.2	0.914899	0.902655
	25	9.9	0.88799	0.876106
	30	9.7	0.870051	0.858407
	35	9.6	0.861082	0.849558
	40	9.6	0.861082	0.849558
	45	9.5	0.852112	0.840708
4 LPM	0	11.9	1.067382	1
	5	11.3	1.013565	0.94958
	10	10.7	0.959747	0.89916
	15	10.3	0.923869	0.865546
	20	10	0.89696	0.840336
	25	9.7	0.870051	0.815126
	30	9.5	0.852112	0.798319
	35	9.4	0.843142	0.789916
	40	9.2	0.825203	0.773109
	45	9.1	0.816234	0.764706
5 LPM	0	14.4	1.291622	1
	5	13.3	1.192957	0.923611
	10	12.2	1.094291	0.847222
	15	11.5	1.031504	0.798611
	20	10.9	0.977686	0.756944
	25	10.7	0.959747	0.743056
	30	10.4	0.932838	0.722222
	35	10.3	0.923869	0.715278
	40	10.1	0.90593	0.701389
	45	9.9	0.88799	0.6875
6 LPM	0	13.5	1.210896	1
	5	12.1	1.085322	0.896296
	10	11.3	1.013565	0.837037
	15	10.5	0.941808	0.777778
	20	9.9	0.88799	0.733333
	25	9.5	0.852112	0.703704
	30	9.3	0.834173	0.688889
	35	9.1	0.816234	0.674074
	40	9	0.807264	0.666667
	45	8.9	0.798294	0.659259

Table 3.5: Change in concentration of aqueous phase with time at different gas flow rates for gas injection through central nozzle at 1 cm slag depth.

Experimental conditions	Time (min)	Vol of KOH used (ml)	Wt of acid per liter bath (gm)	(Ct / Co)
3 LPM	0	11.8	1.058413	1
	5	11.5	1.031504	0.974576
	10	11.3	1.013565	0.957627
	15	11.2	1.004595	0.949153
	20	11	0.986656	0.932203
	25	10.8	0.968717	0.915254
	30	10.7	0.959747	0.90678
	35	10.5	0.941808	0.889831
	40	10.3	0.923869	0.872881
	45	10.2	0.914899	0.864407
6 LPM	0	12.4	1.11223	1
	5	11.1	0.995626	0.895161
	10	10.2	0.914899	0.822581
	15	9.7	0.870051	0.782258
	20	9.5	0.852112	0.766129
	25	9.1	0.816234	0.733871
	30	8.9	0.798294	0.717742
	35	8.6	0.771386	0.693548
	40	8.5	0.762416	0.685484
	45	8.3	0.744477	0.669355

Table 3.6: Change in concentration of aqueous phase with time at different gas flow rates for gas injection through central nozzle at 5 cm slag depth.

Experimental conditions	Time (min)	Vol of KOH used (ml)	Wt of acid per liter bath (gm)	(Ct / Co)
3 LPM	0	12.2	1.094291	1
	5	11.1	0.995626	0.909836
	10	10.4	0.932838	0.852459
	15	9.9	0.88799	0.811475
	20	9.8	0.879021	0.803279
	25	9.5	0.852112	0.778689
	30	9.4	0.843142	0.770492
	35	9.1	0.816234	0.745902
	40	8.9	0.798294	0.729508
	45	8.8	0.789325	0.721311

6 LPM	0	12.6	1.13017	1
	5	10.5	0.941808	0.833333
	10	9.4	0.843142	0.746032
	15	8.4	0.753446	0.666667
	20	7.9	0.708598	0.626984
	25	7.6	0.68169	0.603175
	30	7.4	0.66375	0.587302
	35	7.1	0.636842	0.563492
	40	6.8	0.609933	0.539683
	45	6.5	0.583024	0.515873

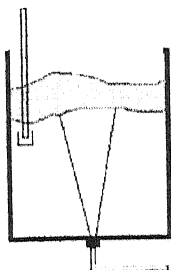
Table 3.7: Change in concentration of aqueous phase with time at different gas flow rates for gas injection through dual nozzle at 1 cm slag depth.

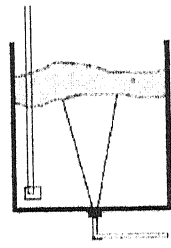
Experimental conditions	Time (min)	Vol of KOH used (ml)	Wt of acid per liter bath (gm)	(Ct / Co)
3 LPM	0	11.1	0.995626	1
	5	10.7	0.959747	0.963964
	10	10.5	0.941808	0.945946
	15	10.2	0.914899	0.918919
	20	10.1	0.90593	0.90991
	25	9.9	0.88799	0.891892
	30	9.8	0.879021	0.882883
	35	9.8	0.879021	0.882883
	40	9.7	0.870051	0.873874
	45	9.6	0.861082	0.864865
6 LPM	0	13.1	1.175018	1
	5	12.3	1.103261	0.938931
	10	11.6	1.040474	0.885496
	15	11.2	1.004595	0.854962
	20	10.9	0.977686	0.832061
	25	10.5	0.941808	0.801527
	30	10.3	0.923869	0.78626
	35	9.9	0.88799	0.755725
	40	9.9	0.88799	0.755725
	45	9.8	0.879021	0.748092

Table 3.8: Change in concentration of aqueous phase with time at different gas flow rates for gas injection through dual nozzle at 5 cm slag depth.

Experimental conditions	Time (min)	Vol of KOH used (ml)	Wt of acid per liter bath (gm)	(Ct / Co)
3 LPM	0	11.9	1.067382	1
	5	11.3	1.013565	0.94958
	10	10.7	0.959747	0.89916
	15	10.4	0.932838	0.87395
	20	10.3	0.923869	0.865546
	25	10.1	0.90593	0.848739
	30	9.8	0.879021	0.823529
	35	9.6	0.861082	0.806723
	40	9.5	0.852112	0.798319
	45	9.5	0.852112	0.798319
6 LPM	0	12.3	1.103261	1
	5	10.6	0.950778	0.861789
	10	9.7	0.870051	0.788618
	15	9.2	0.825203	0.747967
	20	8.6	0.771386	0.699187
	25	8.3	0.744477	0.674797
	30	7.9	0.708598	0.642276
	35	7.7	0.690659	0.626016
	40	7.7	0.690659	0.626016
	45	7.5	0.67272	0.609756

Table 3.9: Change in concentration of aqueous phase with time at different gas flow rates for gas injection through central nozzle at different sampling positions.

Experimental conditions 3 LPM	Time (min)	Vol of KOH used (ml)	Wt of acid per liter bath (gm)	(Ct / Co)
SAMPLING FROM TOP 	0	11.6	1.040474	1
	5	10.8	0.968717	0.931034
	10	10.4	0.932838	0.896552
	15	10.1	0.90593	0.87069
	20	9.9	0.88799	0.853448
	25	9.8	0.879021	0.844828
	30	9.8	0.879021	0.844828
	35	9.5	0.852112	0.818966
	40	9.3	0.834173	0.801724
	45	9.2	0.825203	0.793103

SAMPLING FROM BOTTOM 	0	11.6	1.040474	1
	5	11	0.986656	0.948276
	10	10.6	0.950778	0.913793
	15	10.2	0.914899	0.87931
	20	10	0.89696	0.862069
	25	9.8	0.879021	0.844828
	30	9.7	0.870051	0.836207
	35	9.5	0.852112	0.818966
	40	9.4	0.843142	0.810345
	45	9.4	0.843142	0.810345

3.4 DISCUSSION OF RESULTS

All the results of the change in concentration of benzoic acid with respect to time for various experimental conditions reported in Table 3.2 to 3.7. were subjected to rigorous analysis to determine the influence of operating parameters on the rate of interfacial mass transfer. Evidently, the experimental results suggest that the transfer of benzoic acid from water to oil dependent on gas injection rate, slag depth and the location of the gas injecting nozzle. A detailed analysis of the results is presented below.

3.4.1 Effect of Gas Flow Rate on Mass Transfer

Figure 3.3 shows the variation of fractional concentration (C_t / C_o) of benzoic acid in water resulting due to its transfer to 2lts of oil (Volume fraction of model slag = ϕ = (Volume of model slag / Volume of model bath) = 0.1) vs. time for various gas injection rates through central nozzle. It is to be noted that by plotting (C_t / C_o) against time, it is relatively convenient to assess the rate of interfacial transport and thus compare rates among various configurations. It can be seen from the figure that as the flow rate increases C_t / C_o decreases which implies increased transfer of benzoic acid to the upper phase (oil) This is to be expected since increased gas flow rates causes better stirring (in terms of bulk flow and turbulence in the bulk phase) The decrease in the ratio C_t / C_o is uniform at lower gas injection rates (<3 l/min). At gas injection rates above this the decrease in C_t / C_o is faster initially (up to 15 min) and then the ratio starts to level off. It is evident from the figure that for higher gas flow rate after some time there is no more transfer of benzoic acid from water to oil as the equilibrium is tends to be achieved. To further check that whether there is more transfer of benzoic acid, sample has been taken after 1 hr, 1.5 hr and 2 hr after the start of the experiment. Equilibrium value of the concentration was found to be 0.5382 gm/lts at 3cm slag depth.

Similar types of plots were obtained with other nozzle configurations. Figure 3.4 and 3.5 shows the variation of fractional concentration (C_t / C_o) of benzoic acid in water vs. time for various gas injection rates through dual nozzle and asymmetric nozzle configurations

respectively. Although the individual concentration profile for all the configurations is same, the central nozzle injection shows faster two phase mass transfer at higher flow rates.

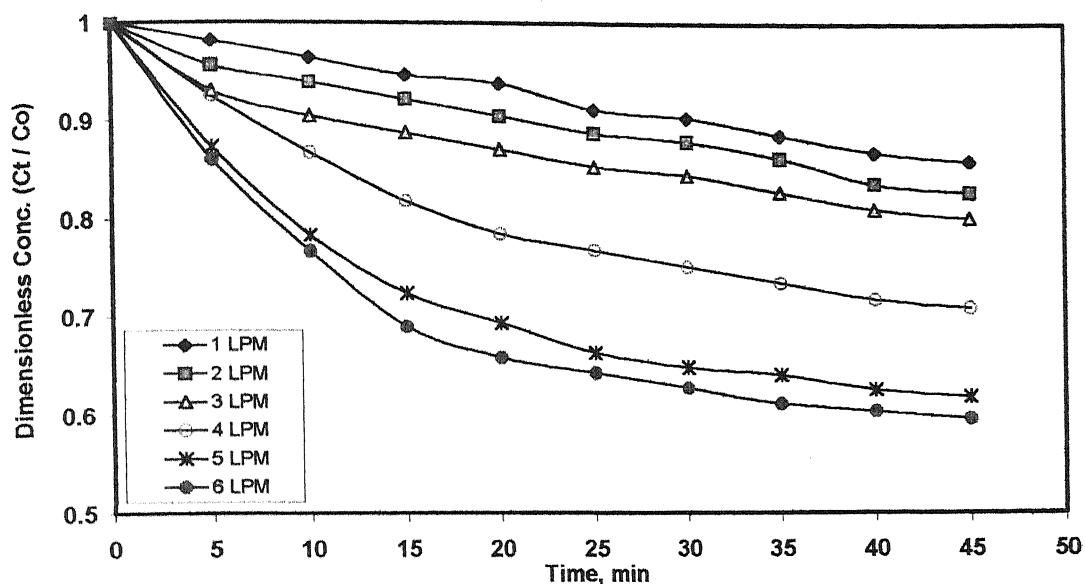


Figure 3.3: Fractional change of concentration of benzoic acid in water as a function of time for gas injection through central nozzle.

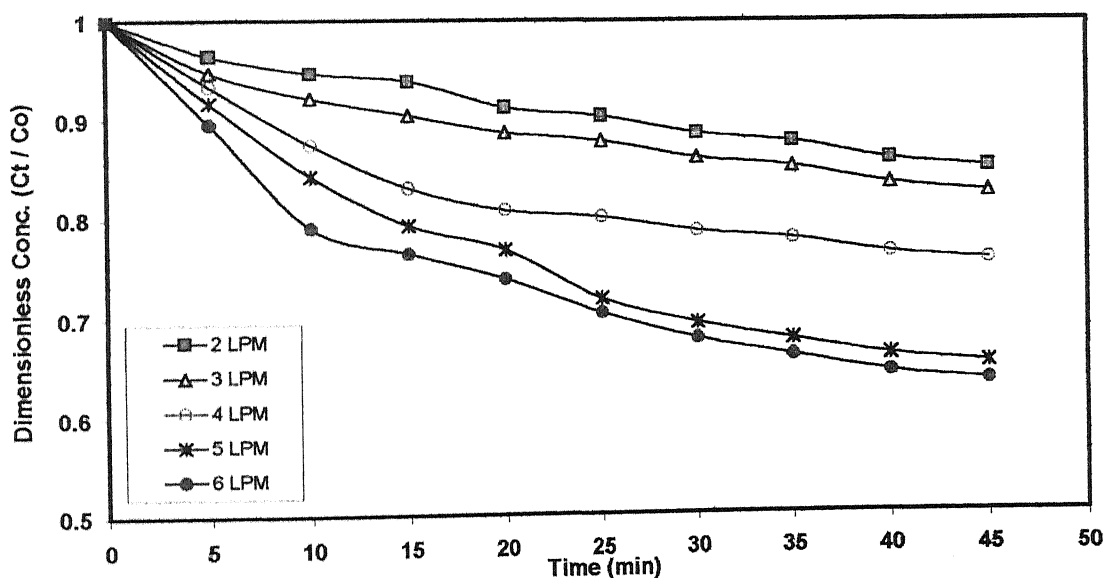


Figure 3.4: Fractional change of concentration of benzoic acid in water as a function of time for gas injection through dual nozzle.

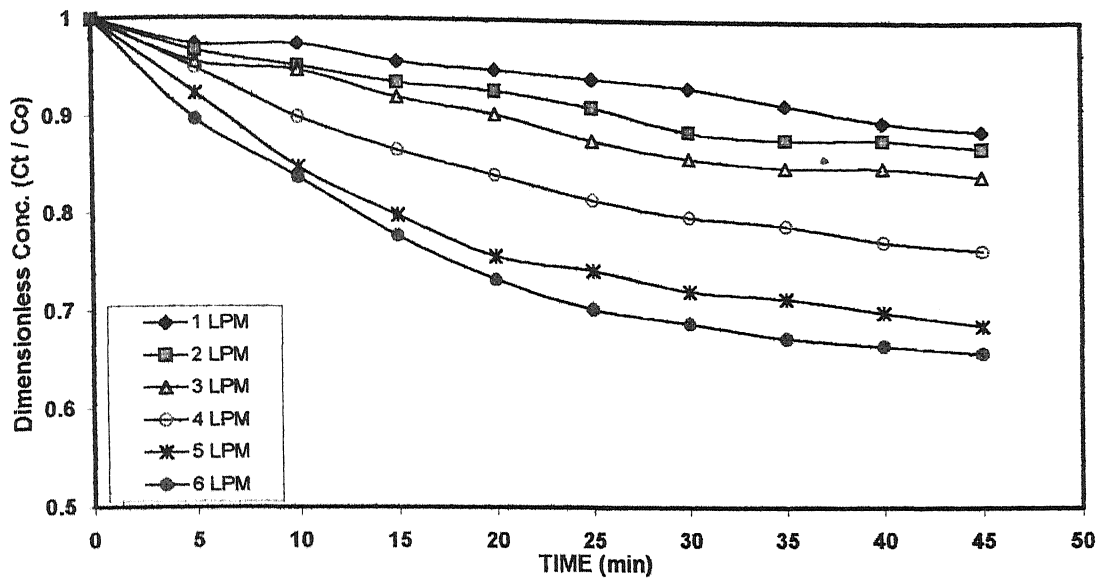


Figure 3.5: Fractional change of concentration of benzoic acid in water as a function of time for gas injection through single asymmetric nozzle.

3.4.2 Determination of Rate Constant

The process of mass transfer between two immiscible liquids can be described by the following first order rate expression [44, 46].

$$\ln \frac{(C_t - C_e)}{(C_o - C_e)} = - \frac{\beta A}{V_w} t \quad (3.10)$$

$$- \ln \frac{(C_t - C_e)}{(C_o - C_e)} = - K t \quad (3.11)$$

Where

$$K = \beta A / V_w \quad (3.12)$$

According to equation (3.10) or (3.11), a plot of $\ln[(C_t - C_e) / (C_o - C_e)]$ against time is linear with slope K . Figures 3.6 to 3.8 show typical semi logarithmic plots of $[(C_t - C_e) / (C_o - C_e)]$ vs. time for different nozzle configurations. The experimental results agree closely with equation (4.14), which suggests that the process of mass transfer is indeed

first order and controlled by the liquid phase mass transfer resistance. The plots show the straight lines, the slopes of which gives value for the rate constant 'K'. It can be derived from the plots 3.6 to 3.8 that the value of K increases with increases in gas injection rate for all configurations which is to be expected.

It can seen from the figures that the Eq. 3.11 describes very well the results of the present investigation which suggests that film diffusion of benzoic acid from water to oil phase is rate controlling step. In this connection it must be noted that film diffusion processes are accelerated by stirring, since stirring enhances velocity and turbulence in the system which in turn enhances the over all transport. The value of the rate constant determines the rapidity of the transfer and therefore, in the following sections, experimental results are visualized in terms of rate constant 'K', determined from Figs. 3.6 to 3.8. Thus $-\ln[(C_t - C_e) / (C_o - C_e)]$ (LHS of the equation 3.11) is plotted as a function of time for injection through a centre, dual and asymmetric nozzles respectively.

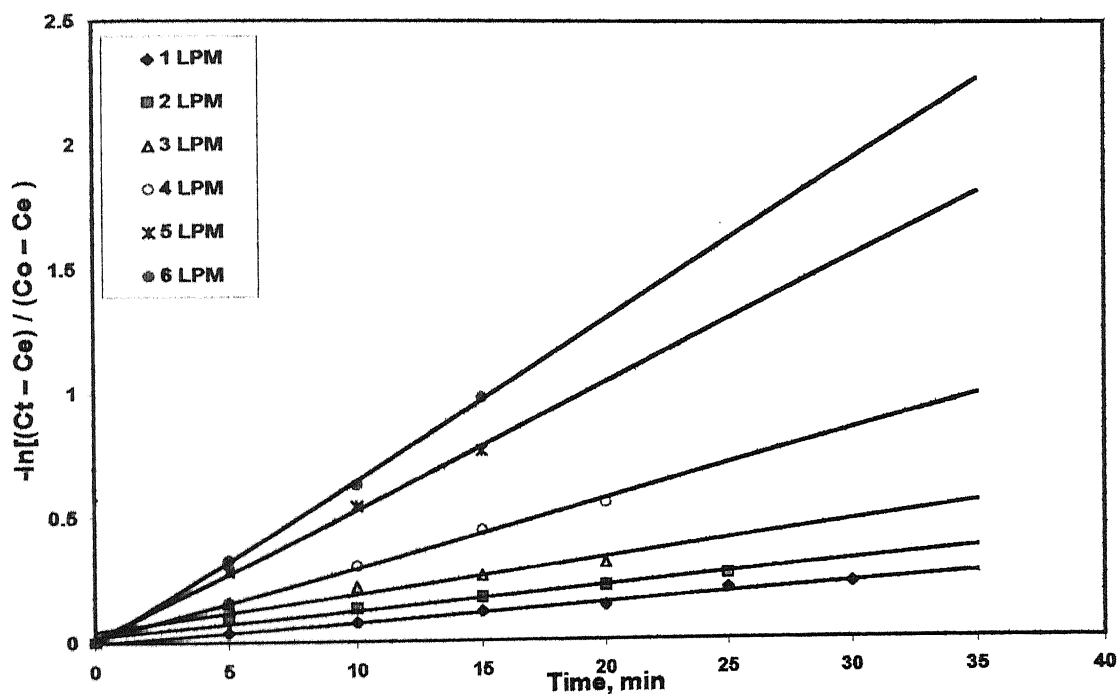


Figure 3.6: Relationship between $-\ln[(C_t - C_e) / (C_o - C_e)]$ and time for central nozzle injection.

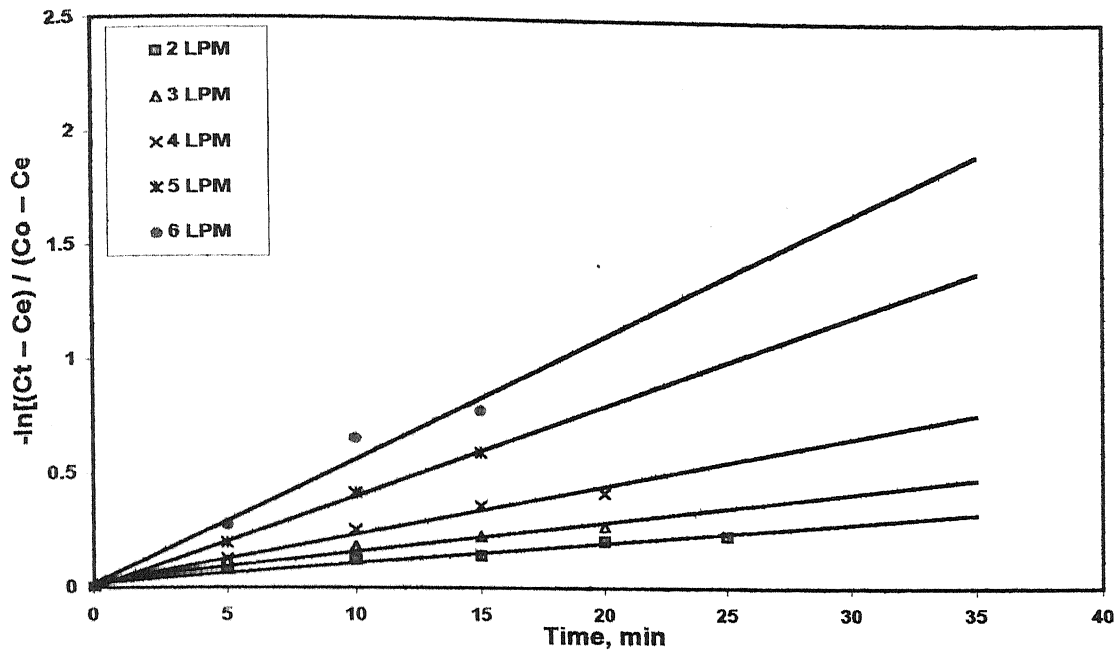


Figure 3.7: Relationship between $-\ln[(C_t - C_e) / (C_o - C_e)]$ and time for dual nozzle injection.

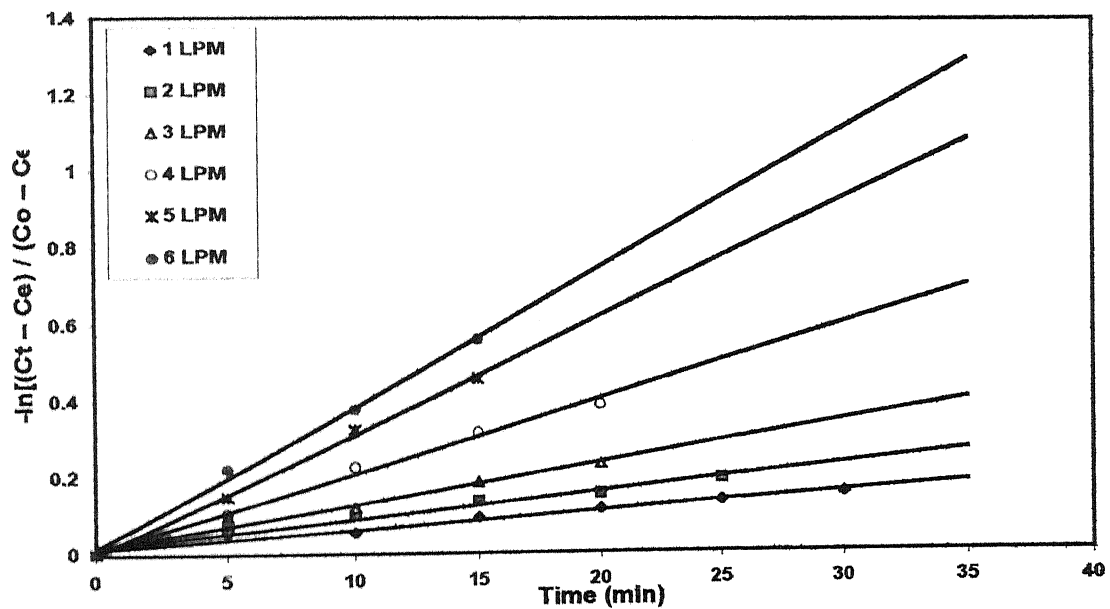


Figure 3.8: Relationship between $-\ln[(C_t - C_e) / (C_o - C_e)]$ and time for single asymmetric nozzle injection.

	MASS TRANSFER PARAMETER, min ⁻¹		
Flow Rate	Central Nozzle	Dual Nozzle	Single asymmetric nozzle
1	0.0077		0.0048
2	0.0099	0.0088	0.0072
3	0.0147	0.0129	0.0111
4	0.028	0.0214	0.0197
5	0.0513	0.0398	0.031
6	0.0649	0.0542	0.0367

Table 3.10: Values of Mass transfer parameter K for different gas injection configurations.

All the values of Mass transfer parameter K for different nozzle configurations are listed in Table 3.10. These values thus derived from the slopes of the lines drawn in Fig.3.6 to Fig 3.8 are analyzed in the following sections.

3.4.3 Effect of Gas Flow rate on Mass Transfer Parameter

Fig. 3.9 shows a plot of mass transfer parameter 'K' as a function of gas flow rate for centre nozzle injection. The mass transfer parameter, increases slowly for increasing flow rate for low flows. There is an abrupt increase on 'K' at higher flow rates (> 3 lpm). A different behavior of interaction between oil and water phases was visually observed with increasing flow rate.

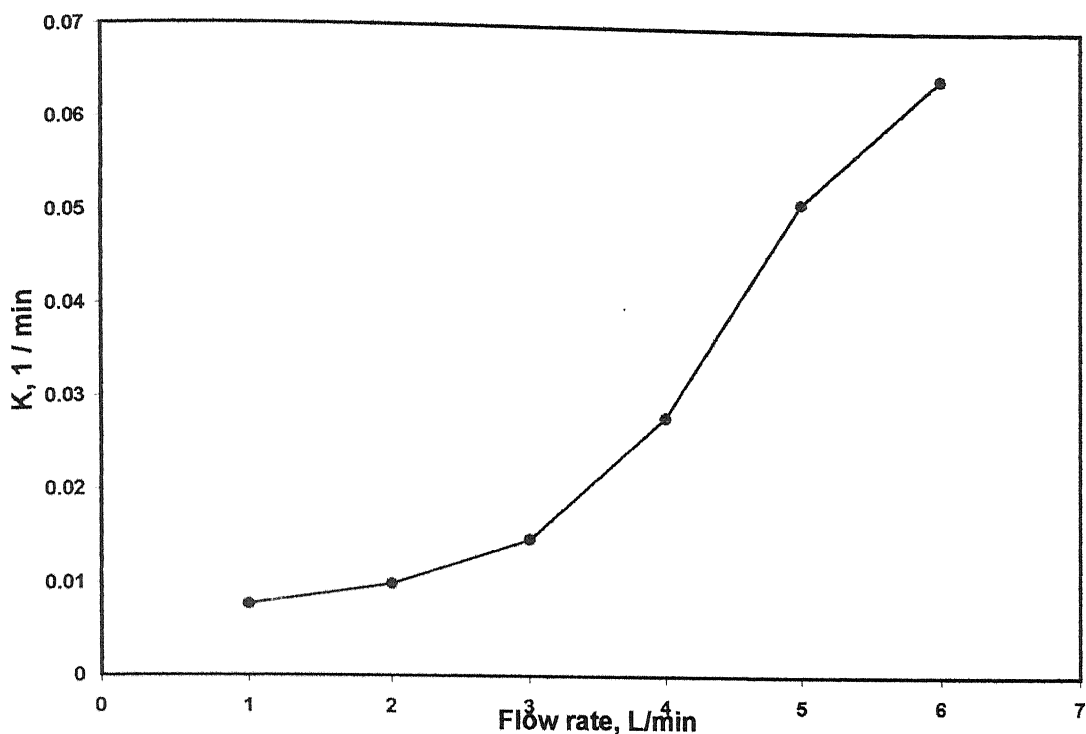


Figure 3.9: Plot of mass transfer parameter, K as a function of gas flow rate for central nozzle injection.

The mass transfer rate is a weak function of flow rate in at low values where the oil layer is very calm, no oil droplets are driven into water, and interface between oil and water phases is close to planar surface except for the very weak wave motion of the interface near the edge of plume eye. The abrupt change in the value of ' K ' at higher flow rate can be explained by observation that the oil layer near the edge of a plume eye continuously forms oil ligaments and then breaks up into more and more droplets which are entrained into water. This phenomenon increases the oil/water interfacial area. At further higher flow rates, nearly the entire oil layer breaks down into oil droplets and the penetration of these oil droplets deep into the water bath occurs. The effect of stronger agitation on the mass transfer rate begins to decrease because the size and number of oil droplets approach steady state. The recirculation and entraining depth of the oil droplets in the liquid bath are the major parameters increasing the mass transfer. Similar trends were observed in previous mass transfer studies [29,35,44].

3.4.4 Effect of Nozzle Configuration

The nozzle position was changed to three different configurations to investigate the effect on mass transfer. The values of K , mass transfer parameter are plotted as a function of gas flow rate for injection through a centre, dual and asymmetric nozzle as shown in Fig 3.11. For gas flow rates below 3 lpm, not much difference in K for three different nozzle arrangements was observed. However, above 3 lpm, centre nozzle arrangement gives faster mass transfer than the other two arrangements. Similar trends were observed in literature and the apparent reason for this is shown schematically in Fig 3.10.

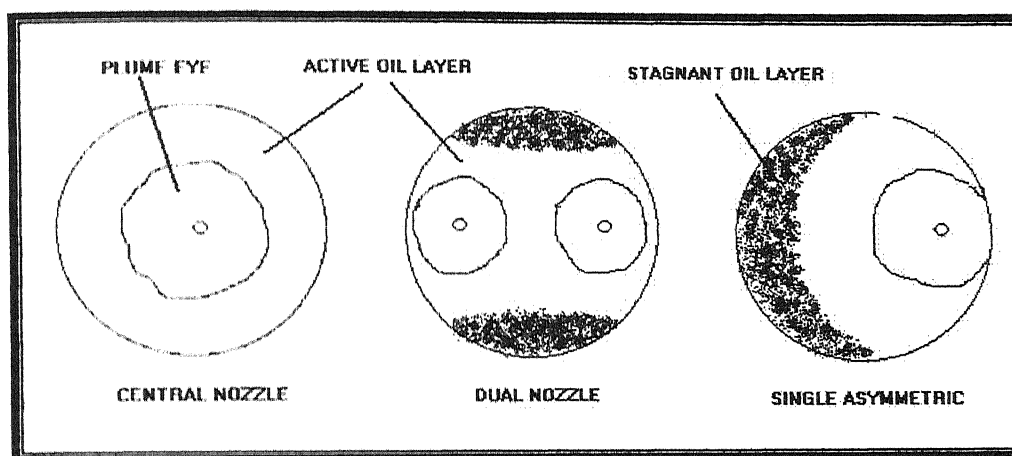


Figure 3.10: A schematic diagram of top views of oil layer during gas injection of high gas flow rates according to the different arrangements of nozzles.

As the mass transfer phenomena is dependent on interfacial area and in case of an off centre arrangements, the oil layer near the vessel wall on the opposite side of the nozzle is not much affected by the gas-liquid plume and the formation of oil droplets starts to appear at much higher gas flow rates because it requires more energy to break down the wider stagnant area of oil at the opposite side of the nozzle position thus having lesser active region as compared to axisymmetric configuration.

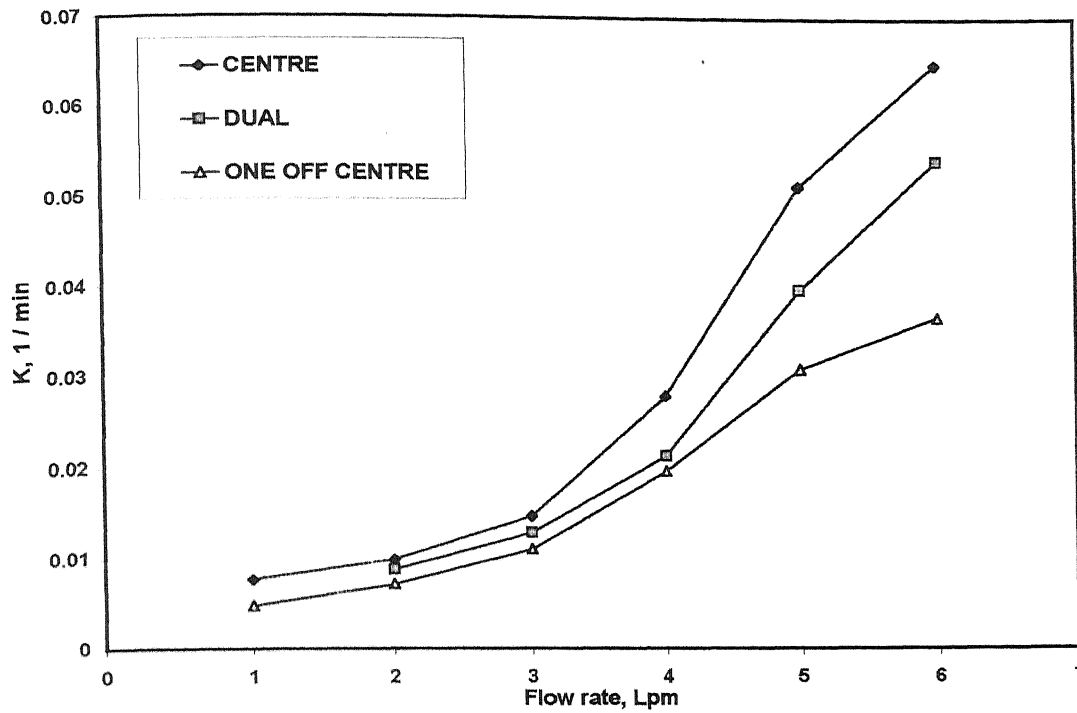


Figure 3.11: Effect of position of a nozzle on the mass transfer parameter.

It was found that mass transfer rate will be fastest for central nozzle arrangement and slowest for asymmetric nozzle arrangement among the three configurations under consideration.

3.4.5 Effect of Oil Volume Fraction

Figure 3.12 and 3.13 shows the effect of slag depths on mass transfer at two different flow rates for central nozzle injection and dual nozzle injection respectively. It can be concluded from the plot that mass transfer is faster at higher slag depths for the same bubbling conditions. The larger amount of oil increases the mass transfer rate by the formation of oil droplets at slightly lower gas flow rates. Also a large oil/water ratio decreases the starting gas flow rate for breaking the oil layer increasing the mass transfer rate. Some of the stirring energy due to the gas injection is consumed in producing turbulence at the interface between two immiscible phases and creating a circulation inside the upper oil phase, which can help break up the upper oil layer.

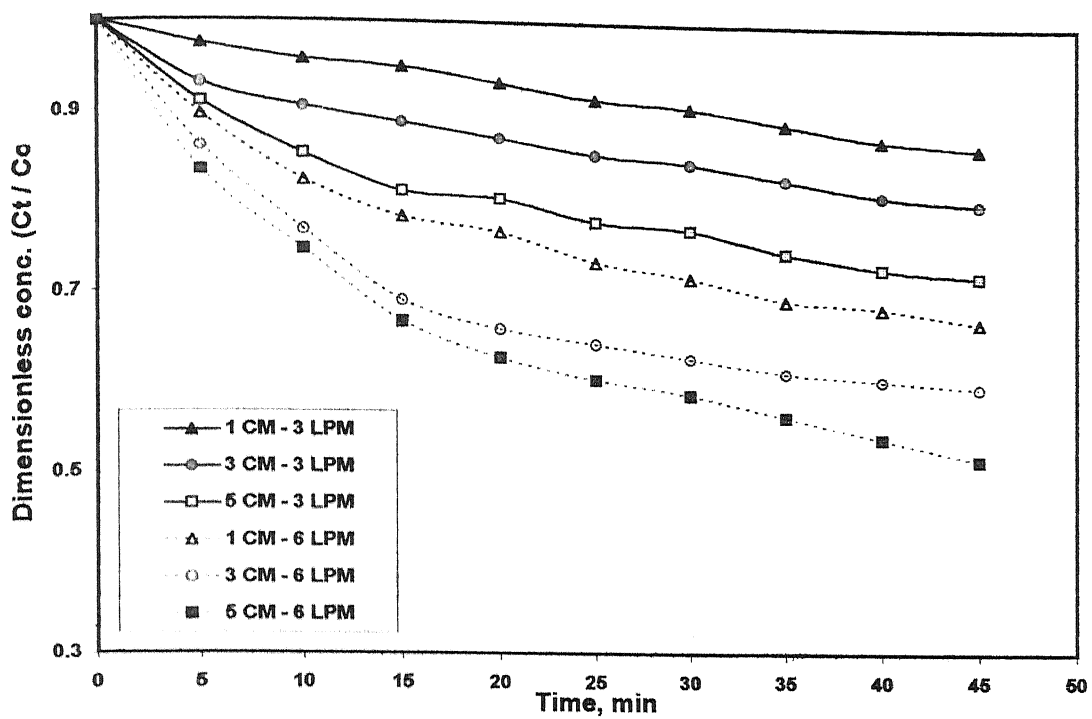


Figure 3.12: Fractional change of concentration of benzoic acid in water as a function of time for different slag depths for central nozzle injection.

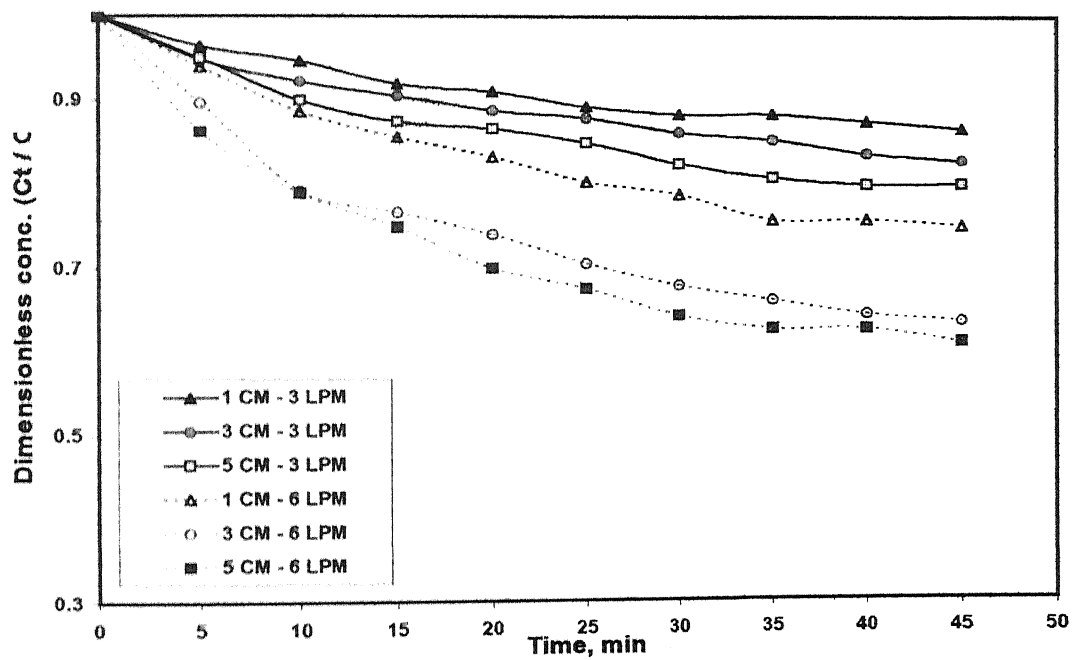


Figure 3.13: Fractional change of concentration of benzoic acid in water as a function of time for different slag depths for dual nozzle injection.

Visual observations indicated that as the oil layer becomes thicker, the oil layer breaks into the droplets more easily due to the formation of more active and stronger circulation inside the oil layer. The mass transfer rate turns out to be very sensitive to the effect of oil volume fraction under conditions tested.

3.4.6 Effect of Location of Sampling on Mass Transfer

To study the effect of the location of sampling point on the transfer of benzoic acid from water to oil phase, samples were drawn from two different places one from top and one from bottom of the bath apart from the usual centre position. Fig 3.14 shows the fractional variation of benzoic acid concentration in the bath with time at three different locations for central nozzle injection at 3 lpm, from which it is evident that the location of the sampling point had no effect on the mass transfer. This also proves that the sample used in this investigation were representative of the entire bath

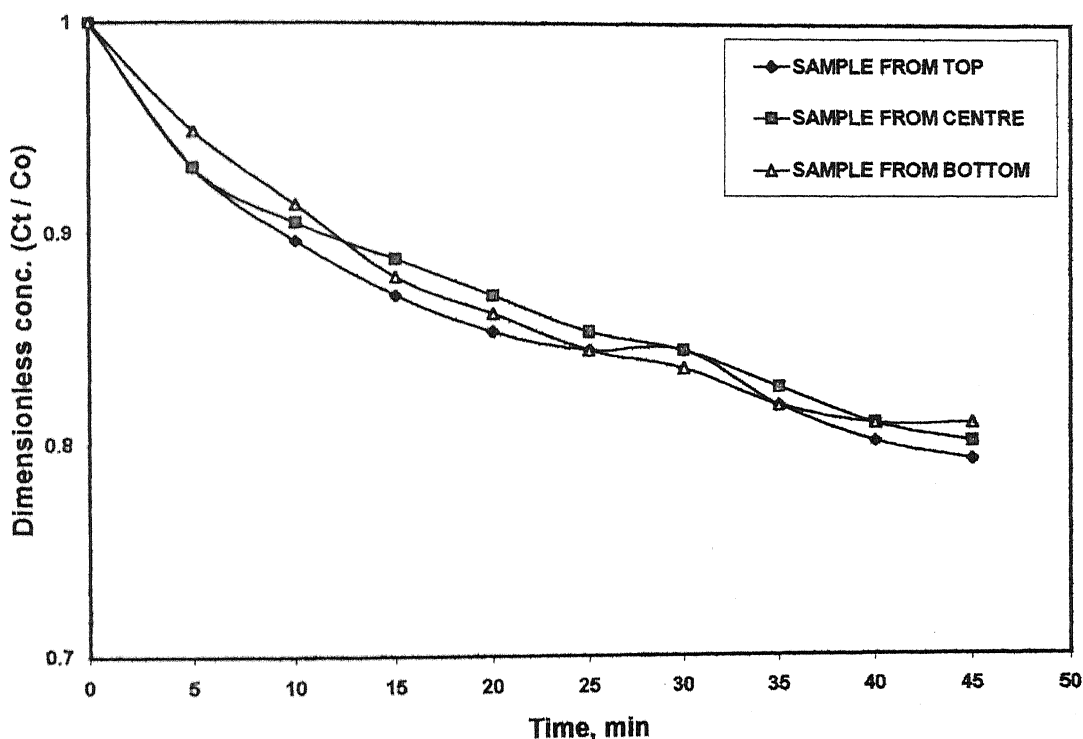


Figure 3.14: Effect of location of sampling point on mass transfer for central nozzle injection.

3.5 MIXING TIME MEASUREMENTS

The intrinsic efficiencies of many chemical processing operations carried out in present day steelmaking ladles are intricately related to mixing phenomena. Mixing enhances chemical reactions by bringing reactants together and removing products from reactant sites. It also influences the extent of thermal and particulate inhomogeneities within the ladle. It is therefore desirable to ascertain the extent of mixing, in order to evaluate the process performance of argon or nitrogen stirred ladles. Although it is desirable to measure the mixing time directly in high temperature melts, it is expensive and difficult. To overcome this problem, cold water model studies are often carried out. Towards these, different experimental techniques have been applied, although methods based on pH and electrical conductivity measurements have been relatively more popular. In the present study, electrical conductivity measurement technique was applied to monitor mixing time in a small ($D = 0.30\text{m}$) cylindrical vessel in the presence of an upper buoyant phase. It must be borne into mind that industrial slag metal system can not be simulated in the laboratory using a cold model analogue. This is owing to the large dissimilarities between the interfacial tensions in the high temperature and cold model system. None the less the influence of an upper buoyant phase can be simulated at least qualitatively using a lower density fluid with respect to the bulk aqueous phase. In the present work, mustard oil was used to simulate the industrial slag phase.

3.5.1 Principles of Electrical Conductivity Measurement Technique

Of the various methods reported in the literature for the measurement of mixing time, electrical conductivity measurement technique is perhaps the best [22]. Acid, alkali or salt solution is added as a pulse tracer and change in electrical conductivity recorded against time elapsed. Both pH and electrical conductivity measurement techniques are very similar in measurement techniques, but the later have some unique advantage over the former. The electrical conductivity probe is sturdy and has faster response. Moreover, electrical conductivity varies linearly with the tracer concentration [47]. The electrical conductivity probe can be used for a wide range of homogenization measurements and thus one can easily estimate the mixing time with sufficient reliability. During a typical

measurement, air is injected into the water bath through the nozzle(s) located at the bottom of the vessel at a specified flow rate for 1 to 2 minutes to ensure the stability of flow in the vessel as well as to homogenize the initial bath composition. On addition of KCl solution as a tracer, considerable oscillations in the form of peaks and valleys are recorded via conductivity probe. These peaks and valleys results from the concentration fluctuations at the probe tip arising from inhomogeneities of the tracer concentration in the bath. The fluctuations gradually diminish as the time progress and attain a steady value which is reflected as an almost steady voltage output from the probe. From such mixing times can be determined fairly accurately.

3.6 MIXING TIME EXPERIMENTS

High temperatures, visual opacity of molten steel and massive size of industrial molten steel processing vessels pose difficulties for direct experimental observations. As it is impractical to carry out any elaborate studies in high temperature steel refining ladles, investigators for the last few decades were carrying out mixing time studies on laboratory scale cold models. Results were then scaled up for practical systems. In this present study, mixing times in presence of simulated slag in gas stirred ladle was measured. Air/N₂ was injected through the bottom of cylindrical vessel filled with water using various combinations of nozzle(s) locations and gas flow rates. The present chapter describes the experimental measurements and parameters of mixing times under a wide variety of operating conditions.

3.6.1 The Criterion for determination of mixing times

The mixing phenomenon in metallurgical systems containing molten metal has been normally characterized by “mixing time” [48]. This is defined as the time taken to attain the desired level of mixing or homogenization in the bath. The desired level of homogenization has been defined by Danckwerts [49] in terms of the degree of mixing, which implies the extent of uniformity of composition desired in the final mixture. One more definition given about the mixing time as the time required for a slug of feed solution to be dispersed homogeneously throughout the vessel in a batch operation or in a

continuous flow system. No matter how well a liquid is mixed, there always exists regions of segregation and the composition of each of these regions is different. However, mixing time has mostly been defined in the literature somewhat arbitrarily for a degree of mixing ranging from 75 to 99%. For the present investigation mixing time is defined as the time required for the conductivity to settle within $\pm 5\%$ deviation around its final value. This definition is referred to as the 95% mixing time criterion

3.6.2 Experimental Setup

The schematic representation of laboratory scale experimental set up is shown in Fig 3.15. The experimental set up employed is a cylindrical Perspex vessels having scale factor 0.08 with respect to a full scale ladle of 150 tonne containing water at room temperature. In this vessel, nozzles were fitted at the bottom at various locations to facilitate gas injection into the water bath.

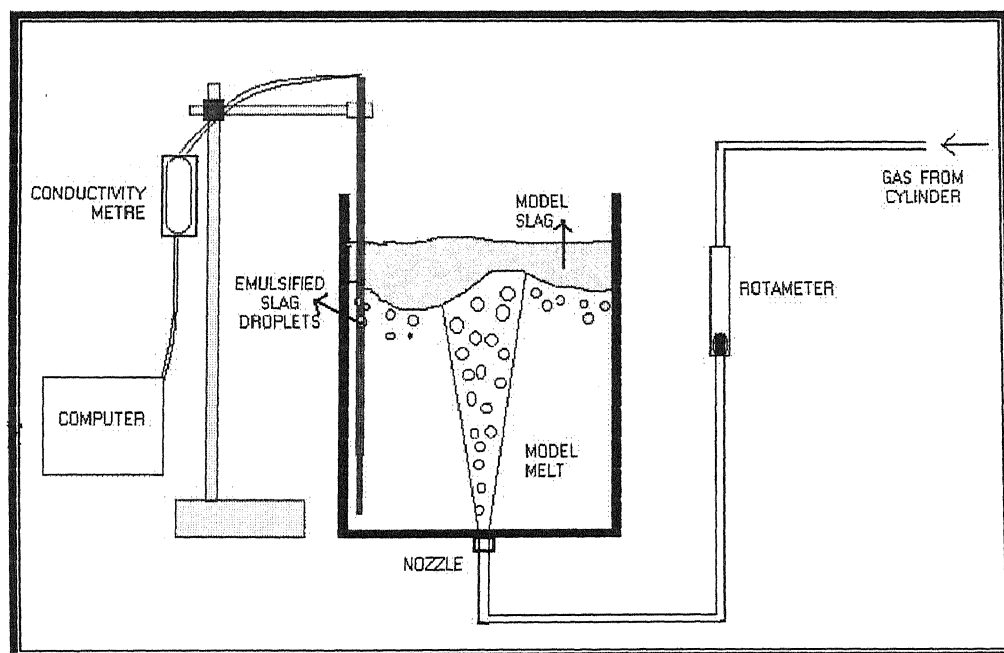


Figure 3.15: A schematic diagram of the experimental setup for mixing time measurements.

Mixing times were measured in the vessel as a function of nozzle configuration and gas flow rate using a EUTECH made CYBERSCAN 200 conductivity meter. Mustard oil

was used for simulating slag. 2 lts of oil was used for every experiment. This is approximately steel slag ratio used in actual practices (normally the slag to metal ratio in ladle treatment is less than 0.1). The probe was located at a dimensionless position of 0.085 above the bottom wall and from the side wall of the ladle. It is assumed that the tip of the probe was kept in the slowest mixing region so that measured 95% mixing times could be interpreted as bulk mixing times [50].

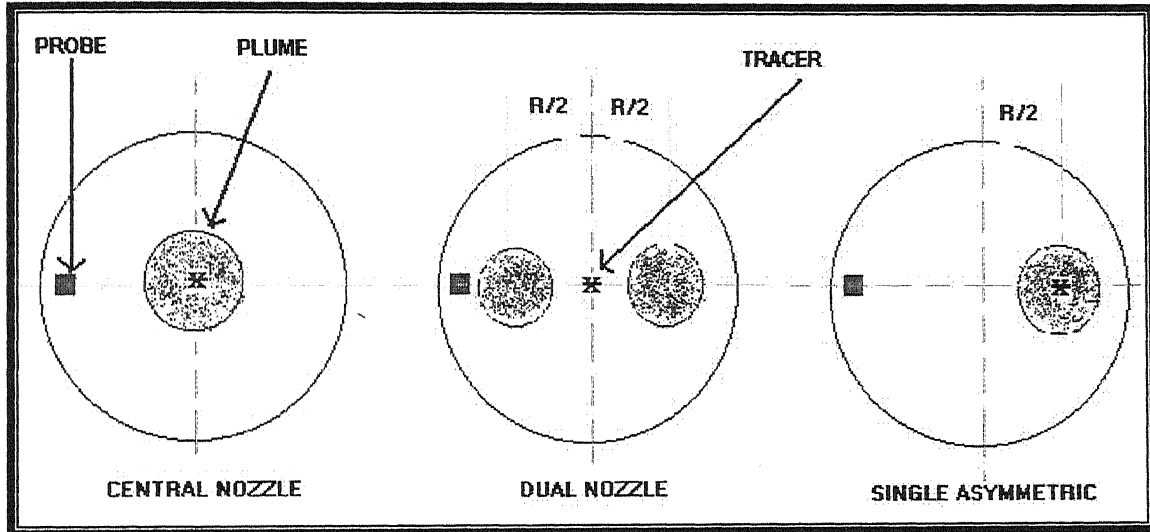


Figure 3.16: Location of tracer additions with respect to nozzle configuration.

The recording of the pulse tracer response was carried out until the concentration of the entire water bath was considered to have reached a homogeneous level. In the present study, the mixing time were estimated as the time required for the monitoring point concentration (or conductivity) to fall continuously within a $\pm 5\%$ deviation band of the well mixed region. For each configuration five experiments were carried out and average mixing time was thereby determined.

3.6.3 Experimental Procedure

Mixing times were measured in cylindrical vessel (I.D. = 0.30m) with and without slag, in which water bath was agitated by injecting air/ N_2 through the combination of nozzles located at the bottom of the vessel. Three different nozzles configurations were investigated and these included axisymmetric central plug, single asymmetric plug

located at $R/2$ and dual plug of diametrically opposite positions of $(R/2)$ as shown in Fig 3.16. Water was filled in the vessel up to the height of 27 cm and mustard oil is then gently poured along the side of the vessel over the water level to make it up to 30 cm height to make $L/D = 1$. Pouring of mustard oil over the liquid bath is done carefully to avoid any formation of emulsion before the gas purging is started. This is done by using a funnel to pour the oil, the tip of which is kept just touching to the upper surface of the liquid so that the oil spreads gently over the surface instead of going deep into the liquid. Since the tracer used is diluted H_2SO_4 having almost same density as that of water it is totally dissolved in water phase itself and the transfer of H_2SO_4 to upper oil phase is negligible. Air/ N_2 is injected at predetermined rate by adjusting the gas tap. The gas flow rates were so chosen to ensure gentle stirring condition as are encountered in actual ladle metallurgy steelmaking operations.

A conductivity probe supplied with digital conductivity meter was employed to record changes in the local ion concentration of pulse tracer (H_2SO_4) addition in the bath. The tracer was added at a point lying midway between the 'eyes' of surfacing plume[63] for dual plug configuration and exactly over the plume in case of single plug configurations as shown in Fig. 3.16. The change in local ion concentration around the probe tip was measured through the changes in water's electrical conductivity and recorded manually via digital conductivity meter as soon as change in electrical conductivity was shown on the monitor of the conductivity meter (typically every 2/3 seconds) and simultaneously stored in a computer using CyberComm Portable software. The recording of tracer response was carried out until the concentration was considered to have reached the homogeneously mixed value. On addition of tracer, considerable oscillations in the form of peaks and valleys were observed after plotting the recorded data's of change in electrical conductivity (mS) vs. time elapsed (s). In all experiments, the tip of the probe was kept at a location close to the bottom of the vessel and near the side wall and collinear with both the injection nozzles. To compare the effect of upper slag layer on mixing time same set of experiments repeated without the slag layer for same configurations. A typical tracer response curve is shown in Figure 3.17

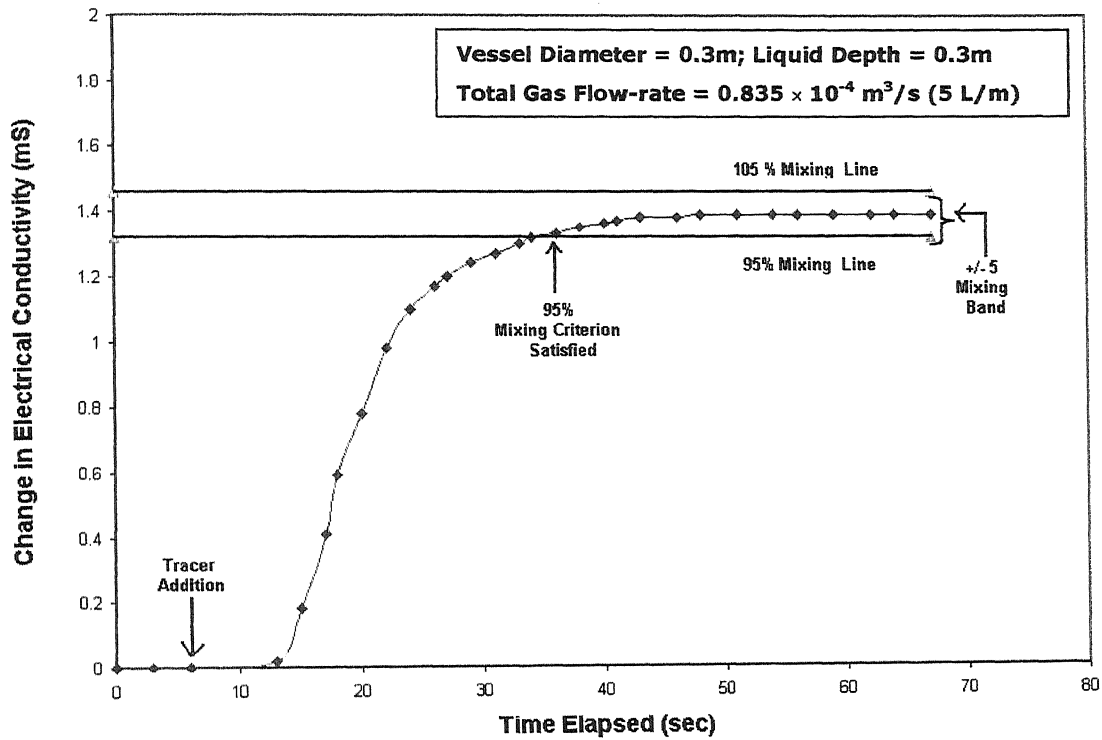


Figure 3.17: A typical tracer response curve illustrating experimentally measured variation of bath electrical conductivity at the monitoring point as a function of time.

3.6.4 Reproducibility of Data

To check the reproducibility of the experimental measurements, these were repeated for five times under identical conditions of gas flow rate and nozzle configuration. Table 3.11 and 3.12 shows discrete experimental mixing time values as well as their average values for a set of three different experimental conditions in the vessel without and with slag respectively. It is estimated from the table that the variation in mixing time, τ_m between run to run was within $\pm 10\%$ in case of no slag and $\pm 18\%$ in presence of slag. Thus it can be concluded that fairly reproducible mixing time values were experimentally measured during the present investigation.

3.7

MIXING TIME EXPERIMENTAL RESULTS

Mixing time experiments were conducted on cylindrical Perspex vessels having scale factor 0.08 keeping the L/D ratio 1. Experiments were done with slag and without slag layer for various gas flow rates and nozzle configurations. In this section the experimental results are presented in a tabular form.

WITHOUT SLAG						
FLOW RATE (LPM)	CENTRAL PLUG					AVERAGE (Sec)
	EXP 1	EXP 2	EXP 3	EXP 4	EXP 5	
1	56	44	46	36	47	45.8
2	40	43	45	49	41	43.6
3	38	35.5	37	35	40	37.1
4	44	30	33.5	26	36	33.9
5	31	28	25	30.5	29	28.7
DUAL PLUG						
2	30	31	35	29	27	30.4
3	26	35	29.5	27.5	24.5	28.5
4	26	14	27.5	32	29	25.7
5	27.5	25.5	24	29	16	24.4
6	24	13	15	27	12	18.2
SINGLE ASYMMETRIC						
1	29	47	37.5	50.5	31.5	39.1
2	42	28	44	38	42	38.8
3	39	30.5	33	38	35	35.1
4	27	25.5	38	36.5	31.5	31.7
5	26	23.5	27.5	31	29.5	27.5

Table 3.11: Experimentally observed mixing time values for varying flow rates at three different nozzle configurations without slag layer.

WITH SLAG						
<i>FLOW RATE (LPM)</i>	CENTRAL PLUG					AVERAGE (Sec)
	EXP 1	EXP 2	EXP 3	EXP 4	EXP 5	
1	58	70	104	64	63	71.8
2	71	51	70	91.5	56	67.9
3	59	82.5	70.5	59	65	67.2
4	66	78	82.5	39	50	63.1
5	41.5	39	38.5	83	71.5	54.7
DUAL PLUG						
2	38	67	42	58	61	53.2
3	57	39	41.5	48.5	41	45.4
4	58	40	51.5	49	31.5	46
5	45.5	33.5	38	52	44	42.6
6	25.5	46	46.5	37	46.5	40.3
SINGLE ASYMMETRIC						
1	50	43	74	67	66	60
2	53	57	48	58.5	77	58.7
3	37.5	51.5	68.5	57.5	66.5	56.3
4	65	51	51.5	45	49.5	52.1
5	55	48	46.5	45	49	48.7

Table 3.12: Experimentally observed mixing time values for varying flow rates at three different nozzle configurations in presence of slag layer of 3cm thickness.

FLOW RATE	CENTRAL NOZZLE	DUAL NOZZLE (R/2-R/2)	SINGLE ASYMMETRIC (R/2)
1	1.567686	---	1.534527
2	1.557339	1.75	1.512887
3	1.811321	1.592982	1.603989
4	1.861357	1.789883	1.643533
5	1.905923	1.745902	1.770909
6	---	2.214286	---

Table 3.13: Ratio of experimental mixing times (τ_m , with slag / τ_m , without slag) for varying flow rates at 3 cm slag depth.

WITH SLAG						
FLOW RATE (LPM)	1 CM SLAG DEPTH					AVERAGE (sec)
	EXP 1	EXP 2	EXP 3	EXP 4	EXP 5	
2	35	41.5	51	42	47.5	43.4
3	52.5	31	45.5	33.5	34	39.3
4	28.5	42.5	43	32.5	31	35.5
5	41	35.5	28	29.5	31	33
6	22.5	32	33.5	30.5	25	28.7
6 CM SLAG DEPTH						
2	67.5	74.5	85.5	89	81	79.5
3	85	71.5	79.5	69.5	82.5	77.6
4	79	62.5	69.5	73	66	70
5	76.5	78	61	74.5	67	71.4
6	59	73.5	65	69	62.5	65.8

Table 3.14: Experimentally observed mixing time values for varying flow rates at 1cm and 6 cm slag depth for dual nozzle configuration.

Table 3.11 shows the experimental mixing times for various gas flow rates at all the three nozzle configurations under consideration without slag. A log-log plot of experimental mixing time against gas flow rates for all configurations without slag is shown in the Fig 3.18. The mixing time is found to be maximum for single central nozzle and minimum for dual nozzle for the same total gas flow rate. However mixing times decreases with increasing flow rates for all the configurations. Among the single nozzle configurations the asymmetric nozzle shows lower mixing time than the central nozzle. It can be said from the plot that optimum mixing condition is achieved while using dual nozzle configuration for the same gas flow rate.

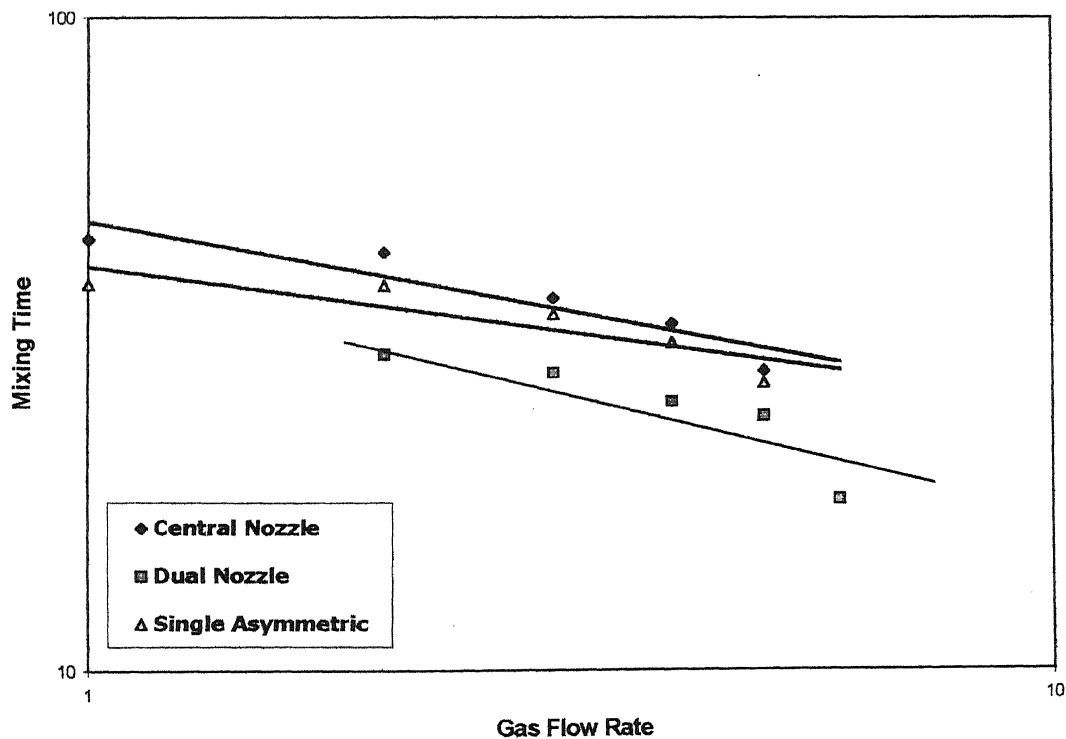


Figure 3.18: Experimentally measured mixing times (sec) as a function of gas flow rate (m^3/sec) for three different nozzle configurations without slag.

Table 3.12 shows the experimental mixing times for various gas flow rates at all the three nozzle configurations under consideration in presence of slag. A log-log plot of experimental mixing time against gas flow rates for all configurations in presence of slag is shown in the Fig 3.19. The mixing time values in this case are quite higher as compared to no slag experiments regardless of the injection configuration. This shows that the presence of upper slag layer has a considerable effect on mixing time. These results are in accordance with the different theories proposed in the literature which states that presence of upper slag layer dissipates the part of the input energy rate to give somewhat longer mixing time. In the presence of the oil layer, some of the stirring energy by gas injection is consumed in producing turbulence at the interfacial region and circulation inside the oil. This gives less energy to be used for mixing phenomenon inside the bulk phase.

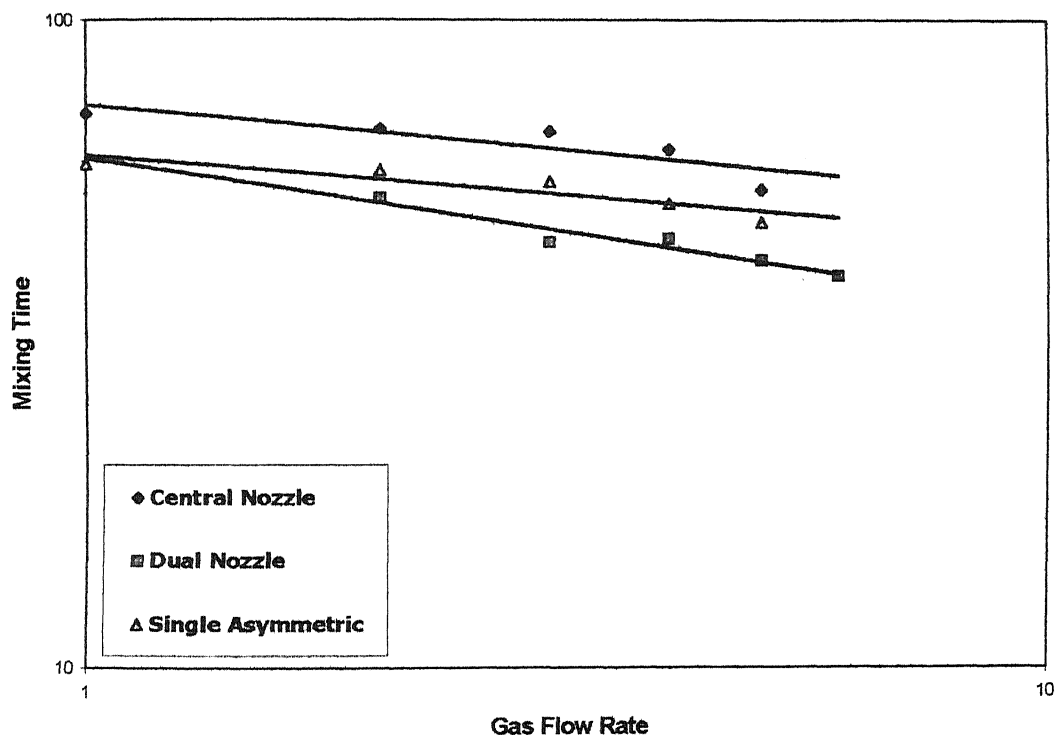


Figure 3.19: Experimentally measured mixing times (sec) as a function of gas flow rate (m^3/sec) for three different nozzle configurations in presence of slag layer (0.03 m thickness).

However the results in presence of slag layer show the similar relative nature among different configurations to without slag experiments. Mixing times decreases with increasing flow rates for all the configurations and dual nozzle configuration gives the optimum mixing condition.

It can be seen from the Table 3.13 that the ratio of mixing time between with slag and no slag condition varies from 1.5 to 2 for central nozzle injection. A closer comparison of with slag and without slag conditions for central nozzle injection is shown on a log-log plot in Fig 3.20. The mixing times in presence of slag are sufficiently high as compared to no slag conditions.

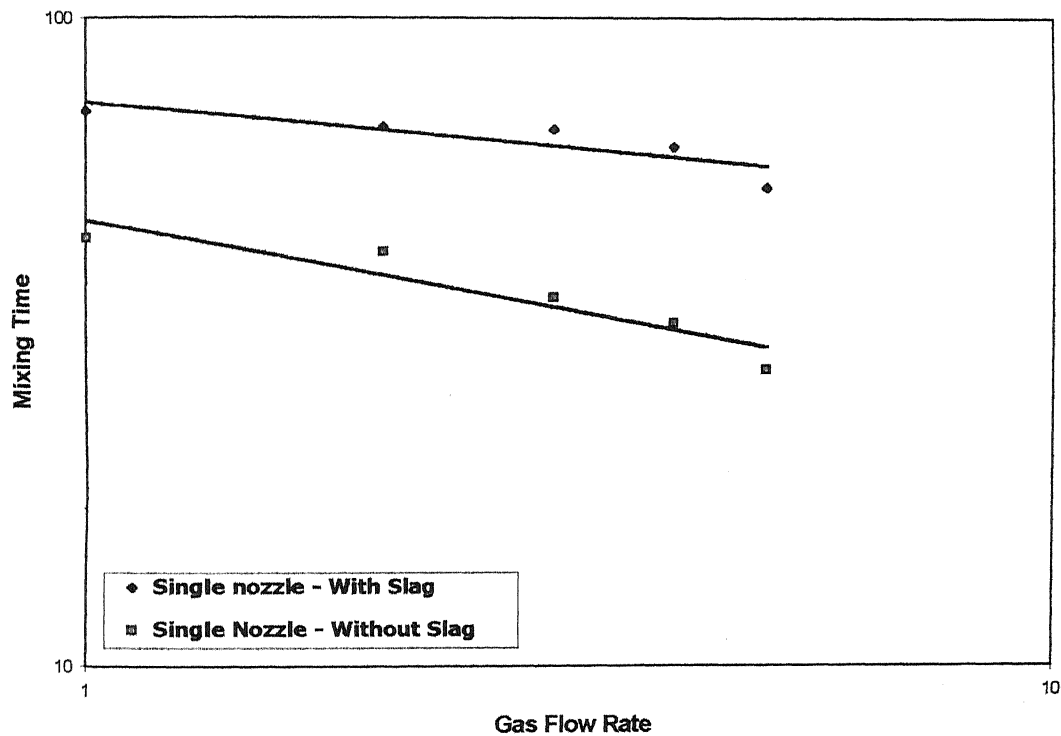


Figure 3.20: Comparison of experimentally measured mixing times (sec) as a function of gas flow rate (m^3/sec) for central single nozzle configuration with 0.03m slag thickness and without slag.

It can also be seen from the Table 3.13 that the ratio of mixing time between with slag and no slag condition for dual nozzle injection varies from 1.75 to 2.20. A closer comparison of with slag and without slag conditions for dual nozzle injection is shown on a log-log plot in Fig 3.21. This clearly shows that the mixing times in presence of slag are sufficiently high as compared to no slag conditions for dual nozzle configuration too.

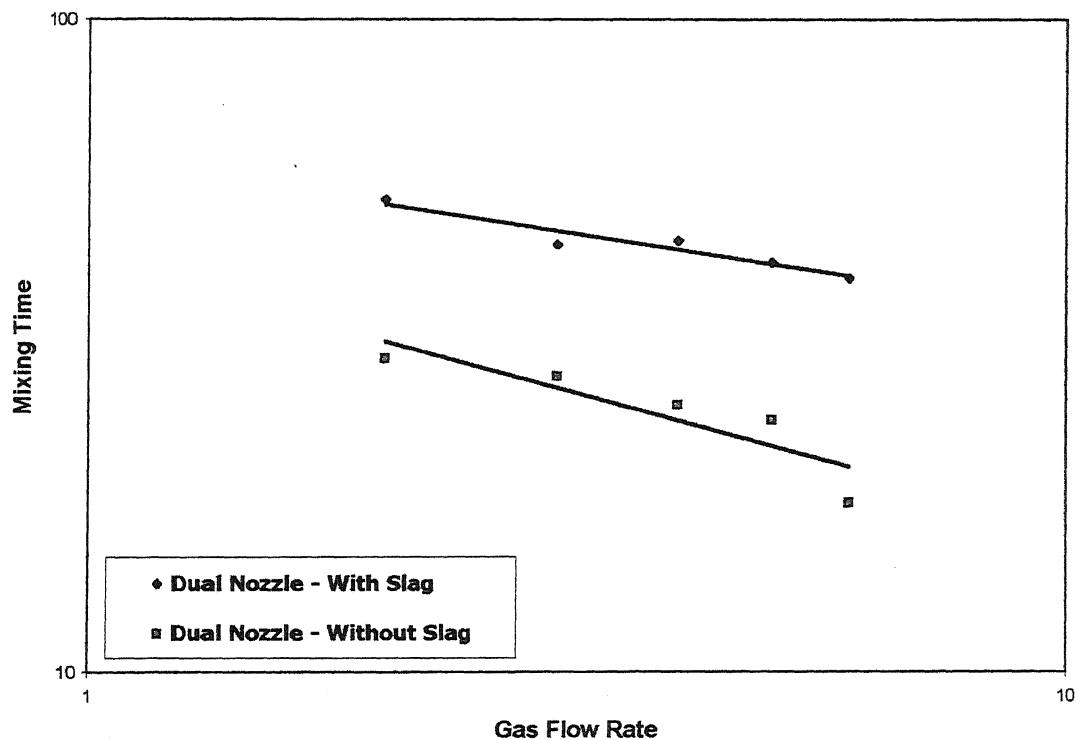


Figure 3.21: Comparison of experimentally measured mixing times (sec) as a function of gas flow rate (m^3/sec) for dual nozzle configuration with 0.03m thickness slag and without slag.

Table 3.14 shows the mixing times at different gas flow rates for 1cm and 6cm slag depth on dual nozzle configuration. Fig 3.22 shows the comparison of mixing times at plotted on a log-log plot for 1cm, 3cm and 6cm slag depths on dual nozzle configuration. It can be concluded from the plot that presence of thicker slag depth gives larger mixing times. This is because the oil layer resists the recirculatory flow and this hindrance increases with increasing oil layer thickness.

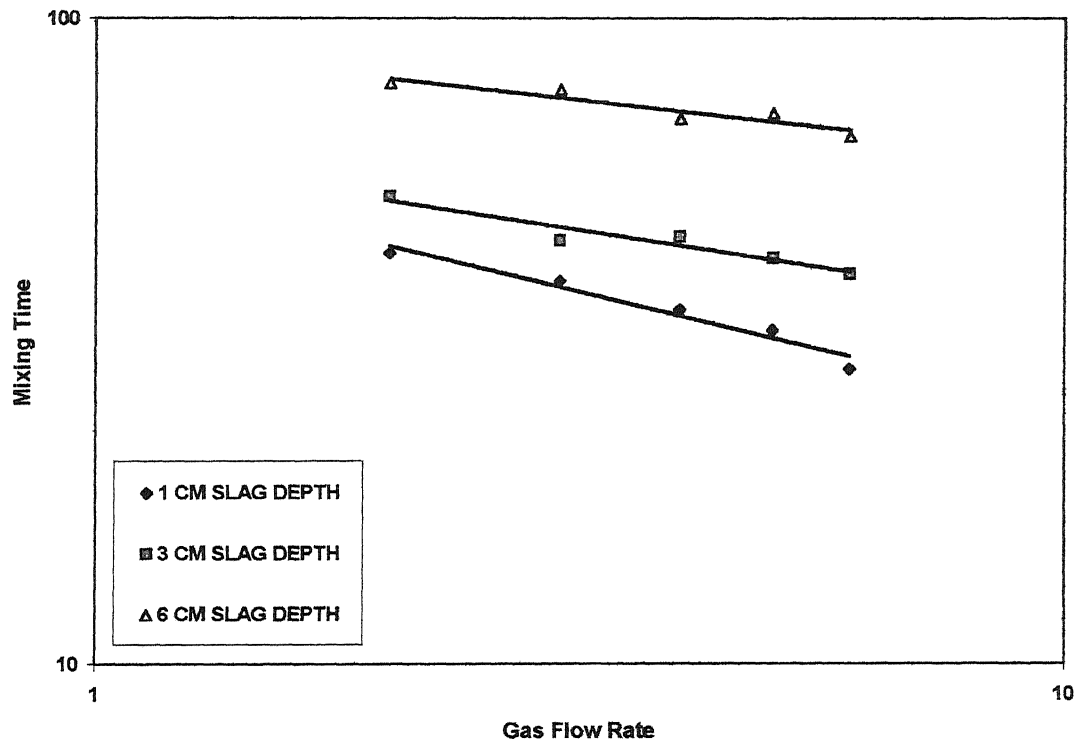


Figure 3.22: Comparison of experimentally measured mixing times at 0.01m, 0.03m and 0.06m slag depths as a function of gas flow rate (m^3/sec) for dual nozzle configuration.

During the pouring of liquid steel from furnace to ladle there is uncontrolled amount of slag carryover and a considerable thickness of slag is always present over the bulk metal during the ladle operations. From the above plots it can be concluded that the presence of upper slag does make a significant increase on mixing times. These findings also indicate the weakness of the existing models and relations to describe the velocity profile and mixing time in bulk phase which were developed without considering the effect of the secondary phase (slag layer).

CHAPTER IV

CONCLUSION TO THE THESIS

Fluid flow, mixing and mass transfer were studied in a cylindrical water model ladle of scale factor of 0.08 of a full scale 150 tonne ladle in presence of an upper buoyant phase with water representing metal and mustard oil representing slag over a wide range of operating conditions (nozzle(s) location, slag depth and the ambient gas flow rate). Presence of oil layer has great influence on fluid flow, mixing and mass transfer behavior in the ladle. On the basis of the results and discussions following conclusions can be drawn.

- i. Video recording method developed in the lab gives a reasonable estimate for the purpose of qualitative analysis and can be applied as a first approximation for rate calculations (dissolution, melting etc.) in such gas agitated systems.
- ii. The mean speed increases with increase in gas flow rate and depth of liquid in the system.
- iii. The velocity magnitude increases with increasing gas flow rate but the axial and radial velocities both are dampened considerably in presence of an upper phase for both single and dual plug bubbling.
- iv. Although mixing time was decreased with increasing gas flow rate, bulk mixing time considerably increased by a factor of 1.5 to 2.25 in presence of upper buoyant phase over the entire gas flow rate for all nozzle configurations.
- v. Better mixing has been observed, as indicated by decreased mixing time for dual plug as compared to centre or off centre single nozzle configuration for same total gas flow rate with and without upper phase.
- vi. For a constant gas flow rate the bulk mixing time was extended with increase of oil thickness.
- vii. Mass transfer from the bulk phase to upper buoyant phase increased with increasing gas flow rates.

- viii. Better mass transfer was observed for single central nozzle injection as compared to dual nozzle injection over entire gas flow rates.
- ix. Increasing the oil to water ratio increased the rate of the two phase mass transfer.

CHAPTER V

RECOMMENDATIONS FOR FUTURE WORK

The scope of the present work can be further expanded considering the following:

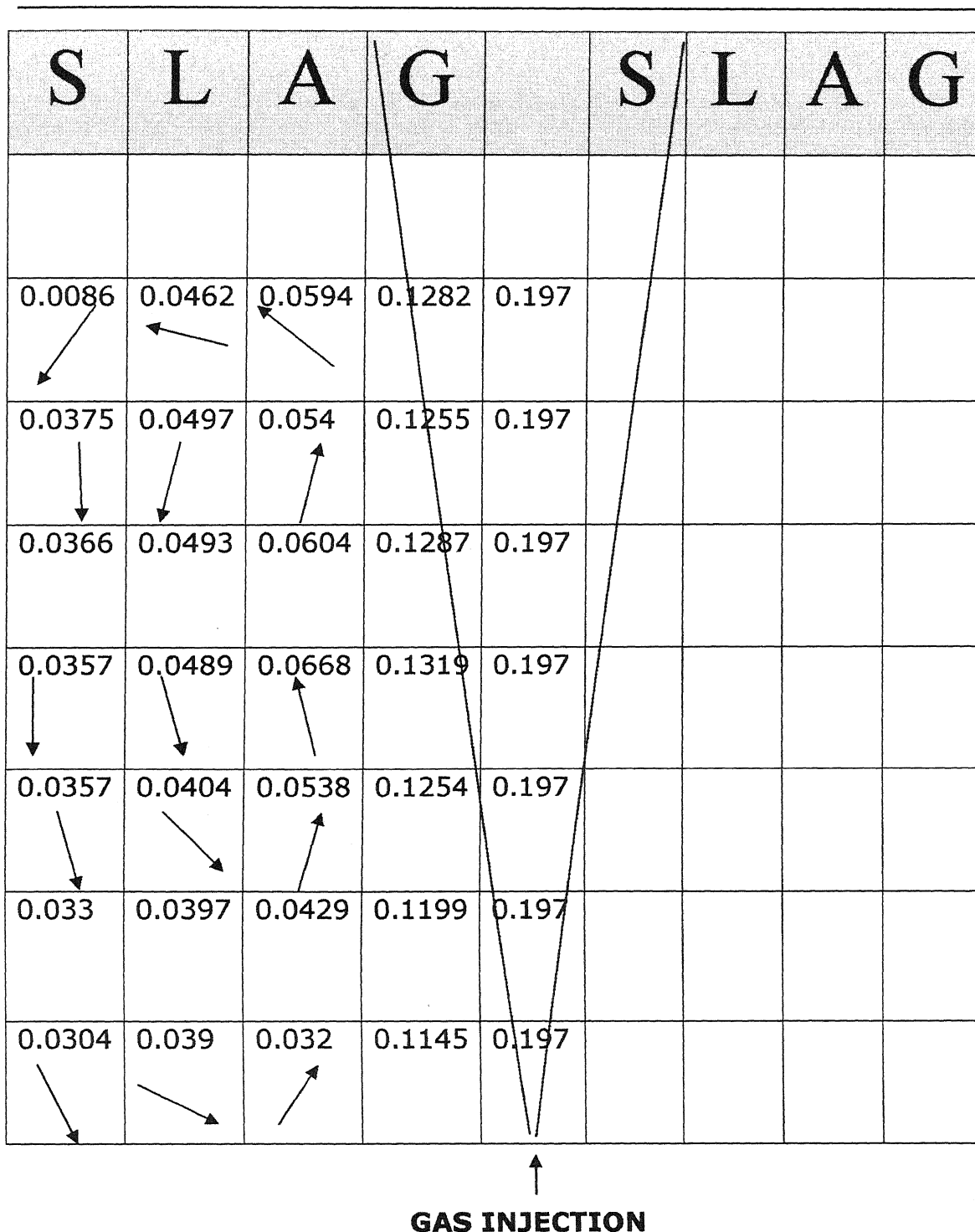
- i. In the present study, the fluid flow, mixing and mass transfer were studied using only mustard oil keeping the density/viscosity fixed. Further investigation can be done to study the effect of various parameters by varying oil densities/viscosities of the buoyant phase.
- ii. The present physical model can be modified with inclined wall instead of the vertical wall, which is more typical of actual practice.
- iii. The present work can also be expanded to different aspect ratios of the vessel.
- iv. Mathematical modeling of twin plug system should be carried out and predicted results be verified against present experimental results.

REFERENCES

1. K.H.Tacke, H.G.Schubert, D.J.Weber and K.Schwerdtfeger, *Metall. Trans.*, 16B, 263, 1985.
2. S.C.Koria and S.Singh, *Steel Res.*, 60, 301, 1989.
3. S.C.Koria and S.Singh, *Trans. Indian Inst. Met.*, 44, 223, 1991.
4. Y.Sheng and G.A.Irons, *Int. J. Multiphase Flows*, 17, 585, 1991.
5. Y.Sheng and G.A.Irons, *Metall. Trans.*, 23B, 779, 1992.
6. M.A.S.C.Castello-Brano and K.Schwerdtfeger, *Metall. Trans.* 25B, 359, 1994.
7. S.T.Johansen and T.A.Engh, *Scand. J. Metall.*, 14, 214, 1985.
8. C.T.Hsiao, T.Lehner and B.Kjellberg, *Scand. J. Metall.*, 9, 105, 1980.
9. S.T.Johansen, D.G.C.Robertson, K.Woje and T.A.Engh., *Metall. Trans.* 19B, 745, 1988.
10. A.H.Castillejos and J.K.Brimacombe, *Metall. Trans.*, 18B, 659, 1987.
11. K.Narita, A.Tomita, Y.Hirooka and Y.Satoh, *Tetsu-to-Hagane*, J.Iron Steel Inst. Jpn), 57, 1101, 1971.
12. S.Joo and R.I.L.Guthrie, *Metall. Trans.*, 23B, 765, 1992.
13. L.Zhang, S.Taniguchi, K.Cai and Y.Qu, *Steel Res.*, 9, 325, 2000.
14. S.Tanaka and R.I.L.Guthrie, *Process Technology Proc.*, 6th Int. Iron Steel Cong., Vol 6, 249, 1986.
15. D.Mazumdar, H.Nakajima and R.I.L.Guthrie, *Metall. Trans.*, 19B, 507, 1988.
16. D.Mazumdar and R.I.L.Guthrie, *Trans. Indian Inst. Met.*, 43, 139, 1990.
17. D.Mazumdar and R.I.L.Guthrie, *Metall. Trans.*, 17B, 725, 1986.
18. G.G.Krishna Murthy and S.P.Mehotra, *Ironmaking and Steelmaking*, Vol 19, 377, 1992.
19. D.Mazumdar and R.I.L.Guthrie, *ISIJ International*, Vol 35, 1, 1995.
20. R. I. L. Guthrie, *Iron & Steelmaker*, 9, 41, 1982.
21. S. Asai, T. Okamoto, H.Ji.Cheng, *Trans. ISIJ*, Vol. 23, 43, 1983.
22. G. G. Krishna Murthy, S. P. Mehrotra and A. Ghosh, *Metall. Trans. B*, Vol. 19B, 839, 1988.
23. J.Mietz and F.Oeters, *Steel Res.*, 59, 52, 1988.

24. K.Nakanishi, J.Szekely and C.W.Chang, *Ironmaking Steelmaking*, 2,115,1975.
25. K.Nakanishi, T.Fujii and J.Szekely, *Ironmaking Steelmaking*, 2, 193,1975.
26. U. P. Sinha and M. J. McNallan, *Metall. Trans. B*, Vol. 16B, 850, 1985.
27. T.Stapurewicz and N.J.Themelis, *Can Metall.Q.*, 26,123, 1987.
28. S. Asai, T. Okamoto, J.C.He and I.Muchi, *Trans. ISIJ*, Vol. 23, 43, 1985.
29. S. H. Kim and R. J. Fruehan, *Metall. Trans. B*, Vol. 18B, 381, 1987.
30. S. Joo and R. I. L. Guthrie, *Metall. Trans. B*, 1992, Vol. 23B, 765, 1992.
31. M.Hirasawa, K.Mori, M.Sano, A.Hatanaka, Y.Shimatani and Y.Okazaki, *Trans. ISIJ*, 27, 277, 1987.
32. M.Hirasawa, K.Mori, M.Sano, Y.Shimatani and Y.Okazaki, *Trans. ISIJ*, 27, 283, 1987.
33. B. Berg, G. Carlsson, M. Bramming, *J. Metal*, 14, 299, 1985.
34. K.Ogawa and T.Onoue, *ISIJInternational*, 29, (2), 148, 1989.
35. J.Mietz, S.Schneider and F.Oeters, *Steel Res.*, 62, (1), 1, 1991.
36. R.P.Singh and D.N.Ghosh, *Ironmaking Steelmaking*, 17, (5), 333, 1990.
37. S.C.Koria and M.R.R.I.Shamsi, *Ironmaking and Steelmaking*, 17, (6), 401, 1990.
38. S.H.Kim, R.J.Fruehan and R.I.L. Guthrie, *Steelmaking Conf. Proc.*, 70, 107, 1987.
39. R.J.Matway, R.J.Fruehan and H.Henein, *Iron Steelmaker*, 16, 51, September 1989.
40. R.J.Matway, H.Henein and R.J.Fruehan, *Iron Steelmaker*, 18, 43, December 1991.
41. H.Schlarb and M.G.Frohberg, *Steel Res.*, 15, (3), 127, 1985.
42. S.Paul and D.N.Ghosh, *Metall. Trans.*, 17B, 461, September, 1986.
43. S.Taniguchi, Y.Okada, A.Sakai and A.Kikuchi, *6th Int. Iron and Steel Congr.*, *ISIJ*, 1990.
44. S.C.Koria and A.Gorge, *Ironmaking and Steelmaking*, 15, (3), 127, 1985.
45. S.C.Koria and S.Pal, *Steel Res.*, 62, (2), 47, 1991.
46. S.C.Koria and S.Pal, *Ironmaking and Steelmaking*, 17, (5), 325, 1990.
47. H. Kramers, G. M. Barrs and W. H. Knoll : *Chem. Engg. Sci.*, 1953, Vol. 2, 35.
48. S. Asai, T. Okamoto, H.Ji.Cheng, *Trans. ISIJ*, Vol. 23, 43, 1983.
49. P.V.Danckwerts, *Chem. Eng. Sci.*, 8, 93, 1958.
50. J.Mandal, M.Tech Thesis, IIT Kanpur, India, July, 2003.

APPENDIX



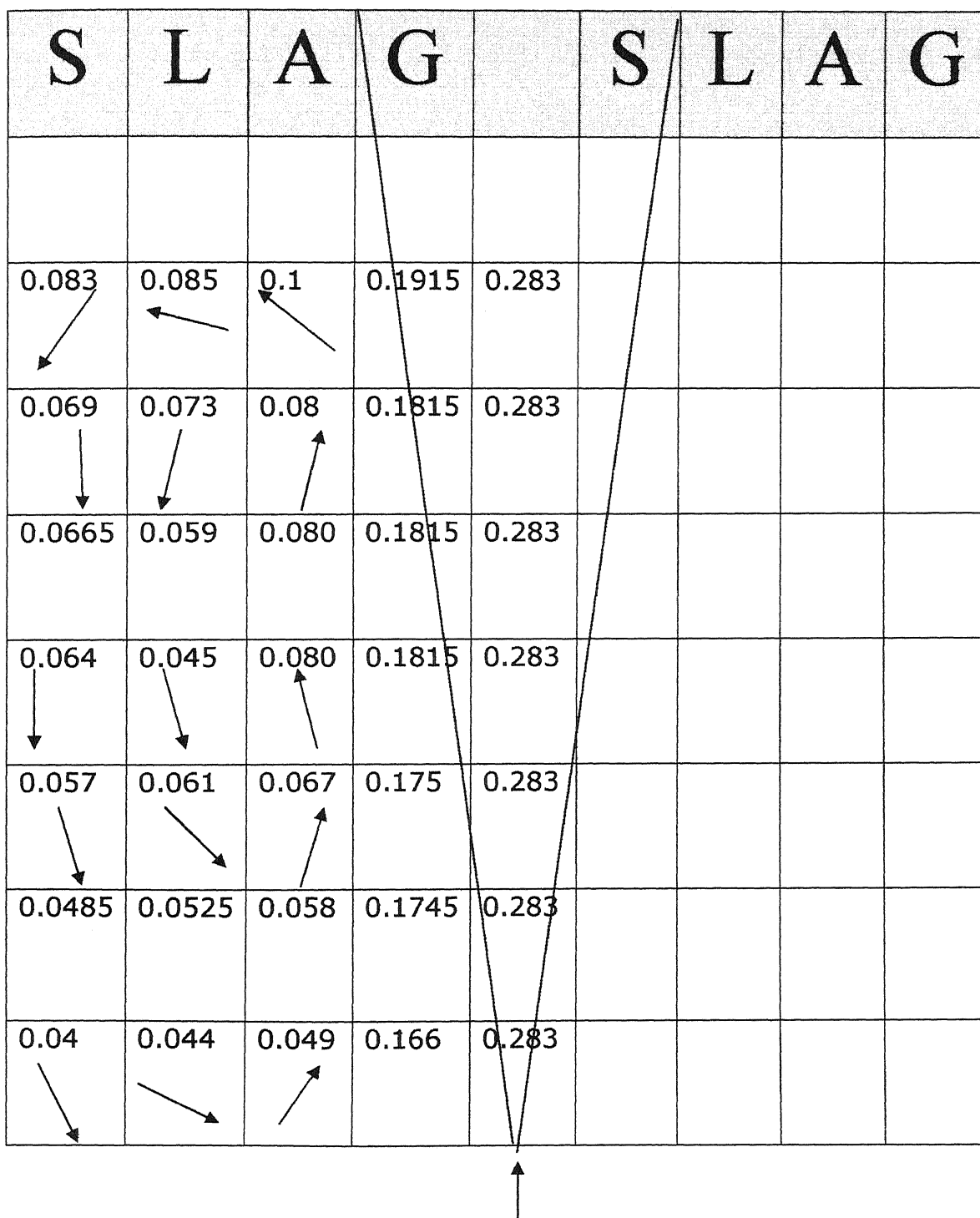
CASE 1: FLOW RATE = 1 LPM SLAG DEPTH = 3.5 CM

S	L	A	G		S	L	A	G
0.040 ↙	0.0489 ←	0.056 ↖	0.152	0.248				
0.053 ↓	0.054 ↙	0.049 ↗	0.1485	0.248				
0.0458	0.0495	0.048	0.148	0.248				
0.0386 ↓	0.045 ↙	0.047 ↗	0.1475	0.248				
0.0329 ↘	0.0423 ↘	0.0409 ↗	0.1444	0.248				
0.0302	0.0393	0.0395	0.1437	0.248				
0.0275 ↘	0.0364 ↘	0.0382 ↗	0.1431	0.248				




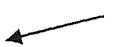
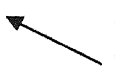

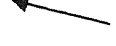
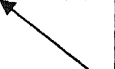












GAS INJECTION

CASE 2: FLOW RATE = 2 LPM SLAG DEPTH = 3.5 CM



GAS INJECTION

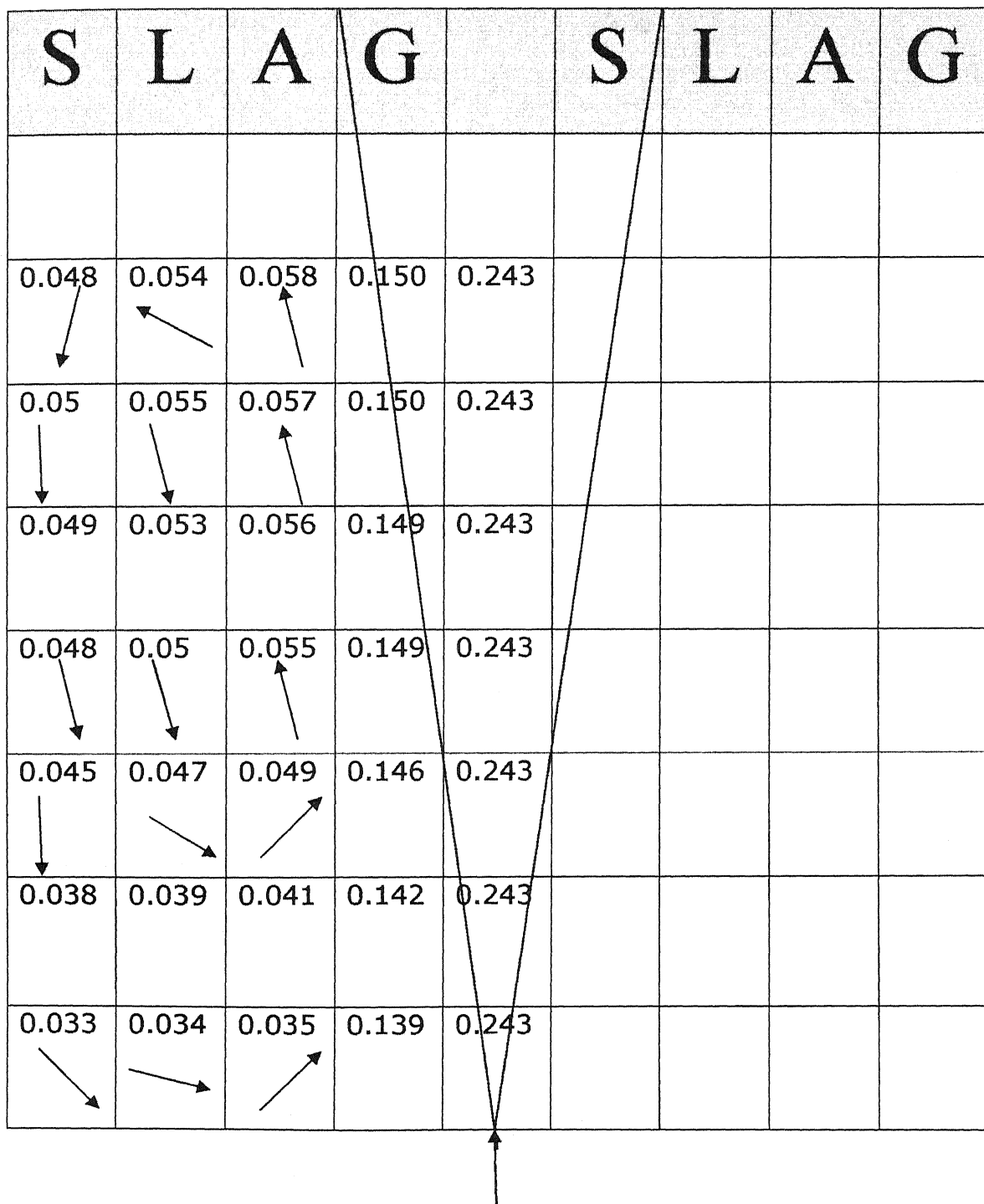
CASE 3: FLOW RATE = 3 LPM SLAG DEPTH = 3.5 CM

S	L	A	G		S	L	A	G
0.065 	0.07 	0.069 	0.1065	0.252				
0.055 	0.063 	0.066 	0.159	0.252				
0.053	0.06	0.059	0.155	0.252				
0.05 	0.057 	0.052 	0.152	0.252				
0.045 	0.051 	0.06 	0.156	0.252				
0.0465	0.0515	0.057	0.154	0.252				
0.048 	0.052 	0.054 	0.153	0.252				
0.029 	0.034 	0.04 	0.146	0.252				



GAS INJECTION

CASE 4: FLOW RATE = 2 LPM SLAG DEPTH = 1 CM



CASE 5: FLOW RATE = 2 LPM SLAG DEPTH = 5 CM